Development of a robust nanoscaffold as a modular vaccine platform



Theodora Bruun

Department of Biochemistry
St. Edmund Hall
University of Oxford

Trinity 2018

This thesis is submitted to the Department of Biochemistry at the University of Oxford, in partial fulfilment of the requirements for the degree of Masters by Research.

Abstract

Protein nanoparticles have been used as platforms to multimerize and present otherwise weakly immunogenic antigens to the immune system. Virus-like particles (VLPs) are self-assembling protein cages, forming the basis of safe and immunogenic vaccines that have been administered to millions of people. However, the creation of chimeric VLPs that display heterologous antigens through either genetic fusion or chemical coupling continues to be a challenge. To address this challenge, a modular vaccine platform has been previously developed that takes advantage of the spontaneous isopeptide bond between the protein domain SpyCatcher and its peptide partner SpyTag. Fusion of SpyCatcher to the surface-exposed N-terminus of the bacteriophage VLP AP205 afforded a particle that could be covalently coupled to a SpyTag-antigen simply by mixing. In the first part of this thesis I establish a methodology for the directed evolution of SpyCatcher-VLPs. I evolve the AP205 coat protein to attempt to address limitations in solubility and yield of the SpyCatcher-AP205 platform. I then extend the scope of SpyCatcher/SpyTag-mediated vaccines by characterizing a new modular platform based on the computationally designed I3-01 nanoparticle. I3-01 was rationally engineered to reduce aggregation by removing two surface-exposed cysteines. This mutated protein was given the name MI3. Genetic fusion of SpyCatcher to the N-terminus of MI3 yielded a platform that was purified in high yield from *E. coli*. I show that SpyCatcher-MI3 is robust and tolerates heating, freezing, and lyophilization. Immunization with SpyCatcher-MI3 particles conjugated with the SpyTagged malarial antigen CyRPA yielded high-avidity antibodies against CyRPA. The SpyCatcher-MI3 platform's stability, simple production method, and modular quantitative coupling should facilitate the development of new vaccines.

Authorship Declaration

I declare that this thesis is entirely my own work except for the cases described below. This thesis has not been submitted for any other degree at the University of Oxford or another institution.

Purified proteins obtained from others:

- CyRPA-SpyTag was produced by Dr. Anne-Marie Andersson
- Pfs25-SpyTag was produced by Dr. Karl Brune
- SpyTag-mClover3 was produced by Dr. Matteo Ferla

Work performed by others:

- TEM images were taken by Dr. Errin Johnson
- Immunizations and ELISAs were performed by Dr. Anne-Marie Andersson

Acknowledgements

This thesis is the culmination of two years of my life at Oxford. First and foremost, I would like to thank Professor Mark Howarth for giving me the opportunity to study here and for providing guidance during the ups and downs of my research.

I could not have done this thesis without the support of the people I worked with. Thank you to the members of the Sherratt and Whitby laboratories for contributing to the wonderful environment in the laboratory. To the members of the Howarth laboratory that I have had the pleasure of getting to know - Robert, James, Niels, MJ, Alberto, Mollie, Anusuya, Georgi, Felix, Arne - I am eternally grateful for your scientific advice, moral support, and stimulating conversation. For bringing great computational skills to the lab I thank Matteo. For being a great housemate I would like to thank JJ. I would also like to extend a very special thank you to Can for being the best friend that someone could ask for, and also for giving me so much of your time and support in the lab. To Irsyad and Anne-Marie: thank you for being my confidants and for all the late-night company. Additionally, it has been an absolute pleasure to work with Anne-Marie and I hope our paths cross again in the future.

I want to thank my college, Teddy Hall, and the Clarendon Council, not just for financial support but also for enriching my social life. Thank you to the Teddy Hall Boat Club for everything you contributed during my two years here. To all the people I interacted with at Oxford whether in small or large ways - thank you for making my time here so special.

Finally, a very special thanks to Evan, Edvard, Felix, and, of course, my parents.

Abbreviations

AP ..... Acceptor peptide

APC ..... Antigen presenting cell

AU ..... Antibody units

BCA ..... Bicinchoninic acid assay

BCR ..... B-cell receptor

Bio ..... Biotin

BirA ..... Biotin ligase

BSA ..... Bovine serum albumin

CFPS ..... Cell-free protein synthesis

CIDR ..... Cysteine-rich interdomain region

CpG ..... 5'-C-phosphate-G-3'

CP3 ..... Coat protein 3

CTL ..... Cytotoxic T Lymphocyte

CyRPA ..... Cysteine-rich protective antigen

DC ..... Dendritic cell

DE ..... Directed evolution

DLS ..... Dynamic light scattering

DMSO ..... Dimethyl sulfoxide

EDTA ..... Ethylenediaminetetraacetic acid

ELISA ..... Enzyme-linked immunosorbent assay

EpPCR ..... Error-prone PCR

EU ..... Endotoxin unit

FPLC ..... Fast protein liquid chromatography

GMP ..... Good manufacturing practice

GST ..... Glutathione S-transferase

ELISA ..... Enzyme-linked immunosorbent assay

HBc ..... Hepatitis B core protein

HBV ..... Hepatitis B virus

HEV ..... Hepatitis E virus

HPV ..... Human papilloma virus

IPTG ..... Isopropyl β-D-1-thiogalactopyranoside

IMAC ..... Immobilized metal ion affinity chromatography

LS ..... Lumazine synthase

MBP ..... Maltose binding protein

MHC ..... Major histocompatibility complex

MQ ..... Milli-Q

MWCO ..... Molecular weight cut-off

Ni-NTA ..... Nickel-nitrilotriacetic acid

PAGE ..... Polyacrylamide gel electrophoresis

PBS ..... Phosphate-buffered saline

PCR ..... Polymerase chain reaction

PDB ..... Protein Data Bank

PEG ..... Polyethylene glycol

PI ..... Protease inhibitors

PMSF ..... Phenylmethylsulfonylfluoride

qPCR ..... Quantitative polymerase chain reaction

RPM ..... Revolutions per minute

RT-PCR ..... Reverse-transcription polymerase chain reaction

SDS ..... Sodium dodecyl sulfate

SEC ..... Size exclusion chromatography

TEM ..... Transmission electron miscroscopy

TEV ..... Tobacco etch virus

TCR ..... T-cell receptor

TLR ..... Toll-like receptor

VLP ..... Virus-like particle

Table of Contents

Abstract i

Authorship Declaration ii

Acknowledgements iii

Abbreviations iv

Table of contents vi

List of figures xi

List of tables xiii

1 Introduction **1**

1.1 Vaccines 1

1.1.1 A brief history of vaccine development 1

1.1.2 Next generation vaccines: virus-like particles 3

1.1.3 VLP immunology 6

1.1.4 VLP decoration 8

1.1.5 Directed evolution of VLPs 10

1.1.6 Protein nanoparticles for vaccine technologies 12

1.2 Spontaneous isopeptide bond-forming technology 14

1.2.1 Introduction and development 14

1.2.2 Preceding work on VLPs and SpyCatcher/SpyTag 17

1.3 Thesis Objectives 18

2 Materials and Methods **19**

2.1 Cloning . . . 19

2.1.1 Polymerase Chain Reaction (PCR) . . . 19

2.1.2 Agarose gel electrophoresis . . . 20

2.1.3 PCR product purification . . . 20

2.1.4 Gibson assembly . . . 20

2.1.5 Transformation of *E. coli* . . . 21

2.1.6 Plasmid purification . . . 21

2.1.7 DNA sequencing . . . 21

2.2 Standard protein expression and purification . . . 22

2.2.1 Media and *E. coli* growth parameters . . . 22

2.2.2 Protein expression . . . 22

2.2.3 Ni-NTA purification of His_6-Tagged Proteins . . . 22

2.3 SDS-PAGE . . . 23

2.4 Protein concentration quantification . . . 24

2.5 Protein biotinylation . . . 24

2.6 TEV protease purification . . . 24

2.7 TEV protease cleavage . . . 25

2.8 SpyCatcher-AP205 VLPs . . . 25

2.8.1 SpyCatcher-AP205 expression . . . 25

2.8.2 Purification . . . 25

2.8.2.1 Immobilized metal affinity chromatography (IMAC) . . . 25

2.8.2.2 Ultra-centrifugation . . . 26

2.9 Directed evolution . . . 27

2.9.1 Error-prone PCR using Mutazyme . . . 27

2.9.2 Electro-competent cells . . . 27

2.9.3 Library transformation . . . 28

2.9.4 Variant capture using protein bait and magnetic beads 28
2.9.5 RNA extraction and purification 29
2.9.6 Reverse-transcription PCR (RT-PCR) 29
2.9.7 Quantitative PCR (qPCR) 29
2.10 SpyCatcher-MI3 nanoparticles 30
2.10.1 Expression 30
2.10.2 Purification by C-tag resin 30
2.10.3 Purification by Ni-NTA resin 31
2.10.4 Purification by gel filtration 31
2.11 Protein characterization and *In Vitro* assays 32
2.11.1 Dynamic light scattering 32
2.11.2 Transmission electron microscopy (TEM) 32
2.11.3 Nanoparticle reactivity 32
2.11.4 SpyCatcher-MI3 thermal resilience analysis 33
2.11.5 SpyCatcher-MI3 freeze-thaw stability 33
2.12 Protein lyophilisation 33
2.13 Nanoparticle vaccines 34
2.13.1 Preparation of SpyCatcher-nanoparticle immunogens 34
2.13.2 Endotoxin removal and quantification 34
2.13.3 SpyCatcher-nanoparticle immunizations 34
2.13.4 End-point ELISA 35
2.13.5 Antibody avidity ELISA 36
2.13.6 Statistical analysis of immunizations 36

3 Directed Evolution of SpyCatcher-AP205 37

3.1 Introduction 37
3.2 Generation of SpyCatcher-AP205 VLPs 38
3.3 Development of directed evolution methodology 41

3.3.1 RNA extraction and RT-PCR . . . 41
3.3.2 Genotype-phenotype correlation . . . 42
3.3.3 Model selection . . . 44
3.3.4 Library construction . . . 49
3.4 Directed evolution 1 . . . 52
3.5 Optimization of methodology . . . 55
3.6 Directed evolution 2 . . . 60
3.7 VLP assembly and disassembly . . . 62
3.8 Discussion . . . 64

4 Characterization of SpyCatcher-MI3 as a vaccine scaffold 68
4.1 Chapter Introduction . . . 68
4.2 Production of SpyCatcher-MI3 . . . 70
4.3 Pushing the limits of SpyCatcher-MI3 . . . 75
4.3.1 Biophysical characterization . . . 75
4.3.2 Reactivity and conjugation of particle . . . 76
4.3.3 Robustness . . . 78
4.4 Immunization trial . . . 80
4.5 Discussion . . . 87

5 Summary and General Discussion 91
Bibliography . . . 97
Appendix . . . 123

List of Figures

1.1 Major milestones in the field of vaccinology. 2

1.2 Activation of humoral and cell-mediated immunity following B- and T- cell antigen presentation. 8

1.3 Protein-based nanoparticles for vaccine platform technologies. 13

1.4 Splitting of the CnaB2 domain yielded two reactive partners capable of forming an irreversible covalent bond. 15

1.5 Splitting of the RrgA domain in three parts yielded a system capable of ligating two peptide tags. 16

1.6 Plug-and-display assembly for modular vaccines. 18

3.1 Characterization of SpyCatcher-CP3 VLPs. 40

3.2 Specific isolation of RNA from SpyCatcher-CP3 VLPs. 42

3.3 RT-PCR amplified RNA from VLPs at a very low concentration. 43

3.4 Establishing SpyCatcher-VLPs have a genotype-phenotype correlation. . . . 45

3.5 Capture of SpyCatcher-VLPs on biotin-binding beads is not selective. 47

3.6 Optimized VLP capture conditions for the directed evolution of SpyCatcher-CP3. 50

3.7 Quantitiative-PCR (qPCR) to assess RNA amounts in model selection experiments. 51

3.8 Results from directed evolution 1 indicated a problem in the methodology. . 54

3.9 Investigating bias for non-VLP forming mutants in the evolution methodology. 57

3.10 Ultra-centrifugation as an improved purification method for SpyCatcher-CP3 VLPs. 59
3.11 Results from directed evolution 2. 61
3.12 A variant from the evolution showed assembly over time. 62
3.13 SpyCatcher-CP3 VLP sizes varied widely under the same purification and storage conditions. 63
3.14 SpyCatcher-CP3 VLP size changed after dialysis into a high-salt buffer. . . . 64

4.1 I3-01 forms a hollow dodecahedral protein nanocage after mutations at key interface residues. 69
4.2 Modification of the I3-01 scaffold 72
4.3 Mutations in I3-01 and the addition of C-tag improved the solubility of nanoparticles. 73
4.4 SpyCatcher-MI3 was high yielding and less prone to aggregation than SpyCatcher-I301. 74
4.5 SpyCatcher-MI3 assembles into well-formed particles. 75
4.6 SpyCatcher-MI3 reaction with model protein partner SpyTag-MBP. 76
4.7 SpyCatcher-MI3 nanoparticles efficiently reacted with a variety of antigens. . 78
4.8 SpyCatcher-MI3 can be functionalized directly in lysate. 79
4.9 SpyCatcher-MI3 nanoparticles were robust to freezing, lyophilization, and heating. 81
4.10 SpyCatcher-MI3 is highly soluble and stable to storage. 82
4.11 Minimal sequence similarity to MI3 or SpyCatcher in the human genome. . . 83
4.12 Preparation of SpyCatcher-nanoparticle immunogens. 85
4.13 Plug-and-Display immunization with CyRPA immunogens. 86

List of Tables

2.1 Genotypes of *E. coli* host strains. 21

3.1 Optimization of the model selection conditions. 48

3.2 Mutational spectrum of the CP3 library compared to reported results. 53

3.3 VLP expression protocol versus standard expression for soluble protein. . . . 55

4.1 Dynamic light scattering of SpyCatcher-MI3 nanoparticles after heating, freezing, and lyophilization. 80

Chapter 1

Introduction

1.1 Vaccines

1.1.1 A brief history of vaccine development

Vaccines are the most effective medical intervention for preventing and controlling infectious diseases (Delany et al., 2014). The number of lives saved per year, thanks to vaccines, is estimated to be around 2-3 million (Karch and Burkhard, 2016). A selected timeline of major vaccine milestones is shown in Figure 1.1. In the 18^{th} century, Edward Jenner succeeded in developing the world's first vaccine. By inoculating people with material found in cow-pox pustules, Edward Jenner noticed that he was able to stop people from becoming ill with smallpox (Karch and Burkhard, 2016). The next major leap in vaccinology occurred when Louis Pasteur discovered the concept of attenuation (Hajj Hussein et al., 2015). By growing organisms under suboptimal conditions, or treating them with chemicals, it is possible to diminish the virulence of a pathogen (Galen et al., 2014). Injection with less-virulent strains of a bacteria can lead to protection when later challenged by a non-attenuated version. The first attenuated vaccine was created against rabies in 1885 (Delany et al., 2014). Attenuated/killed whole vaccines for typhoid fever, cholera, and the plague bacillus followed shortly after (Plotkin and Plotkin, 2011).

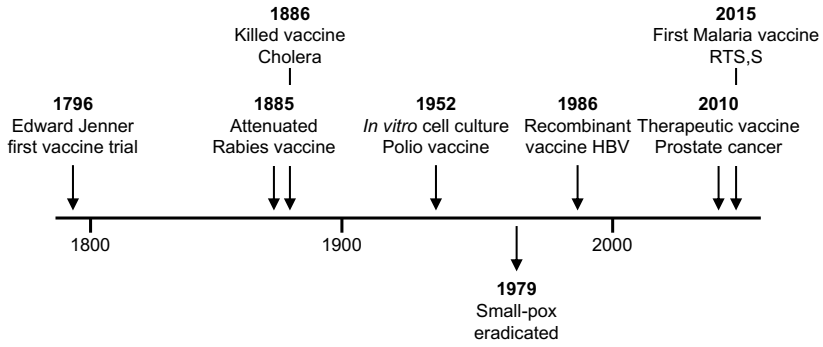


Figure 1.1. Major milestones in the field of vaccinology. Before Edward Jenner's vaccine experiment in the late 18th century, variolation had been practiced in India, China, and Western Asia. Advances in cell culture techniques and molecular biotechnology paved the way for more sophisticated vaccine technologies in the late 20th and 21st century. Timeline adapted from Karch and Burkhard, 2016; Delany et al., 2014.

In 1979 small-pox was officially declared eradicated thanks to a global vaccination effort (Tomori, 2011). Although this was a cause for celebration, and proved the power of vaccination, there were many concerns with the use of attenuated/killed whole pathogens. First, there were safety and cost-concerns with the large-scale culturing of live pathogens for vaccines (Thomassen et al., 2013). Second, live vaccines can cause serious medical side-effects in certain individuals and could sometimes revert to virulence once injected (Huang et al., 2004). Thus, with the invention and widespread use of the recombinant biological/genetic techniques, interest in the vaccine field shifted to creating recombinant subunit vaccines (Karch and Burkhard, 2016; Delany et al., 2014). Producing a vaccine based on a recombinantly produced protein is safer and cheaper (Moyle and Toth, 2013). However, although the safety profile of subunit vaccines is improved, it comes at a cost of reduced immunogenicity. The superior immunogenicity and efficacy of whole organism vaccines is likely due to the fact that they expose the immune system to multiple copies of each antigen and they contain many other immunostimulating molecules (Karch and Burkhard, 2016). To help boost the immunogenicity of recombinant proteins, huge efforts have been directed towards the development of potent adjuvants (Alving et al., 2012; Mbow et al., 2010). However, another approach to increasing the immune response to subunit vaccines involves repetitive antigen

display through the use of virus-like particles (VLPs) (Wu et al., 2015).

The first VLP-based vaccine was licensed in 1986 and was based on the protein antigen S (HBsAg) of the Hepatitis B virus (HBV) (Meireles et al., 2015). HBsAg forms 22 nm VLPs that are $\sim$ 1,000$\times$ more immunogenic than monomeric HBsAg (Cabral et al., 1978). The physical characteristics and immunostimulatory properties of VLPs will be discussed in detail in section 1.1.3 and section 1.1.2.

Thanks to the ability to create chimeric constructs, i.e. VLPs displaying non-native epitopes, vaccines against a broad range of targets are currently being developed (Rohovie et al., 2017; Chackerian, 2007; Frietze et al., 2016). This includes many diseases that have evaded traditional vaccine efforts and continue to pose a global public health challenge. For example, there is no effective vaccine against AIDS, malaria and tuberculosis, which collectively kill more than 5 million people a year (Rappuoli and Aderem, 2011). Traditional vaccines have been successful at preventing infection from pathogens that have low antigen variability and can be treated by antibodies (Rappuoli and Aderem, 2011). However, traditional vaccines fail to protect against pathogens that require T-cell mediated immunity, have highly variable genomic sequences, and have complex host life-cycles.

1.1.2 Next generation vaccines: virus-like particles

In the 1950s to 1980s, the term "virus-like particle" was applied to particles that resembled viruses in shape and size, and were seen by researchers studying papillomas, hepatomas, and tumours by transmission electron microscopy (Adams and Prince, 1957; Roingeard, 2008). Since their initial discovery, as characterization and knowledge of these particles has improved, the term virus-like particle has come to define spontaneous self-assembling nanoparticles. VLPs are formed from viral structural proteins but lack the genomic component responsible for the infectious nature of natural viruses. The fact that VLPs are hard to distinguish from infectious virus to the human immune system make VLPs attractive candidates for vaccines and vaccine platforms (Frietze et al., 2016; Chackerian, 2007; Zeltins,

2013). There are currently over 150 VLPs noted in the literature that come from 35 different families including animal viruses (e.g. parvovirus), plant viruses (e.g. tobacco mosaic virus), and bacteriophages (e.g. Qβ, AP205, MS2) (Zeltins, 2013). VLPs can be enveloped or non-enveloped, spherical or rod-shaped, and are typically in the size range of 20-200nm (Kushnir et al., 2012). VLPs can be made in mammalian cell culture, bacteria, yeast, transgenic plants, and baculovirus/insect cells (Kushnir et al., 2012). Although the use of VLPs in vaccines is one of the most common applications (Jennings and Bachmann, 2008), VLPs are also attractive imaging agents, nanobioreactors, and therapeutic tools (Uchida et al., 2018; Wilhelm et al., 2016; Shi et al., 2017). Because of their structure, VLPs can be functionalized externally or they can be exploited as hollow nanocages (Rohovie et al., 2017). Since the first hepatitis B VLP vaccine was commercialized in 1986, a number of companies have seen VLP-based vaccines successfully reach the market. Currently licensed VLP-based vaccines include those HBsAg VLPs (Engerix, Recombivac), HPV VLPs (Gardasil, Cervarix), HEV VLP (Hecolin), and an influenza virus VLP (Flublok) (Kushnir et al., 2012). Many other VLP-based vaccines are also at different stages in clinical trials (Kushnir et al., 2012). VLP-based vaccines are now being developed to target not just infectious diseases, but also autoimmune diseases, cancer, Alzheimer's disease, and allergies (Delany et al., 2014; Lee et al., 2016; Jennings and Bachmann, 2008).

Although there are many licensed VLP-based vaccines, reducing cost, accelerating the manufacturing process, and ensuring proper purity and quality are still critical areas for research and innovation. VLP size and complexity are two factors that produce challenges in the downstream processing of VLP vaccines, particularly when scaling up purification processes (Effio and Hubbuch, 2015). While ultracentrifugation remains one of the most widely used purification methods, ultracentrifugation is time-intensive and often low yielding (Effio and Hubbuch, 2015; Vicente et al., 2011). Because VLPs are produced using recombinant technology, there are two types of impurities that must be taken into account when designing purity guidelines for commercial VLP vaccines: process- and product-related impurities

(Effio and Hubbuch, 2015; Nestola et al., 2015). Process-related impurities can refer to host-cell impurities like cells, DNA, and endotoxins (a particular concern of *E. coli* expression systems). Process-related impurities can also include nucleases, anti-foam reagents, or media components that are introduced during upstream or downstream processing. Product-related impurities are those formed from the incorrect or inappropriate aggregation, folding, or treatment of VLP subunits. Removing or limiting the amount of these impurities is crucial to the safety of a vaccine. VLP purity for clinical usage is recommended to be >95 %, with endotoxin levels bellow 20 EU/mL (Brito and Singh, 2011).

The choice of expression system determines the clarification, purification and polishing steps necessary to produce VLPs according to good manufacturing practice (GMP). In a recent review that examined the successful production of 174 VLPs, the expression host systems that were most common were found to be bacterial, insect, and yeast systems (28 %, 28 %, and 20 % of all cases respectively) (Zeltins, 2013). Complex VLPs (ones with a lipid envelope and composition from multiple viral proteins), necessitate the use of a eukaryotic host where assembly occurs *in vivo* (Effio and Hubbuch, 2015). However, mammalian cell culture is expensive and cells have a low growth rate (Kim and Kim, 2017). High production cost is also a drawback of insect expression systems and, while bacterial and yeast systems are cheap, recombinant protein expression in bacteria and yeast may increase the amount of misfolded protein (Kim and Kim, 2017).

Choosing an expression host system is also important because the expression system can affect not just the final quantity but also the quality of VLP produced (Kim and Kim, 2017). For example, in a recent paper it was shown that, while recombinant *Mr*NV VLPs produced in *E. coli* were unstable and heterogeneous, when the same VLPs were produced in a baculovirus system (*Spodoptera frugiperda*) the VLPs were stable, homogeneous, and higher yielding (8.5 mg/L: a 5-fold improvement) (Kueh et al., 2016). In another example, polyomavirus VP1 VLPs produced in *E. coli* were polymorphic compared to the same VLPs produced in Sf9 insect cells (Salunke et al., 1989).

Host systems may affect particle assembly due to difference in cellular and biochemical conditions. Differences in cellular redox state, the presence of molecular chaperones, temperature, pH, and salt concentration all affect interactions between coat proteins during assembly. The use of cell-free protein synthesis (CFPS) technology has shown promise for VLPs and has some important benefits compared to other expression systems. For example, MS2 and HBV VLPs were assembled via *E. coli*-based CFPS at a 10× greater yield than previously reported production methods (Bundy et al., 2008). Furthermore, the methodology is easily scalable and has the potential to be much cheaper than other current VLP process technologies. Other benefits of CFPS include the ability to produce proteins that would not be tolerated normally. For example, the synthesis of Qβ (a bacteriophage VLP) via CFPS allowed researchers to incorporate protein A2, a protein that is toxic to living cells (Smith et al., 2012). The use of CFPS is also critical in cases where it is necessary to have unnatural amino acids incorporated into the desired VLP (Lu et al., 2013; Patel and Swartz, 2011). The ability to control the redox potential at all stages of CFPS also allowed researchers to produce HBc VLPs with disulfide bonds (Bundy and Swartz, 2011).

1.1.3 VLP immunology

The immune system is extremely complex and involves the integration of a wide range of signals and cellular responses. The immune system is often divided into the innate immune system and the adaptive immune system, although in reality the two overlap and functionally interact with each other (Parkin and Cohen, 2001). The innate immune system is highly conserved amongst species and provides the first line of defence against pathogens. The innate immune system is crucial for survival and is responsible for antigen presentation and activation of the adaptive immune system. The adaptive immune system relies on T- and B-lymphocytes to generate antigen-specific responses (Parkin and Cohen, 2001). These responses may take days or weeks to develop but can be retained in specific memory cells. The activation of memory cells confers protective immunity upon future re-exposure to the

same pathogen (Parkin and Cohen, 2001). The adaptive immune system is thus the basis of vaccination and the success of VLP-based vaccines relies on the strong stimulation of both B- and T- cell responses. Specifically, the stimulation of long-lived T-helper cell-dependent IgG responses is the cause of the success of prophylactic vaccines, while therapeutic vaccines (for example, vaccines against cancer) focus on generating $CD4^+$ and $CD8^+$ T-cell responses (Bachmann and Jennings, 2010).

The natural immunogenic properties of VLPs can be summarized as being due to their repetitive structure, their size, and their ability to induce innate immunity that appropriately stimulates adaptive immune responses (Jennings and Bachmann, 2008). VLP size ($\sim$ 20-200 nm) means they can drain directly into lymph nodes to be taken up by antigen presenting cells (APCs), or they can be actively transported to lymphoid tissue after uptake by dendritic cells (DCs) (Jennings and Bachmann, 2008). Lymph nodes house the germinal centers, the place where B cells undergo maturation (hypermutation and antibody class switching). Professional APCs are able to present VLP-derived epitopes, via MHC class I and II molecules, to $CD4^+$ T-helper and $CD8^+$ cytotoxic T cells (Figure 1.2)(Reimann and Schirmbeck, 1999). These activated T-cells can then stimulate B-cells in a T-cell dependent way. The activation of T-helper cells is crucial for helping primed B-cells differentiate into plasma cells that secrete antibodies (Stanley, 2008). Additionally, a proportion of plasma cells become memory B-cells.

The size and shape of VLPs means they can directly bind and stimulate B-cells. Because VLPs are comprised of many identical copies of coat proteins, their surfaces display antigens in a repetitive and dense array. B-cells are evolutionarily primed to respond strongly to these geometric displays via B-cell receptor (BCR) cross-linking (Figure 1.2) (Chackerian, 2007; Bachmann and Jennings, 2010). BCR cross-linking is an example of T-cell independent activation that results in strong antibody responses. VLPs also directly induce DC maturation, increasing the speed and strength of the immune response (Dalod et al., 2014; Chackerian, 2007). DC maturation refers to the enhancement of properties like antigen processing and

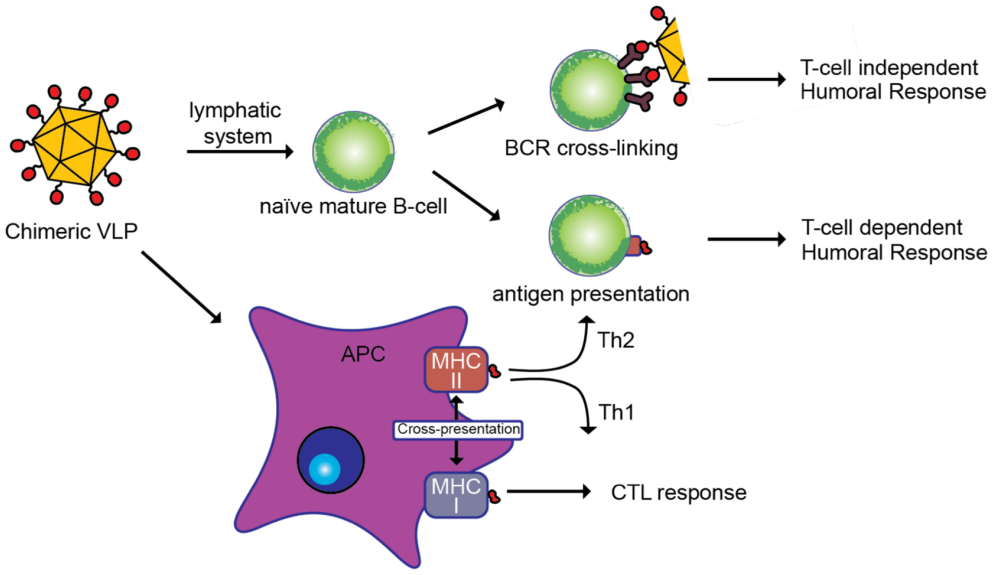


Figure 1.2. Activation of humoral and cell-mediated immunity following B- and T- cell antigen presentation. VLPs can stimulate the adaptive immune system through both B- and T-cell activation thanks to their size, shape, and geometry. Figure adapted from Parkin and Cohen, 2001 and Rehm, 2017.

presentation, and T-cell stimulation via co-stimulatory signals. Some documented examples of VLP-induced DC maturation include responses triggered by HPV (human papilloma virus) and HIV gag VLPs (Lenz et al., 2001; Tsunetsugu-Yokota et al., 2003).

Finally, some VLPs can encapsulate nucleic acids or be deliberately loaded with ligands that stimulate the innate immune system through activation of pathogen-associated molecular pattern recognition receptors (Jennings and Bachmann, 2008; Zabel et al., 2013; Schmitz et al., 2012). Examples of such ligands include single-stranded RNA, double-stranded RNA, and CpGs (DNA rich in non-methylated CG motifs). Immunostimulatory ligands can also be loaded directly on a chimeric VLP or injected in combination with VLPs as an adjuvant (Cheng et al., 2016; Perez et al., 2016).

1.1.4 VLP decoration

To serve as general vaccine platforms VLPs must be efficiently functionalized with heterologous antigens. There are two general approaches to for creating chimeric VLPs. The first

approach is direct genetic fusion to a VLP coat protein. The second approach involves installing an antigen in a secondary step. While genetic fusion of an antigen to a VLP has been done successfully (Mateu, 2011), the approach has limitations including the fact that it can be destabilizing to the VLP (which means placement of antigen requires extensive trial-and-error) (Chackerian, 2007), or genetic fusions can prevent the VLP from forming entirely (Stockley and Mastico, 2000; Peabody et al., 2008). Furthermore, folding and structure of the antigen may be compromised on the VLP, and the size of the antigen can be a limiting factor (Jain et al., 2015; Peabody et al., 2008). Finally, the antigen and VLP may have different optimal expression systems - particularly in cases where the antigen requires specific post-translational modifications (i.e. disulfide bond formation or glycosylation) (Smith et al., 2013). Thus, strategies to install an antigen onto a VLP in a secondary step are often advantageous.

Different approaches to VLP decoration have different drawbacks and advantages. It is unlikely that a single method will be satisfactory in every context. However, when developing technology for chimeric VLP formation, there are a number of criteria that an ideal method should fulfill. The method should yield quantitative coupling, produce a homogeneous end-product, and be reproducible from batch to batch. To reduce production cost, the reaction should use a minimal amount of reagents and have a short reaction time. The reaction must also occur in conditions that are suitable for both VLP and antigen.

Techniques for VLP conjugation have been summarized in a number of excellent reviews (Rohovie et al., 2017; Chackerian, 2007; Frietze et al., 2016; Lee et al., 2016; Mohsen et al., 2017). A classic approach to VLP decoration involves the use of chemical cross-linkers. Chemical techniques exploit five naturally occurring reactive amino acids: cysteine, lysine, tyrosine, glutamic acid and aspartic acid (Lee et al., 2016). Covalent chemical coupling can also occur with the incorporation of unnatural amino acids on the surfaces of VLPs (Smith et al., 2013). VLPs can also be engineered to contain methionine analogues capable of conjugation via click chemistry (Patel and Swartz, 2011). Some non-covalent approaches

to decorate VLPs have exploited the interaction between His-Tag and Ni-NTA (Koho et al., 2015) or the affinity between biotin and avidins (Chackerian et al., 2001). Non-covalent approaches, however, may be less desirable than covalent approaches because the coupling between VLP and antigen is less robust and could be subject to dissociation or reshuffling. Chemical approaches have limitations, including difficulty in producing homogeneous and quantitative coupling, and slow reaction kinetics (Ng et al., 2012; Wang et al., 2002a; Leneghan et al., 2017). With cysteine coupling, the need to introduce cysteines in non-native placements can cause aggregation, or the use of a reducing agent can be disruptive for the antigen and/or VLP (Wang et al., 2002b).

There are a number of covalent approaches that involve genetic engineering (Lee et al., 2016). Some examples include sortase-mediated ligation (Tang et al., 2016), the use of HaloTag (Sun et al., 2015), and spontaneous isopeptide bond forming technology, which will be discussed in more detail in section 1.2 and section 1.2.2. A drawback of HaloTag is its size (33 kDa), which can be disruptive when fused to proteins. Sortase-mediated conjugation suffers from requiring high molar excess of conjugating peptide.

1.1.5 Directed evolution of VLPs

Directed evolution is an integral method in protein engineering and synthetic biology. Directed evolutions mimic the process of natural selection to evolve a protein toward a specific goal, or to explore structure-function relationships (Jäckel et al., 2008; Gillam et al., 2014). An advantage of directed evolution is that we can achieve improvements or find solutions to problems despite gaps in our knowledge of structure and function. The success of directed evolution in accelerating the pace of scientific discovery is evident from the number and quality of improvements that have been achieved in diverse areas such as enzyme catalysis, protein folding, and antibody development (Arnold et al., 2001; Porter et al., 2016; Könning and Kolmar, 2018; Sachsenhauser and Bardwell, 2018).

Common principles that are crucial to the success of any evolution include establishing

a genotype-phenotype relationship and a good selection/screening strategy with sufficient selection pressure (Packer and Liu, 2015). Creating a high quality library of variants is one of the most important factors for an evolution (Tee and Wong, 2013). Genetic diversity can be introduced into a protein through three main strategies: random mutagenesis, focused mutagenesis, and DNA recombination (Tee and Wong, 2013). Focused mutagenesis is advantageous because it decreases the library size that is theoretically necessary to cover the entire mutational space of a given sequence. The maximum library size that can be created by any laboratory technique places an appreciable limit on the number of variants that can be accessed for screening (Jäckel et al., 2008). Although focused mutagenesis can help address this shortcoming, it also relies on identifying areas or amino acids that are likely determining a specific or desired function. Thus, there is a risk of focusing incorrectly on a particular area if structure-function is not well understood.

Directed evolution has been applied successfully to VLPs in many instances. MS2 bacteriophage VLPs have been the focus of a number of such experiments. MS2 is a bacteriophage of the *Leviviridae* family of small viruses that infects different types of Gram-negative bacteria. The MS2 coat protein has been mutagenized to select for particle size (Asensio et al., 2016), explore assembly (Peabody and Al-Bitar, 2001), and to understand and evolve RNA binding (Wang et al., 1997; Peabody, 1993). MS2 VLPs have also been used as a platform for the development of random sequence peptide libraries for affinity selection (Chackerian et al., 2011; Peabody et al., 2008; Crossey et al., 2015).

A classic example of directed evolution on a VLP involved the capsid of lumazine synthase (Worsdorfer et al., 2011). First, scientists engineered the lumazine synthase capsid to spontaneously assemble around a toxic HIV protease through electrostatic interactions. When co-expressed in *E. coli*, the growth advantage to the bacterial cell from protease encapsulation by VLP promoted evolution of the capsid over four rounds of mutagenesis and selection. The final capsid variant had a 5- to 10-fold higher nucleic acid loading capacity. In another example of a directed evolution, three rounds of evolution on a synthetic nu-

cleocapsid, 153-50, yielded particles with a more than 133-fold improved genome packaging ability (Butterfield et al., 2017). This experiment showed that synthetic nanoparticles can be evolved to obtain properties of VLPs that are desirable for vaccine purposes.

However, directed evolution is not the only technique that protein engineers can employ to alter VLP properties. Structure-based design of proteins has been employed in a number of cases to modify recombinant VLPs for vaccine technologies (Frietze et al., 2016). To allow conjugation of antigens onto VLPs some engineering strategies have involved creating reactive handles on the surface of VLPs through the introduction of cysteines or lysines. To enhance stability, cysteines that form intersubunit disulfide-bonds can also be introduced in VLPs (Fiedler et al., 2012b). Many computational tools including homology modelling, bioinformatics, and MD simulation are used to predict and explore VLP and epitope structure and assembly dynamics (Lua et al., 2014).

1.1.6 Protein nanoparticles for vaccine technologies

Although VLPs may be the most popular and extensively explored immunogenic antigen carriers, there are a number of other particles that have been used as antigen multimerization scaffolds (Rehm, 2017). These nanoparticles are typically composed of either lipids, proteins, polymers, or inorganic materials (Rehm, 2017). However, nanoparticles that form from self-assembling proteins are of particular interest since they most closely mimic VLPs (Karch and Burkhard, 2016). Furthermore, VLPs and similar protein nanocages, are less toxic than metal nanoparticles, often exhibit better stability compared to liposomes, and are more uniform than non-biological polymers (Schrand et al., 2010; Zylberberg and Matosevic, 2016; Malyala and O'Hagan, 2017; Irvine et al., 2015).

A number of protein-based nanoparticles are shown in Figure 1.3. Coiled-coils are oligomerization domains that are composed of a minimum of 2 helical proteins (Fletcher et al., 2012). The use of coiled-coils as vaccines has been reported (Ogun et al., 2008; Harakuni et al., 2016; Li et al., 2016). By using isopeptide bond-forming technology it was

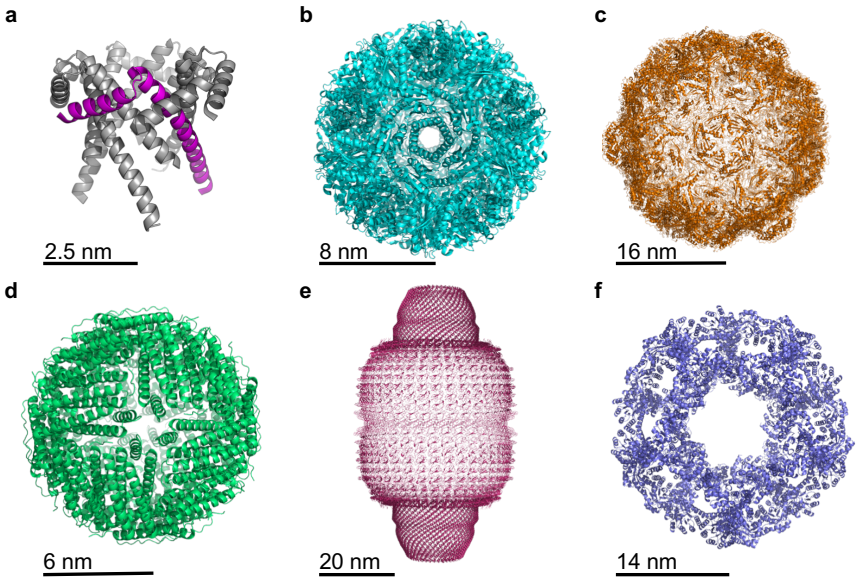


Figure 1.3. Alternate protein-based nanoparticles for vaccine platform technologies. Examples of self-assembling proteins that can be functionalized to display antigens. **(a)** Heptameric coiled-coil IMX313 (PDB:2YF2). One monomer shown in purple. **(b)** Lumazine synthase from *Bacillus anthracis* (PDB:1HQK). **(c)** *Myxococcus xanthus* encpasulin protein (PDB:4PT2). **(d)** *Helicobacter pylori* ferritin (PDB:3BVE). **(e)** Rat liver vault protein cage (PDB:4V60). **(f)** Computationally designed synthetic nanoparticle I3-01 (PDB file downloaded from `https://www.nature.com/articles/nature18010supplementary-information`).

possible to fuse two different antigens on either end of the coiled-coil IMX313 scaffold (Brune et al., 2017). The incorporation of multiple antigens onto one particle is an interesting area of investigation (Menon et al., 2018).

An example of a naturally-assembling protein cage is lumazine synthase (LS), an enzyme found in plants, bacteria, and fungi (Rehm, 2017). LS has been shown to be efficiently taken up by APCs and can be conjugated to display foreign epitopes (Ra et al., 2014). Recently, circular permutation of lumazine synthase yielded variants that could assemble into different-sized spherical and tubular protein cages (Azuma et al., 2018).

Two other naturally occurring protein cages that resemble VLPs include ferritin and encapsulins. Ferritins store iron within a protein cage that assembles from 24 monomers (He and Marles-Wright, 2015). Ferritin nanocages have been used in a wide number of applications including as vaccines (He and Marles-Wright, 2015; Rehm, 2017; Karch and

Burkhard, 2016; López-Sagaseta et al., 2016). Encapsulins are bacterial proteins that have also been engineered successfully to display foreign epitopes. In one study, encapsulins presenting the gp350 antigen from the Epstein-Barr Virus elicited stronger antibody titers than soluble antigen alone (Kanekiyo et al., 2015).

Vault proteins occur in eukaryotes and differ in structural organization to the hitherto described nanoparticles (Figure 1.3e). They can be produced in high yield and have been explored in a variety of therapeutic applications (Rome and Kickhoefer, 2013). However, they can only be functionalized to display antigens within the vault cavity, reducing their ability to stimulate humoral responses (Champion et al., 2009).

Recently, researchers have also explored the ability to create synthetic VLP-like nanoparticles using symmetry modelling and computational analysis. Techniques developed and refined by the David Baker group have allowed for the accurate design of a number of cages with varying valencies, architectures, sizes, and assembly properties (King et al., 2012; Bale et al., 2015; King et al., 2014; Bale et al., 2016; Hsia et al., 2016). One example of a designed synthetic nanocage is shown in Figure 1.3f. This protein, named I3-01, is a dodecahedron assembled from 60 trimeric subunits. To date, there has been no published report of the use of these cages as vaccine platforms. However, their shape and size make them likely targets for diverse biotechnological applications.

1.2 Spontaneous isopeptide bond-forming technology

1.2.1 Introduction and development

Isopeptide bonds are amide bonds that form between side-chains of amino acids (Zakeri and Howarth, 2010). Naturally occuring isopeptide bonds include those catalyzed by transglutaminases and ubiquitin ligase (Lorand and Graham, 2003; Pickart, 2001) and autocatalytic intermolecular isopeptide bonds formed in HK97 phage (Wikoff et al., 2000). The first intramolecular isopeptide bond was discovered in the major pilin protein Spy0128 of a

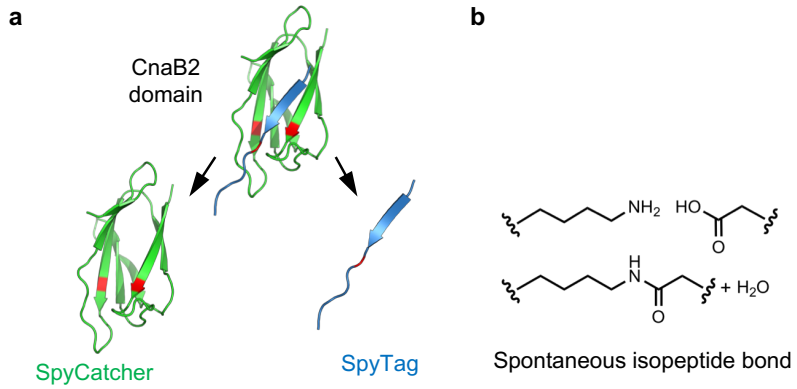


Figure 1.4. Splitting of the CnaB2 domain yielded two reactive partners capable of forming an irreversible covalent bond. (a) Cartoon of the CnaB2 split (PDB:4MLS). SpyCatcher (green) and SpyTag (blue) are shown, with the catalytic triad highlighted in red. SpyCatcher contains the catalytic Glu and reactive Lys. SpyTag contains the reactive Asp residue. **(b)** Molecular illustration of the amidation reaction occurring between SpyCatcher and SpyTag, resulting in the loss of a molecule of water.

Gram-positive bacterium *Streptococcus pyogenes* (Kang et al., 2007). Intramolecular isopeptide bonds can improve thermostability and can confer increased resistance to proteolysis (Alegre-Cebollada et al., 2010; Kang and Baker, 2009). A triad of residues is necessary for a spontaneous isopeptide bond to form (Veggiani et al., 2014). The reaction is catalyzed by a glutamic or aspartic acid that is positioned opposite an asparagine or aspartic acid. Nucleophilic attack by lysine on asparagine forms an amide bond with loss of NH_3 while attack on aspartic acid results in the loss of H_2O.

By splitting the isopeptide bond-containing domain of Spy0128, two fragments were created that could covalently associate upon mixing (Zakeri and Howarth, 2010). Although the two parts, pilin-C and isopeptag, reacted slowly, the experiment demonstrated the feasibility and potential of split isopeptide bonds as a bioconjugation strategy.

Since Spy0128, other covalent bioconjugation systems have been developed. The SpyTag-SpyCatcher system was created by splitting the CnaB2 domain of the fibronectin binding protein FbaB from *Streptococcus pyogenes* (Figure 1.4) (Zakeri et al., 2012). The split created a 13-residue Tag and a 113 residue binding partner ($\sim$ 15 kDa), which react quickly under a wide range of conditions (reaction half time is just over 1 min). SpyTag-SpyCatcher

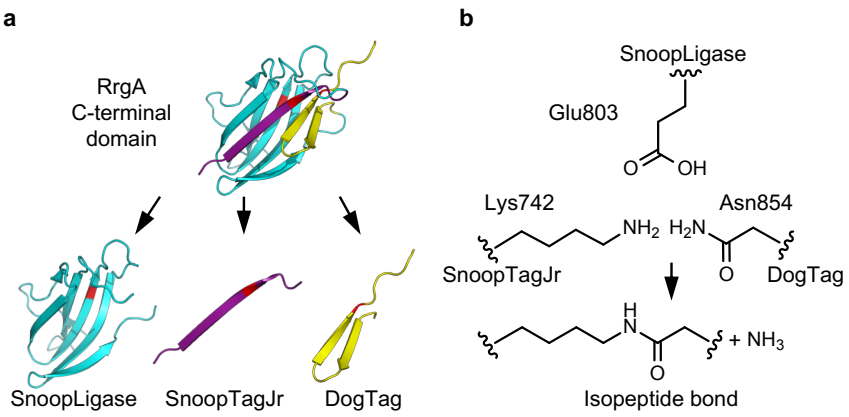


Figure 1.5. Splitting of the RrgA domain in three parts yielded a system capable of ligating two peptide tags. (a) Cartoon of the RrgA split (PDB:2WW8). SnoopLigase (cyan), SnoopTagJr (purple), and DogTag (yellow), with the catalytic residues highlighted in red, are shown. **(b)** Molecular illustration of the transamidation reaction between SnoopTagJr (Lys 742) and DogTag (Asn854), catalyzed by SnoopLigase (Glu 803).

technology has been used in a wide range of applications including enzyme stabilization (Schoene et al., 2014), nanoparticle functionalization (Brune et al., 2016), the study of membrane dynamics (Keeble et al., 2017), and cancer cell death signal activation (Veggiani et al., 2016).

An orthogonal Catcher-Tag pair, SnoopCatcher and SnoopTag, was created by splitting the C-terminal domain of RrgA from *Streptococcus pneumoniae* (Veggiani et al., 2016). The system was tolerant to a wide range of conditions although it reacted slightly slower than SpyCatcher-SpyTag (the reaction half time for SnoopCatcher is 2.5 min). SnoopCatcher/SnoopTag has enabled the creation of a modular vaccine platform that can immunize against two antigens at the same time (Brune et al., 2017).

However, in both systems, a limiting factor is the size of the Catcher, which when fused to a protein can affect expression and proper folding. To address this problem a three-part split of the CnaB2 domain created a SpyLigase (11 kDa protein), that was able to catalyze a covalent bond between a 13 aa SpyTag (containing the reactive Asp), and 11 aa KTag (containing the reactive Lys) (Fierer et al., 2014). However, the system rarely had yields above 50 %. An improved ligase was created by splitting the RrgA domain into three parts

to yield SnoopLigase, SnoopTagJr, and DogTag (Figure 1.5) (Buldun et al., 2018). This system showed conjugation up to 95 % under mild conditions, and has hitherto been used to confer exception thermoresilience to two enzymes through cyclization (Buldun et al., 2018).

1.2.2 Preceding work on VLPs and SpyCatcher/SpyTag

Spontaneous isopeptide bond-forming technology has been exploited to create modular "plug-and-display" vaccine platforms (Figure 1.6). SpyCatcher has been fused to the N-terminus of the coat protein from bacteriophage AP205 to create VLPs that could be quantitively coupled with SpyTag-antigens (Brune et al., 2016; Thrane et al., 2016). In a reverse approach, SpyTag has also been fused to both the N- and C-terminus of AP205 to allow conjugation with SpyCatcher-tagged antigens (Thrane et al., 2016). Conjugation at both termini increases the theoretical maximum conjugation number from 180 to 360 antigens. However, conjugation efficiency can decreases with increased steric hindrance.

Conjugated SpyCatcher-VLPs were able to induce robust, functional antibody responses after a single immunization (Brune et al., 2016). The controlled orientation and precise coupling of the Catcher/Tag platform has also been shown to be have an advantage in the quality of antibody response. In a direct comparison between three vaccine platforms (Qβ, IMX313, and AP205), SpyCatcher-AP205 VLPs conjugated to a malarial antigen induced the best quality of antibodies (Leneghan et al., 2017). The Spy-AP205 platform has also been used for immunizations against cancer (Thrane et al., 2016; Palladini et al., 2017), and against allergy-associated cytokines (Thrane et al., 2016). Thus, the platform can tolerate antigens produced in different expression hosts, of varying size, and against a variety of immunological targets.

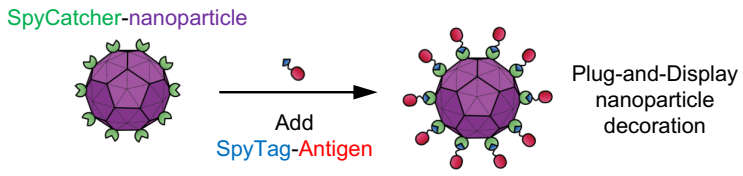


Figure 1.6. Plug-and-display assembly for modular vaccines. Genetic fusion of SpyCatcher onto a coat protein affords a nanoparticle moiety that is easily functionalized by mixing with any SpyTag-antigen.

1.3 Thesis Objectives

The underlying goal of this thesis was to create a scalable vaccine platform that exploits SpyCatcher-SpyTag reactivity. Preceding work in the Howarth laboratory had developed a SpyCatcher-VLP based on the AP205 bacteriophage. The platform achieved quantitative coupling and was successful at stimulating antibody responses against complex malarial antigens. However, the platform had serious limitations including aggregation, instability, and poor yield.

Thus, the first goal was to establish a methodology for the directed evolution of SpyCatcher-VLPs, and to evolve the AP205 coat protein for solubility and high-yield production in *E. coli*. The second goal of this thesis was the development and characterization of a new SpyCatcher vaccine platform based on the robust, computationally designed nanocage I3-01. Finally, I prepared immunological grade formulations of the new platform, to evaluate the immunological properties of a computationally designed nanoparticle-based vaccine.

Chapter 2

Materials and Methods

2.1 Cloning

2.1.1 Polymerase Chain Reaction (PCR)

DNA oligonucleotides for DNA amplification were designed in SnapGene (`http://www.snapgene.com/`), checked for hairpins using the OligoAnalyzer tool from Integrated DNA Technologies (IDT) (`https://eu.idtdna.com/calc/analyzer`), and ordered from IDT. Desiccated oligonucleotides were reconstituted to a concentration of 100 µM in Buffer EB (10 mM Tris-HCl, pH 8.5). Working stocks of 10 µM were created and stored at -20 °C. Polymerase chain reactions (PCR) were done with 0.2 ng DNA (0.5 µL of 10 ng/µL stock), 0.5 µM of each forward and reverse primer (1.25 µL of a 10 µM stock), 9.5 µL Milli-Q (MQ) water, and 12.5 µL of 2× Q5 high fidelity master mix (New England Biolabs) to a final volume of 25 µL. Thermocycling was done in a C1000 Thermal Cycler (Bio-Rad). Standard conditions were: initial denaturation for 30 s at 95 °C, 30 cycles of denaturation at 95 °C for 20 s, annealing at 60 °C for 15 s, extension at 72 °C (40 s/kb extension time), and final extension at 72 °C for 2 min.

2.1.2 Agarose gel electrophoresis

PCR reaction volumes of 25 µL were mixed with 5 µL of 6× loading dye [0.15 % (w/v) Ficoll-400, orange G dye, MQ-water] and loaded onto an agarose gel [0.5, 1, or 2 % (w/v) depending on DNA fragment size] containing 0.01 % SybrSafe (Thermo Fisher Scientific). Agarose gels were run at 130 V in TAE buffer (40 mM Tris base, 20 mM acetic acid, 1 mM EDTA, pH 8.0) for ~ 45 min and imaged on an XcitaBlue Conversion Screen using a Gel Imager Universal Hood II (Bio-Rad). Images were analyzed with Image Lab Version 5.2.1 (Bio-Rad).

2.1.3 PCR product purification

PCR products were excised from an agarose gel and purified using PCR Clean-Up Kit (Promega). Purified DNA concentration was determined using an ND-1000 Nanodrop.

2.1.4 Gibson assembly

Gibson assembly was performed as previously described (Gibson et al., 2009) with modifications to two of the enzymes. A Phusion-like DNA polymerase was cloned and purified by Dr.Karl Brune in the Howarth lab based on a patent (Wang et al., 2011). A *Taq* DNA ligase was also cloned and purified by Dr.Karl Brune. Gibson Assembly Master Mix (2×) was stored in 10 µL aliquots at -20 °C until use. Purified PCR fragments were mixed on ice in either equimolar ratio or a molar ratio of 3:1 for insert:vector, in a total reaction volume of 10 µL. This mixture was then added to 10 µL of Gibson Assembly Master Mix (the mixture containing the enzymes), mixed thoroughly by pipetting, and then incubated in a pre-heated C1000 cycler set to 50 °C for 30 min up to 16 h.

2.1.5 Transformation of *E. coli*

A 50 µL or 100 µL aliquot of chemically competent or electro-competent cells was thawed on ice for 10 min, before addition of either 1 µL of supercoiled plasmid or 8 µL of Gibson assembly product. The aliquot was kept on ice for 10 min before heat shock for 45 s in a 42 °C water bath. Aliquots were immediately incubated on ice for 2 min, then recovered in SOC media (300 µL). For plasmid purification, NEB Turbo or XL1-Blue cells were used. BL21 (DE3) RIPL (Agilent) or C41 cells (a kind gift from Anthony Watts, University of Oxford) were used for protein expression.

Table 2.1. Genotypes of *E. coli* host strains.

Strain	Genotype
NEB Turbo	glnV44 thi-1 Δ(lac-proAB) galE15 galK16 R(zgb-210::Tn10)Tet^S endA1 Δ(mcrB-hsdSM)5, (r_K^- m_K^-) F' [traD36 $proAB^+$ $lacI^q$ lacZΔM15lfhuA2]
XL1-Blue	endA1 gyrA96(naI^R)thi-1 recA1 relA1 lac glnV44 F'[::Tn10 $proAB^+$ $lacI^q$ lacZΔM15] hsdR17(r_K^- m_K^+)
C41(DE3)	F^- ompT gal dcm $hsdS_B$(r_B^- m_B^-)(DE3)
BL21 (DE3) RIPL	B F^- ompT hsdS(r_B^- m_B^-) dcm^+ Tet^r gal λ(DE3) endA Hte [argU proL Cam^r] [argU ileY leuW $Strep/Spec^r$]

2.1.6 Plasmid purification

Plasmid purification was done using the GeneJET Plasmid Miniprep Kit (Thermo Fisher Scientific) or the QIAprep Spin Miniprep Kit (Qiagen). Double the amount of recommended buffer volumes were used on pellets obtained from a 5 mL or 10 mL *E. coli* overnight culture of NEB Turbo or XL1-Blue cells.

2.1.7 DNA sequencing

All constructs were verified by Sanger sequencing performed by Eurofins Genomics (Ebersberg, Germany). Either standard primers from Eurofins were used (T7 and T7 term) or custom sequencing primers were designed.

2.2 Standard protein expression and purification

2.2.1 Media and *E. coli* growth parameters

All media were purchased from the Media Glassware Sterilization Laboratory at the University of Oxford Department of Biochemistry. LB-Miller (high salt): 10 g tryptone, 5 g yeast extract, 10 g of NaCl in 1 L of MQ water. 2× TY: 16 g tryptone, 10 g yeast extract, 5 g NaCl in 1 L of MQ water with pH adjusted to 7.0. Media were sterilized by autoclaving for 20 min at 121 °C. Bacterial cultures were grown in an Infors Multitron shaker (Infors UK Ltd) with a 2.5 cm throw at 200 rpm. Specific temperatures used varied depending on the protein and are described in subsequent sections.

2.2.2 Protein expression

Proteins were expressed in *E. coli* BL21 (DE3) RIPL (Agilent). Single colonies from overnight growth on antibiotic resistant LB-agar plates were picked into 10 mL of LB-Miller, or 2× TY media, containing either 0.5 mg/mL kanamycin or 0.1 mg/mL ampicillin depending on the expression plasmid's resistance gene. The culture was grown overnight and then added to 1 L of the same media containing the same antibiotic with 0.8 % (w/v) glucose. Inoculated cultures were incubated at 37 °C with shaking at 200 RPM. At OD_{600} 0.5 cultures were induced with 0.42 mM IPTG and grown at 30 °C for 4-6 h. Cultures were then centrifuged for 15 min at 5,000×g at 4 °C, washed in PBS, and frozen at -80 °C.

2.2.3 Ni-NTA purification of His_6-Tagged Proteins

1 L *E. coli* culture derived pellets were resuspended in 10 mL cold Ni-NTA binding buffer (50 mM Tris base, 300 mM NaCl, pH 7.8) with the addition of 1 mM phenylmethane sulfonyl fluoride (PMSF) (Sigma) and 1 mg/mL EDTA-free mixed protease inhibitors (PI) (Roche). Pellets were thawed for $\sim$ 1 h in a water bath at room temperature (RT). Samples were then sonicated on ice three times (1 min on, 1 min off), using a Sonics Vibra-Cell sonicator

(Ultrasonic Processor). Total lysate was aliquoted into 2 mL volumes and centrifuged for 30 min at 16,900×g at 4 °C. The cleared lysate was then added to 1 mL packed Ni-NTA resin (Qiagen) per 1 L of bacterial culture. Lysate was incubated with resin for $\sim$ 1 h at 4 °C on a rolling shaker. Following incubation, the resin was applied to a polyprep column (Bio-Rad) by gravity filtration at 4 °C. Resin was washed five times with 10× resin volume of 10 mM imidazole in Ni-NTA binding buffer followed by one wash with 2× resin volume of 30 mM imidazole in Ni-NTA binding buffer. The column was then capped, and resin incubated for 10 min in one resin volume of Ni-NTA buffer containing 200 mM imidazole. Elutions were repeated until all protein was eluted (monitoring of fractions was done using a Nanodrop). Elutions were pooled and dialyzed three times against an appropriate buffer in 1000-fold excess at 4 °C with stirring.

2.3 SDS-PAGE

SDS-PAGE (sodium dodecyl sulfate polyacrylamide gel electrophoresis) was performed with 12-18 % Tris-glycine gels using an XCell SureLock system (Life Technologies). Protein samples were loaded with 6x SDS-PAGE loading buffer (20 % glycerol, 100 mM Tris-HCl, 4 % SDS, 0.2 % bromophenol blue, with or without 100 mM 2-mercaptoethanol). Samples were boiled for 3 min at 99 °C using a C1000 thermal cycler (Bio-Rad) before loading on a gel. SDS-PAGE was performed at 200 V in 25 mM Tris-HCl, 192 mM glycine, 0.1 % (w/v) SDS for 1 h 10 min. All gels were loaded with PageRuler Prestained Protein Ladder (Thermo Fisher Scientific) as a molecular weight marker. Gels were stained with InstantBlue Coomassie stain (Expedeon), destained using Milli-Q water, and imaged using ChemiDoc XRS imager and ImageLab (version 5.2) software (BioRad). ImageLab was also used for band quantification (densitometry).

2.4 Protein concentration quantification

Protein concentration was determined by one of two ways: either by measuring A_{280} using an ND-1000 Nanodrop and dividing the value by the ExPASy ProtParam (`https://web.expasy.org/protparam/`) generated extinction coefficient, or by using the bicinchoninic acid (BCA) assay according to the manufacturer's protocol (Thermo Fisher Scientific). BCA assay was only used for VLPs, nanoparticles, or for vaccine formulations.

2.5 Protein biotinylation

Proteins containing an AP site (also known as an AviTag) (GLNDIFEAQKIEWHE) were site-specifically biotinylated by BirA (*E. coli* biotin ligase) as described previously (Fairhead and Howarth, 2015). AP-protein at 100 µL was incubated with 5 mM $MgCl_2$, 1 mM ATP, 1.5 mM biotin in 100 % DMSO, and 6.7 µM GST-BirA (glutathione-S-transferase fused BirA) in PBS, for 1 h at 25 °C. Then, the same amount of GST-BirA was added to the reaction and mixed well before incubation for another 1 h. To remove GST-BirA, the reaction was incubated with 100 - 200 µL of glutathione-HiCap resin (Qiagen) for 1 h at 4 °C on a rotator. The sample was then centrifuged for 30 min at 16,900×g at 4 °C and the supernatant removed. Supernatant was then dialyzed three times into appropriate buffer in 1000-fold excess using a 3.5 kDa MWCO cellulose membrane (Spectrum Labs).

2.6 TEV protease purification

The MBP-TEV protease plasmid was obtained from Dr.Anthony Keeble of the Howarth lab. The protein was expressed and purified in standard conditions with two modifications. During purification no PI or PMSF was added to the lysate and post Ni-NTA elution the protein was dialyzed against the activity buffer (50 mM Tris-HCl, 0.5 mM EDTA, pH 8.0).

2.7 TEV protease cleavage

Cleavage reactions were performed in the activity buffer (50 mM Tris-HCl, 0.5 mM EDTA, pH 8) at 34 °C for 2 h in a benchtop thermocycler with shaking at 800 RPM. To cleave, MBP-TEV protease was added to either a final concentration of 0.7 mg/mL, or an optimal amount was determined through a titration curve for specific proteins and conditions.

2.8 SpyCatcher-AP205 VLPs

2.8.1 SpyCatcher-AP205 expression

E. coli C41(DE3) cells were transformed with pGEM-SpyCatcher-AP205 (GenBank accession number KU302810) and grown for 16 h at 37 °C, on an LB-agar plate containing 100 µg/mL ampicillin. 10 single colonies were picked into 1 L of 2× TY media containing 20 µg/mL of ampicillin, and cultures were incubated overnight at 37 °C with slow shaking (30 - 60 RPM). The next day, 1 L of fresh 2× TY was diluted 1:1 with the overnight culture, and ampicillin was added to 20 µg/mL, assuming all ampicillin degraded overnight. The culture was incubated at 37 °C with shaking at 100 RPM until A_{600} 0.5. The culture was then cooled to 22 °C for 30 min prior to induction. Cultures were induced with 0.42 mM IPTG and a few drops of antifoam A (Sigma) were added. Protein was expressed at 200 RPM at 22 °C for 16-20 h.

2.8.2 Purification

2.8.2.1 Immobilized metal affinity chromatography (IMAC)

A 1 L culture-derived pellet was resuspended at RT for 1 h in 10 mL lysis buffer [20 mM Tris-HCl, 150 mM NaCl, 75 mM imidazole, 0.2 mg/mL lysozyme, 1 mM PMSF, 25 U/mL benzonase, 0.1 % (v/v) Tween-20, pH 7.8 at 4 °C]. The lysate was sonicated 4 times (30 s on, 1 min off). The lysate was spun twice at 16,900×g for 30-45 min at 4 °C. The supernatant

was then filtered through a 1.2 µm glass filter device (Sartorius) and then through a 0.45 µm surfactant-free cellulose acetate filter device (Nalgene). The filtrate was incubated with 250 U benzonase (Sigma) for 5 min at RT. 1 mL of packed Ni-NTA agarose (Qiagen), equilibrated to 75 mM imidazole, was added to the cleared lysate and incubated on a rotary shaker for 30 min at 4 °C. The resin was then added to a polyprep column by gravity filtration and washed 5× with 10 column volumes of wash buffer [50 mM Tris-HCl, 150 mM NaCl, 100 mM imidazole, 0.1 % (v/v) Tween-20, pH 7.8 at 4 °C]. To elute, the polyprep column was capped, 1 mL of elution buffer added (2 M imidazole, 50 mM glycine, 25 mM sodium citrate, 0.1 % (v/v) Tween-20, pH 8.5 at 4 °C), the resin incubated for 5 min, and the process repeated four times. Eluate was spun down for 30 min at 16,900×g at 4 °C before transfer to a 300 kDa MWCO cellulose ester dialysis tubing (SpectrumLabs). Protein was dialyzed overnight at 4 °C, against a 1,000-fold excess of 50 mM glycine, 25 mM sodium citrate, 0.1 % (v/v) Tween-20, pH 8.0. Dialysis was repeated an additional 2 times for 3 h with fresh buffer. After dialysis, the sample was spun once more at 16,900×g at 4 °C for 30 min, to remove aggregates.

2.8.2.2 Ultra-centrifugation

The protocol for ultra-centrifugation was adapted from a number of sources (Buck and Thompson, 2007; Buck et al., 2004; Thrane et al., 2016). Gradient was prepared from Optiprep Density Gradient Medium (Merck). A 46 % working solution of Optiprep was made by dilution with a diluent buffer (PBS and 0.8 M NaCl). Subsequently three gradient layers of 23 %, 29 %, and 35 % Optiprep were made by diluting the working solution with diluent buffer. 8 mL of each gradient layer was then under-layered into 38.5 mL thin-wall, polypropylene tubes (Beckman Coulter) using a 10 mL syringe and a 21G needle. Layers were allowed to settle for 1 - 2 h. 14.5 mL of cleared lysate or diluted purified virus-like particle, was added carefully onto the gradient. Tubes were balanced to ± 5 mg. Tubes were centrifuged at 140,000×g for 16 h at 4 °C, in an SW28 rotor (Beckman Coulter). Then,

tubes were punctured at the bottom with a 23G needle and 1 mL fractions were collected for analysis.

2.9 Directed evolution

2.9.1 Error-prone PCR using Mutazyme

The library of VLP variants was assembled from two PCR-amplified fragments by Gibson assembly. The vector backbone was amplified from the pGEM-SpyCatcher-AP205cp3 plasmid with standard PCR conditions (section 2.1.1). The insert (CP3) was mutagenized using GeneMorph II Random Mutagenesis Kit (Agilent), according to the manufacturer's protocol. PCR reactions were then purified and assembled as described in section 2.1.3 and section 2.1.4. Colonies from each condition were mini-prepped and sequenced as described in section 2.1.6 and section 2.1.7 to obtain an empirical mutation rate.

2.9.2 Electro-competent cells

Electro-competent cells were made fresh for each round of the evolution. To make electro-competent cells, a glycerol stock of BL21 (DE3) RIPL cells was picked into 10 mL of 2× TY containing 0.5 mg/mL chloramphenicol. After overnight growth, the culture was added to 500 mL of 2× TY media and grown at 37 °C with shaking at 210 rpm until A_{600} 0.5. The culture was immediately put in an ice-water bath and swirled continuously by hand for 10 min. The culture was then poured into 50 mL falcon tubes and spun at 2,000×g for 8 min. The tubes were decanted quickly and 20 mL of ice-cold 10 % glycerol was poured into each tube. The cells were resuspended gently and combined into 50 mL falcon tubes. The cells were centrifuged again at 2,000×g for 8 min and supernatant decanted. Each tube was resuspended in 20 mL ice-cold 10 % glycerol and combined into 40 mL volumes before a final spin for 8 min at 2,000××g. The liquid was decanted and the cells resuspended in a minimal amount of residual supernatant. The efficiency of the cells is proportional to the

cell concentration. If necessary, a small amount of 10 % glycerol was added to resuspend the cells. The concentrated cell mixture was aliquoted into pre-chilled 0.1 cm electroporation cuvettes (Thermo Fisher) in a volume of 50 µL for electroporation.

2.9.3 Library transformation

Assembled DNA, prepared as described in section 2.9.1, was purified using a MiniElute DNA purification kit (Qiagen). 1 µL of purified DNA was electroporated into 50 µL of electro-competent cells prepared as in 2.9.2. Following electroporation, 1 mL of warmed SOC media was immediately added to the cuvettes and the cells were recovered at 37 °for 1 h with shaking at 200 rpm. Transformants were plated on extra large ($\sim$ 16 cm diameter) LB agar plates containing 100 µL/mL carbenicillin. Plates were incubated at 37 °C overnight to give confluent bacterial growth. To harvest the library, 5 mL of LB media was added to each plate, and plates were scraped with a plastic spreader. Cells were pelleted at 500 $\times g$ for 8 min. Then, cells were resuspended in 5 mL 2× TY media and either stored as a 20 % glycerol stock or added directly to 1 L of 2× TY media for protein expression.

2.9.4 Variant capture using protein bait and magnetic beads

Purified SpyCatcher-VLPs were incubated with 1 µL of benzonase ($\sim$ 250 U/µL) (Sigma) at 25 °C for 1 h. Eppendorf tubes (1.5 mL) were blocked with blocking buffer [50 mM glycine, 25 mM sodium citrate, 1.0 % (v/v) Tween-20, 10 % (w/v) bovine serum albumin (BSA), pH 8.0] for a minimum of 1 h. HaloTag magnetic beads (Promega) were blocked with blocking buffer for 30 min at 25 °C while shaking at 1000 rpm. In a blocked and rinsed Eppendorf tube, benzonase-treated VLPs were diluted to 5 µM in a total volume of 1 mL. The VLPs were pre-cleared by incubation with 40 µL of blocked beads for 10 min with shaking at 1000 rpm, before beads were captured using a magnetic rack and supernatant was aspirated. The VLPs in solution were reacted with 2.5 µM SpyTag protein partner for 1 h at 25 °C. 40 µL of blocked beads were then added to the sample and allowed to react for 10 min at 25 °C,

while shaking at 1000 rpm. Beads were captured using a magnetic rack and washed once with 150 µL of buffer and then three times with 150 µL of citrate phosphate buffer pH 4.0 (25 mM citric acid, 25 mM sodium phosphate). Each wash step included an incubation for 2 min with shaking at 1000 rpm. The beads were then resuspended in 140 µL of TEV protease activity buffer (0.5 mM EDTA, 50 mM Tris, pH 8.0). MBP-TEV protease (0.7 mg/mL) was added to the solution and incubated for 2 h at 34 °C with shaking at 800 rpm.

2.9.5 RNA extraction and purification

RNA extraction was done in a fume hood to minimize contamination. All surfaces, gloves, and pipettes were wiped down with 70 % ethanol before the procedure. Gloves were changed often during RNA extraction. RNA extraction from SpyCatcher-AP205 VLPs was done using either the PureLink Viral RNA/DNA Mini Kit (Thermo Fisher Scientific) or the QIAamp Viral RNA Mini Kit (Qiagen).

2.9.6 Reverse-transcription PCR (RT-PCR)

Reverse-transcription PCR was performed using the OneStep RT-PCR Kit (Qiagen) according to the manufacturer's protocol. Between 1 pg - 2 µg/reaction of RNA was added to each reaction. Concentration of RNA was determined using an ND-1000 Nanodrop (Nanodrop) and measuring absorbance at A_{260}.

2.9.7 Quantitative PCR (qPCR)

Quantitative-PCR was performed in a Rotagene-Q Machine (Qiagen). General reaction set up was: 7.5 µL of SensiMix No-ROX kit (2×) (Bioline), 0.375 µL of each forward and reverse primer (10 µM), 5 µL template DNA (concentration ranged between 0.001-0.1 ng/µL), 1.75 µL MQ water. The cycling program was: initial denaturation at 95 °C for 10 min, 45 repeats of denaturation at 95 °C for 10 s, annealing at 60 °C for 15 s, and extension at 72 °C for 20

s.

2.10 SpyCatcher-MI3 nanoparticles

2.10.1 Expression

Transformed BL21 (DE3)-RIPL cells were grown for 16 h at 37 °C on LB-Agar plates containing 50 µg/mL kanamycin. A single colony was picked into a 10 mL starter culture of LB medium containing 50 µg/mL kanamycin. The culture was incubated for 16 h at 37 °C with shaking at 200 rpm. The entire 10 mL culture was then diluted into 1 L LB containing 50 µg/mL kanamycin and incubated at 37 °C with shaking at 200 rpm. At A_{600} 0.8, cultures were induced with 0.5 mM IPTG and grown for 16-20 h with shaking at 200 rpm at 22 °C.

2.10.2 Purification by C-tag resin

One 500 mL culture-derived pellet was resuspended in 10 mL lysis buffer (25 mM Tris base, 150 mM NaCl, 0.1 mg/mL lysozyme, 1 mg/mL protease inhibitors (PI), 1 mM PMSF, pH 8.5 at 4 °C) for 1 h at RT. The lysate was then sonicated (10 s on, 10 s off) for 5 min before centrifuging at 16,900 $\times g$ for 30 min at 4 °C. Capture Select C-Tag Affinity Matrix (Thermo Fisher Scientific) (7.5 mL) was added to cleared lysate and incubated on a rotary shaker at 4 °C for 1 h. The mixture was then added to a polyprep column by gravity filtration and washed with 10 column volumes of 25 mM Tris base, 150 mM NaCl, pH 8.5 at 4 °C. Elution buffer (20 mM Tris base, 2 M $MgCl_2$, pH 7.4) was added to the column and incubated for 5 min before each elution. Protein in elution was monitored by A_{280}. Total eluate was then diluted with a 10× stock of 250 mM Tris, 1.5 M NaCl, pH 8.5, before concentrating in a 20 mL 100 kDa MWCO Vivaspin ultrafiltration unit (Sartorius).

2.10.3 Purification by Ni-NTA resin

A 1 mL culture-derived pellet was thawed in 20 mL lysis buffer (25 mM Tris-HCl, 150 mM NaCl, 0.1 mg/mL lysozyme, 1 mg/mL PI, 1 mM PMSF, pH 8.5 at 4 °C), at RT for 1 h. The lysate was then sonicated (10 s on, 10 s off) for 5 min before spinning at 16,900 $\times g$ for 30 min at 4 °C. The cleared lysate was divided into two 15 mL falcon tubes and 2 mL packed Ni-NTA resin was added to each tube. Lysate and resin were incubated for 1 h at 4 °C on a rolling shaker. Tubes were then spun at 4000 $\times g$ for 1 min before supernatant was removed. Resin was washed five times with 10 mL wash buffer (25 mM Tris-HCl, 150 mM NaCl, 15 mM imidazole, pH 8.5 at 4 °C). After each wash, the tubes were spun at 4000 $\times g$ for 1 min and the supernatant was removed. Resin was then incubated in 2 mL elution buffer (25 mM Tris-HCl, 150 mM NaCl, 200 mM imidazole, pH 8.5 at 4 °C) for 10 min before centrifugation. Ten elution steps were performed.

2.10.4 Purification by gel filtration

Protein was centrifuged at 16,900 $\times g$ for 30 min to remove aggregates before applying to a previously equilibrated HiPrep 16/60 Sephacryl S-500 HR (GE Healthcare) or a HiPrep 16/60 Sephacryl S-400 HR on a fast protein liquid chromatography (FPLC) system Purifier 10 (GE Healthcare). The mobile-phase column buffer was 25 mM Tris base, 150 mM NaCl, pH 8.5 and the applied flow-rate was 1.0 mL/min, all at 4 °C. Protein elution was monitored by A_{280}. For the S-500 column, elutions in the 65-90 mL range were collected. On the S-400 column, elutions in the 45-65 mL range were collected and concentrated.

2.11 Protein characterization and *In Vitro* assays

2.11.1 Dynamic light scattering

Protein samples were centrifuged for 30 min at 16,900 $\times g$ at 4°C to remove aggregates. 20 µL of protein was loaded into a reusable cuvette. Each protein sample was measured at three dilutions at 20 °C using an Omnisizer (Viscotek) with 10 scans of 10 s each. The intensity distribution from the scans was plotted and the mean and standard deviation calculated in Excel.

2.11.2 Transmission electron microscopy (TEM)

SpyCatcher-MI3 VLPs (0.2 mg/mL) were applied to freshly glow-discharged carbon 200 mesh copper grids for 2 min, blotted with filter paper, and stained with 2 % uranyl acetate (w/v) for 10 s, then blotted and air dried. Grids were imaged in a FEI Tecnai T12 transmission electron microscope at 120 kV using a Gatan US1000 CCD camera. Using FIJI (ImageJ) particle diameter was measured. Measurements were plotted with 2 nm bin size and the mean and standard deviation were calculated in Excel.

2.11.3 Nanoparticle reactivity

A 1.5× molar excess of SpyTag-linked partner was used in reactions with SpyCatcher-AP205. A 3× molar excess of SpyTag-linked partner was used in reactions with SpyCatcher-MI3. Reactions were performed in either PBS for SpyCatcher-AP205, or 25 mM Tris base, 150 mM NaCl, pH 8.5, for SpyCatcher-MI3. Reactions were stopped by addition of 6× SDS-PAGE loading buffer and boiling for 3 min at 95 °C. SDS-PAGE analysis was performed as previously described in section 2.3. To assess the percentage of particles that had reacted with antigen, a sample of unreacted particles at the same starting concentration was run on the gel and defined as 100 % unreacted. % conjugation was defined as 100×[1-(particle band after antigen incubation)/(particle band in the absence of antigen)].

2.11.4 SpyCatcher-MI3 thermal resilience analysis

SpyCatcher-MI3 particles at 30 µM were incubated at a given temperature for 1 h. A typical experiment consisted of incubation at 25 °C, 37 °C, 55 °C, 75 °C, and 95 °C. Samples were then centrifuged for 30 min at 16,900 $\times g$ at 4 °C and supernatant removed for analysis via DLS and SDS-PAGE with Coomassie staining. For quantification by densitometry, assays were performed in triplicate. The sample held at 25 °C was defined as 100 % soluble.

2.11.5 SpyCatcher-MI3 freeze-thaw stability

100 µL of 20 µM SpyCatcher-MI3 particles were frozen in the -80 °C freezer for 20 min and thawed in a benchtop C1000 Thermal Cycler (Bio-Rad) for 15 min at 25 °C. For analysis, samples (after either 1× or 4× freeze-thaw) were spun for 30 min at 16,900 $\times g$. The supernatant was run on SDS-PAGE with Coomassie staining and analyzed by densitometry. The sample without freeze-thaw was defined as 100 % soluble. All samples were run in triplicate and plotted values represent the mean ± 1 s.d.

2.12 Protein lyophilisation

A 100 µL aliquot of SpyCatcher-MI3 (10 µM) in PBS was prepared in 100 µL thin-wall PCR tubes (StarLab). Samples were frozen in a dry ice-ethanol bath for 30 min. A BenchTop 2K freeze-dryer (VirTis) was used for 24 h at 0.14 mbar and -72.5 °C. Lyophilized sample was reconstituted in the same volume and spun at 16,900 $\times g$ for 30 min, before analysis via SDS-PAGE and DLS.

2.13 Nanoparticle vaccines

2.13.1 Preparation of SpyCatcher-nanoparticle immunogens

SpyCatcher-MI3 VLPs (10 µM) were incubated with 3× molar excess of CyRPA-SpyTag and SpyCatcher-AP205 VLPs were incubated with 1.5 × molar excess of CyRPA-SpyTag for 16-18 h at RT. The reactions were then dialyzed 4 times in a 300 kDa MWCO cellulose ester dialysis tubing against 4,000× excess PBS with 0.1 % (v/v) Tween 20 to remove unreacted CyRPA-SpyTag. Vaccine doses were matched to 1 µg CyRPA-equivalent for each group and diluted with sterile endotoxin-free PBS (home-made) to a final volume of 25 µL per dose. Each batch was prepared within 5 days prior to immunization and kept at 4 °C.

2.13.2 Endotoxin removal and quantification

Endotoxin was removed from proteins using Triton X-114 phase separation as described previously (Aida and Pabst, 1990). Proteins were transferred to 1.5 mL endotoxin-free microcentrifuge tubes (StarLab, Cat. No. E1415-1510), and 1 % (v/v) Triton X-114 was added to each sample. Samples were then incubated on ice until all Triton X-114 was dissolved, followed by another 5 min incubation on ice. Samples were then incubated at 37 °C for 5 min and centrifuged for 1 min at 16,900 $\times g$ at 37 °C. The supernatant was pipetted off and the entire procedure repeated two times. Endotoxin concentration was determined using the Pierce LAL Chromogenic Endotoxin Quantitation Kit (Thermo Fisher Scientific) according to the manufacturer's instructions. For all vaccines, endotoxin level was below 2 EU/mL.

2.13.3 SpyCatcher-nanoparticle immunizations

All animal experiments and procedures were performed according to the UK Animals (Scientific Procedures) Act Project License (PPL 30/2414 and 30/2889) and approved by the Oxford University Local Ethical Review Body. Age-matched female BALB/c mice (En-

vigo), housed in specific-pathogen free environments, were immunized with equal amounts of vaccines intra-muscularly into each leg. Female mice were chosen because male mice often display greater aggression and may require separation in individual cages. The number of mice needed was determined based on the statistical power of the sample. Immunizations were performed as a prime-boost regimen (prime on day 0, boost on day 14). The vaccines were prepared in sterile endotoxin-free PBS and formulated in the adjuvant Addavax (InvivoGen) (25 µL/per dose). Blood samples were harvested to obtain sera for analysis of endpoint ELISA titers. Blood samples were left to clot overnight at 4 °C, and sera were transferred to fresh Eppendorf tubes after 10 min centrifugation at 8,600 $\times g$. Six mice were used for each condition.

2.13.4 End-point ELISA

End-point ELISAs were performed by Dr.Anne-Marie Andersson. MaxiSorp plates (Thermo Fisher Scientific) were coated overnight at 4 °C with CyRPA at 1 µg/mL in coating buffer (15 mM sodium carbonate with 35 mM sodium bicarbonate, pH 9.6). Plates were washed six times with PBS/T (PBS with 0.5 % (v/v) Tween-20) and blocked with PBS/T with 10 % skim milk for 1 h at 25 °C. Plates were washed six times with PBS/T and incubated with duplicates of 3-fold serially diluted serum samples for 2 h at 25 °C. Following a wash step with PBS/T, goat anti-mouse total IgG conjugated to alkaline phosphatase (Sigma-Aldrich) (1:3,000 dilution in PBS/T) was added to the plates and the plates were incubated for 1 h at 25 °C. After a final wash step with PBS/T, p-nitrophenylphosphate (Sigma-Aldrich) (1 mg/mL) diluted in 1 M diethanolamine, pH 9.8 (Thermo Scientific) was used as a developing substrate. A_{405} was obtained using a SpectraMAX M3 plate-reader (Molecular Devices). The end-point titer is defined as the x-axis intercept of the dilution curve at an absorbance value greater than the mean A_{405}, plus three standard deviations for a serum sample from a naive mouse at a serum dilution of 1:100.

2.13.5 Antibody avidity ELISA

End-point ELISAs were performed by Dr.Anne-Marie Andersson. Antibody avidity was assessed at day 28 using a sodium thiocyanate (NaSCN) displacement ELISA. MaxiSorp plates (Thermo Fisher Scientific) were coated with CyRPA overnight at 4 °C and blocked and washed with PBS/T as described above. Serum samples were individually diluted to reach an A_{405} of approximately 1.5 and plated in duplicate. Three of the samples from the CyRPA-SpyTag immunized group were analyzed at their maximum reachable A_{405} at 0.4, 0.5, and 0.9. Following 2 h incubation at 25 °C, and washing with PBS/T, the indicated concentration of NaSCN (0-7 M) was added to the wells. The plates were incubated for 15 min at 25 °C, followed by washing with PBS/T, and then incubated with secondary antibody and substrate as above. The intercept at which the molar concentration of NaSCN had reduced the A_{405} to 50 % for individual samples was used to give IC_{50}.

2.13.6 Statistical analysis of immunizations

Statistical analysis for ELISAs was performed by Dr.Anne-Marie Andersson using GraphPad Prism 7.0d. Comparisons were made using a Kruskal-Wallis test. Dunn's multiple comparison post-test was performed for significant values. p values above 0.05 were reported as non-significant (n.s.).

Chapter 3

Directed Evolution of SpyCatcher-AP205

3.1 Introduction

Virus-like particles (VLPs) are attractive vaccine scaffolds (Mohsen et al., 2017; Jennings and Bachmann, 2008; Zeltins, 2013). The physical properties of VLPs make them excellent at stimulating humoral immune responses (Bachmann and Jennings, 2010). The ability to use VLPs as platforms for antigen multimerization has expanded their utility and broadened their scope to include development of vaccines against a variety of targets including cancer, allergies, and Alzheimer's disease (Kushnir et al., 2012).

The Catcher-Tag system developed in the Howarth laboratory is a bioconjugation method that covalently links a peptide tag with a protein "catcher" through an irreversible covalent bond (Zakeri and Howarth, 2010). Previous work in the Howarth laboratory, specifically the efforts of Dr. Karl Brune, fused SpyCatcher onto the N-terminus of coat protein 3 (CP3) from the ssRNA *Acinetobacter* phage AP205 (Brune et al., 2016). SpyCatcher-CP3 VLPs formed the basis of a "plug-and-display" vaccine platform that could be decorated with any SpyTag-antigen. However, a number of properties of SpyCatcher-CP3 VLPs limit their

translational potential to industry or clinic. Some of the greatest drawbacks of SpyCatcher-CP3 VLPs are their low stability, solubility, tendency to aggregate, and their extremely low yield ($\sim$ 1 mg/L of *E. coli* culture).

Hence, the first aim of my work was to test out a methodology for the directed evolution of SpyCatcher-VLPs and then to try to evolve the AP205 coat protein to produce a soluble protein that could be produced in high yield in *E. coli*.

In this chapter, I describe the characteristics of SpyCatcher-CP3 VLPs and the development of a directed evolution methodology based on RNA encapsulation inside SpyCatcher-VLPs. I then attempt to evolve SpyCatcher-CP3 two times, with optimization and refinement of the methodology following the first evolution. Ultimately, neither evolution yielded an improved version of SpyCatcher-CP3. Possible explanations for the observed results as well as future directions are discussed.

3.2 Generation of SpyCatcher-AP205 VLPs

AP205 is a ssRNA bacteriophage of the *Leviviridae* family that infects Gram-negative bacteria (Klovins et al., 2002; Shishovs et al., 2016). Recombinant expression of AP205 produces capsids that have T=3 symmetry, are 27-30 nm in diameter, and are formed from 180 copies of the coat protein (Klovins et al., 2002). A unique structural feature of the AP205 capsid means both termini are exposed on the surface of the capsid and are thus particularly amenable to genetic conjugation (Tissot et al., 2010; Klovins et al., 2002). Previous engineering in the Howarth lab by Karl Brune fused ΔN1SpyCatcher to the N-terminus of CP3 (GenBank accession number KU302810) (Brune et al., 2016). ΔN1SpyCatcher was used because the truncated version of SpyCatcher is less immunogenic and is thus more desirable for vaccine applications (Liu et al., 2014).

To test whether I could produce properly assembled SpyCatcher-VLPs, I followed the optimized expression protocol experimentally produced by Karl Brune. This protocol involves

transforming with a modified high-copy number pGEM plasmid, reduced antibiotic concentration to improve bacterial density, and extended expression over 2 days. SpyCatcher-CP3 VLPs purified from cell lysate by immobilized metal affinity chromatography (IMAC) were analyzed for VLP formation, size, and RNA-encapsulation (Figure 3.1). By SDS-PAGE, disulfide bonded high molecular weight (HMW) species, which disassembled into a monomer band under reducing conditions, could be observed (Figure 3.1a). The VLPs were also analyzed by native agarose gel electrophoresis and stained and imaged with SybrSafe (to visualize nucleic acid) before staining with Coomassie (a protein staining dye). The co-localization of protein and RNA band indicate RNA packaging in VLPs, consistent for AP205 (Figure 3.1b) (Shishovs et al., 2016). The proper formation of VLPs was confirmed by TEM (Figure 3.1c). Manual measurement of particles from TEM using ImageJ gave a diameter of 16.5 ± 1.6 nm (mean ± 1 s.d., n = 50). Dynamic light scattering (DLS) of SpyCatcher-VLPs gave a size distribution of particles with a hydrodynamic radius of 16.6 nm ± 7 nm (mean ± 1 s.d.) (Figure 3.1e). Reactivity of SpyCatcher-VLPs was tested by reaction with the model protein SpyTag-MBP. After reaction at room temperature for 2 h with 1.5× molar excess SpyTag-MBP, full conjugation was observed via SDS-PAGE (Figure 3.1f).

Expression and purification of SpyCatcher-VLPs was attempted a number of times. Karl Brune reported yields ranging up to approximately 4 mg/L of *E. coli* culture. Despite my best efforts, and numerous attempts, I was only able to obtain yields in the range of 0.1 - 1 mg/L. To obtain enough protein for subsequent experiments I simply expressed and purified batches of 6 - 12 L cultures. SpyCatcher-CP3 VLPs were prone to aggregation and the tendency to aggregate was exacerbated after freezing. Thus, VLPs were stored at 4 °C. However, even when when storing at 4°C, centrifugation was always required before use to remove visible aggregates: leading to significant protein loss over time. Storage at high concentration further increased the propensity to aggregate. I estimated that SpyCatcher-CP3 VLP concentration for storage should not exceed 30 µM.

Thus, the solubility and yield of SpyCatcher-AP205 is a limiting factor not just for

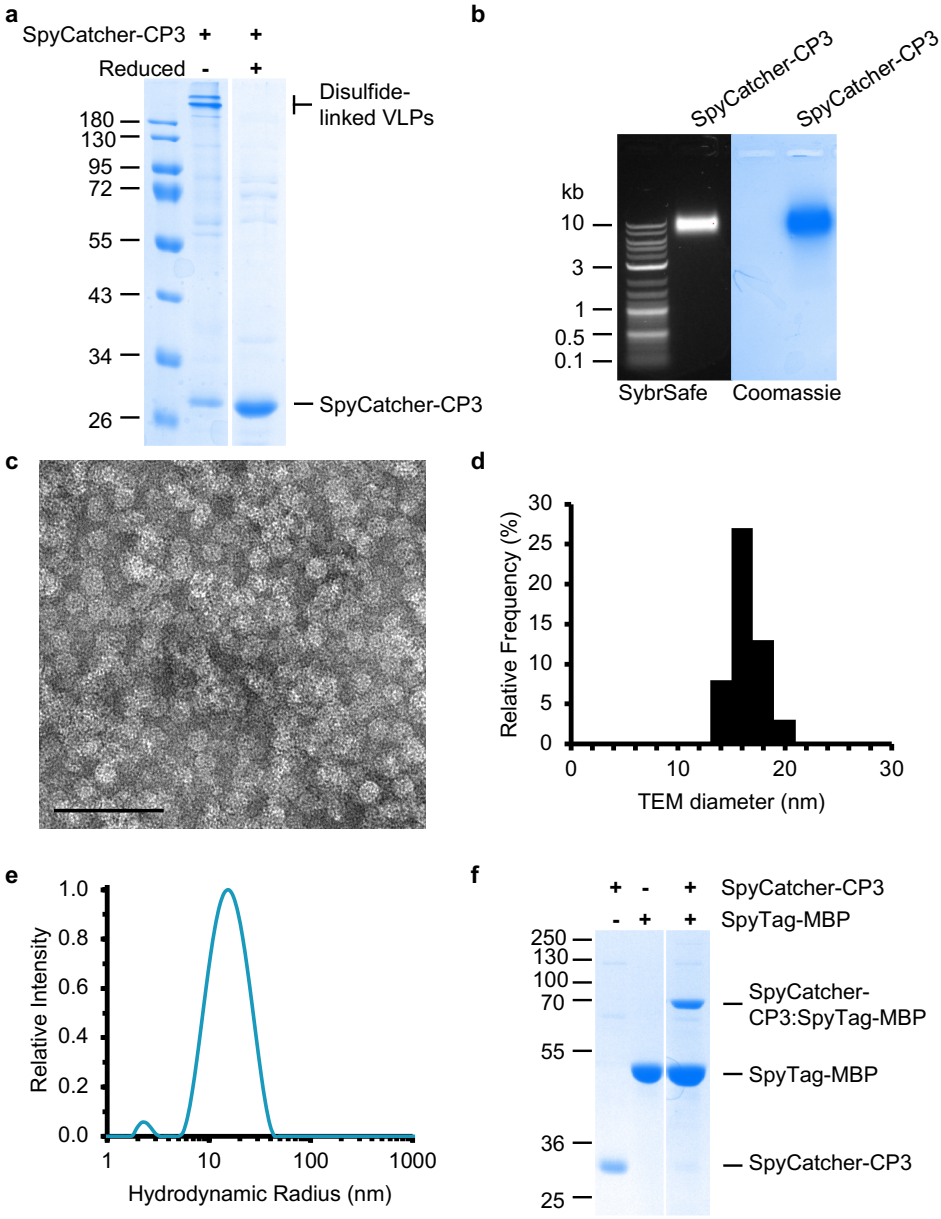


Figure 3.1. Characterization of SpyCatcher-CP3 VLPs. **(a)** IMAC purified SpyCatcher-CP3 VLPs visualized on non-reduced (left lane) and reduced (right lane) SDS-PAGE with Coomassie staining. **(b)** Agarose gel electrophoresis of SpyCatcher-CP3 VLPs first imaged with SybrSafe (to visualize nucleic acid) followed by staining with Instant Blue (a dye containing protein staining agent Coomassie). **(c)** Negatively-stained TEM image of SpyCatcher-CP3 VLPs. Scale bar 100 nm. **(d)** Size distribution of SpyCatcher-CP3 VLPs from TEM measured with FIJI Image processor (n=50). **(e)** Dynamic light scattering (DLS) determination of hydrodynamic radius (R_h) of SpyCatcher-CP3 VLPs. **(f)** Reaction of SpyCatcher-CP3 VLPs with model reaction partner SpyTag-MBP for 2 h at 25 °C before boiling and analysis by reducing SDS-PAGE with Coomassie staining.

lab-scale work but also for translating SpyCatcher-AP205 VLPs into a viable platform for industrial and clinical applications. To address these issues I designed a directed evolution on the SpyCatcher-AP205 protein. The choice of directed evolution versus rational engineering was motivated by two main reasons. First, directed evolution has been used successfully on VLPs in the past: notably on MS2 VLPs which are from the same family as AP205 (Peabody and Al-Bitar, 2001; Chackerian et al., 2011; Asensio et al., 2016). MS2 VLPs encapsulate their own RNA and thus provide a genotype-phenotype relationship. Second, chimeric VLP assembly is particularly sensitive to errors from protein misfolding because VLP assembly is cooperative. It is also challenging to rationally engineer the AP205 protein because one must predict the way that a mutation will affect the interaction between the 180 monomeric proteins. It is likely that there are many aspects of the interactions between monomers and dimers that cannot be predicted by rational design. Using directed evolution helps us circumvent the gap in our understanding of AP205 assembly. Improved variants identified from an evolution could also potentially help us elucidate links between structure and assembly of AP205 VLPs.

3.3 Development of directed evolution methodology

3.3.1 RNA extraction and RT-PCR

For any directed evolution to be successful a number of key factors must be satisfied, including the presence of a genotype-phenotype correlation, sufficient selection pressure, and a diverse library (Packer and Liu, 2015). The first thing I did, after validating SpyCatcher-VLP assembly and biophysical characteristics, was establishing whether RNA could be extracted and selectively amplified from SpyCatcher-VLPs. For the initial test, 10 µM of purified SpyCatcher-VLPs were subjected to lysis and RNA purification using a commercial viral RNA isolation kit. In brief, the procedure involved incubating the VLPs under highly denaturing conditions, adsorption of RNA onto a silica membrane, wash steps, and elution

into RNase-free buffer. The purified RNA was then subjected to reverse-transcription PCR (RT-PCR) and the subsequent DNA was run on an agarose gel to visualize product. As a negative control, RNA purified from a non-VLP transformed *E. coli* culture was subjected to RT-PCR with the same primers. The results from the agarose gel analysis indicated that the primers specifically amplified SpyCatcher-CP3 RNA (Figure 3.2).

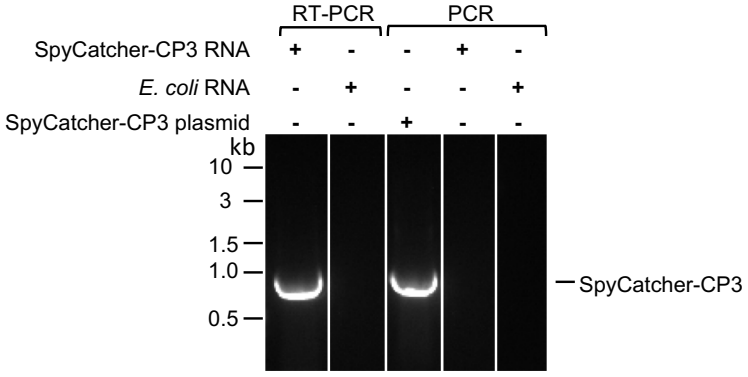


Figure 3.2. Specific isolation of RNA from SpyCatcher-CP3 VLPs. RNA was purified from SpyCatcher-CP3 VLPs as well as from an *E. coli* cell lysate (negative control) and subjected to reverse-transcription PCR (RT-PCR) using primers designed to bind the SpyCatcher-CP3 sequence. Genetic material was successfully and specifically purified only from VLPs.

I next decided to explore the detection threshhold of procedure, i.e. what was the lowest concentration of VLPs where RNA could still be amplified. RT-PCR on RNA extracted from 0.05 nM of VLPs still produced a visible DNA product by agarose gel, meaning that the isolation and amplification procedure was sensitive enough to detect RNA from as few as $\sim$ 30 VLPs (Figure 3.3).

3.3.2 Genotype-phenotype correlation

Although I had shown that RNA could be amplified from VLPs, it was critical to determine whether VLPs would selectively package their own RNA and not other recombinant protein RNA. In the context of the directed evolution we can imagine that there would be hundreds of thousands of unique SpyCatcher-CP3 sequences. Some of these variants would form VLPs but many would encode non-functional or insoluble protein. If VLPs encapsulate

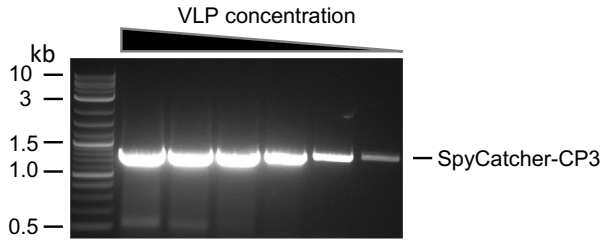


Figure 3.3. RT-PCR amplified RNA from VLPs at a very low concentration. RNA was purified from SpyCatcher-CP3 VLPs in a dilution series (5 µM, 0.5 µM, 0.05 µM, 5 nM, 0.5 nM, 0.05 nM). Purified RNA was subjected to reverse-transcription PCR (RT-PCR) using primers designed to bind the SpyCatcher-CP3 sequence.

both their own and other SpyCatcher-CP3 variant RNA then it would be impossible to establish a genotype-phenotype correlation and distinguish between desirable and non-desirable mutations.

To probe the selectivity of RNA packaging in SpyCatcher-VLPs, I designed an experiment to mimic the conditions the VLPs would experience during the evolution. These conditions involve SpyCatcher-VLPs mixing with protein/RNA from SpyCatcher-CP3 variants that do not form VLPs (Figure 3.4a). A 500 mL *E. coli* culture transformed with the SpyCatcher-CP3 plasmid, was induced and expressed as normal. At the same time, another 500 mL *E. coli* culture was inoculated with cells transformed with SpyCatcher002-superfolderGFP (SpyCatcher002-sfGFP). The SpyCatcher002-sfGFP protein would serve as a surrogate for a "non-VLP forming" variant that would exist in the library. After expression for 4 h, the two cultures were mixed to form a 1 L culture with equal cell density from both cultures (based on OD600). The culture was then pelleted and and the cleared lysate purified via IMAC to isolate SpyCatcher-VLPs. The VLPs were then subjected to the RNA extraction and RT-PCR but this time with primers specific for sfGFP. Analyzing the DNA product of the RT-PCR on an agarose gel showed a strong DNA band corresponding to the expected product size of the sfGFP construct. This indicated that foreign non-VLP RNA was co-purified with the VLPs (Figure 3.4b). However, there were two possible scenarios in which foreign RNA could be amplified in concert with the VLPs. As visualized in Figure 3.4a, non-VLP RNA could either be co-packaged inside the VLPs, or simply stuck to the outside

of the VLPs through non-specific interactions. If it was the latter, then there would be the possibility of using a nuclease to degrade unprotected RNA. If it was the case that SpyCatcher-VLPs encapsulate foreign RNA, it would have been impossible to continue with the DE.

To distinguish between these two scenarios another sample of the same SpyCatcher-VLPs (purified in the presence of SC002-sfGFP) was incubated with benzonase at a concentration of 25 U/µL for 1 h at 25 °C. Afterwards, benzonase was removed through IMAC purification, and the RNA from the VLPs was extracted and subjected to RT-PCR. Analysis by agarose gel showed no band was amplified with the sfGFP primers, while the RNA inside the VLP was protected and amplified robustly by SpyCatcher-CP3 specific primers (Figure 3.4b). This indicated that the foreign RNA was stuck to the outside of the VLPs perhaps through electrostatic interactions and was not actually encapsulated inside the VLPs.

3.3.3 Model selection

Since two of the crucial controls had been verified (RNA amplification and the genotype-phenotype correlation), I moved on to establishing a method for SpyCatcher-VLP capture and enrichment. A previously established directed evolution strategy from the Howarth laboratory selected for SpyCatcher-phage through reaction with biotinylated SpyTag and capture with biotin-binding magnetic beads (Keeble et al., 2017). I decided to adapt this protocol for use in the directed evolution of SpyCatcher-CP3. A cartoon of the model selection protocol is shown in Figure 3.5a. The first step would involve mixing SpyCatcher-VLPs with biotinylated-SpyTag-MBP. Biotin-binding magnetic beads would then be added to the mixture and captured using a magnetic rack. The beads would be washed to remove any unbound species like misfolded or aggregated VLPs, or any particles without a functional SpyCatcher accessible on the surface. Following the washes, the VLPs remaining on the beads would be lysed directly and the RNA purified and taken forward. To test that this process would work, I used 5 µM of purified SpyCatcher-CP3 VLPs and incubated the protein with

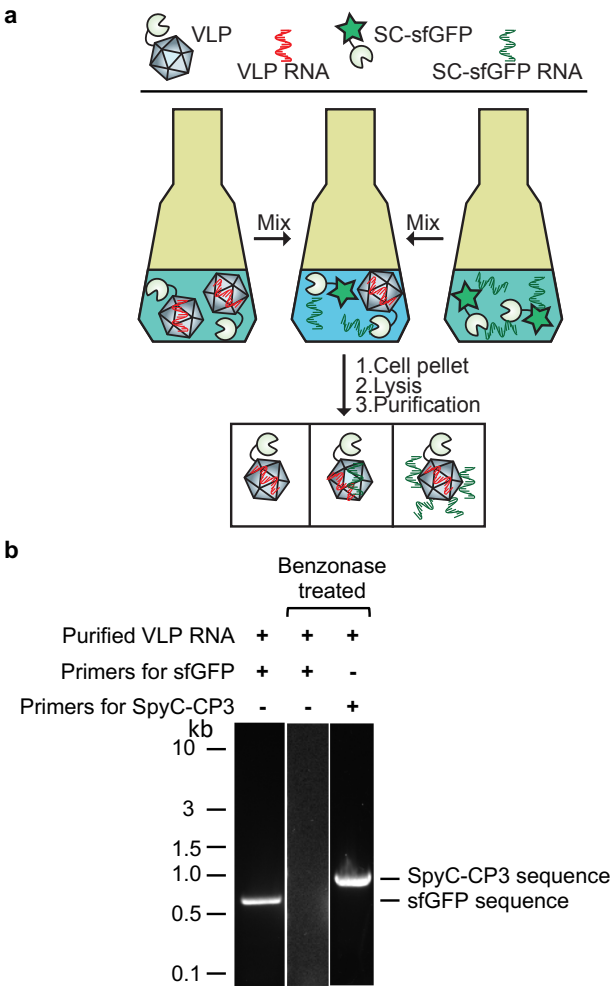


Figure 3.4. Establishing SpyCatcher-VLPs have a genotype-phenotype correlation. (a) A cartoon of the experiment. A 500 mL *E. coli* culture expressing SpyCatcher-CP3 VLPs was mixed with a 500 mL *E. coli* culture that had expressed a non-VLP protein (SpyCatcher002-sfGFP). The 1 L mixed culture was pelleted and then SpyCatcher-VLPs purified as normal from lysate. RNA was purified from VLPs and amplified via RT-PCR before and after benzonase treatment. RT-PCR used primers specific for either SpyCatcher-CP3 sequence or sfGFP.

bio-SpyTag-MBP in a 1:1 molar ratio for 1 h (Sample 1). Two negative control samples of the same concentration were also processed in parallel. Sample 2 contained CP3-DogTag VLPs incubated with bio-SpyTag-MBP. Since DogTag has no reactivity with SpyTag, these VLPs should not be bound or captured on the magnetic beads and thus no RNA should be amplified from these samples (Buldun et al., 2018). Sample 2 was a control making sure that only VLPs with reactive SpyCatcher displayed on their surface would get selected.

Sample 3 was a negative control for non-specific binding on the magnetic beads. This sample contained only SpyCatcher-CP3 VLPs and no bio-SpyTag-MBP bait. Thus, during the wash step all VLPs in sample 2 and 3 should be removed and no RNA amplified. A cartoon of the three samples is illustrated in Figure 3.5b. However, in the very first test I attempted, I saw no difference in VLP capture between any of the three samples, indicating that VLPs were not getting selectively captured via the SpyCatcher-SpyTag interaction (Figure 3.5c).

Since the initial model capture did not exhibit the desired selectivity, I turned my attention to optimizing different properties of the procedure. Since VLPs seemed to be non-specifically bound to the beads, I added 3 % BSA to all buffers and I blocked both Eppendorf tubes and beads for 1 h with BSA before use. I also tried casein instead of BSA and used different bead washes. Washes ranged in harshness from 0.5 % Tween-20 to phosphate-citrate pH 4. All conditions were assessed by agarose gel and the intensity of amplified DNA for each sample is summarized in Table 3.1.

Since neither increasing blocking or washing seemed to have any effect on the selectivity, I tried using streptavidin agarose resin rather than streptavidin magnetic beads. However, using the resin also proved unsuccessful (Table 3.1 line 5). Thus, I cloned a TEV cleavage site into my SpyTag-MBP to facilitate cleavage of specifically bound VLPs. I also introduced a bead pre-clearing step that involved adding a small amount of blocked beads to the VLPs before reaction with the SpyTag bait. The idea behind the pre-clearing step was to remove some of the protein species in solution that were being non-specifically captured. These

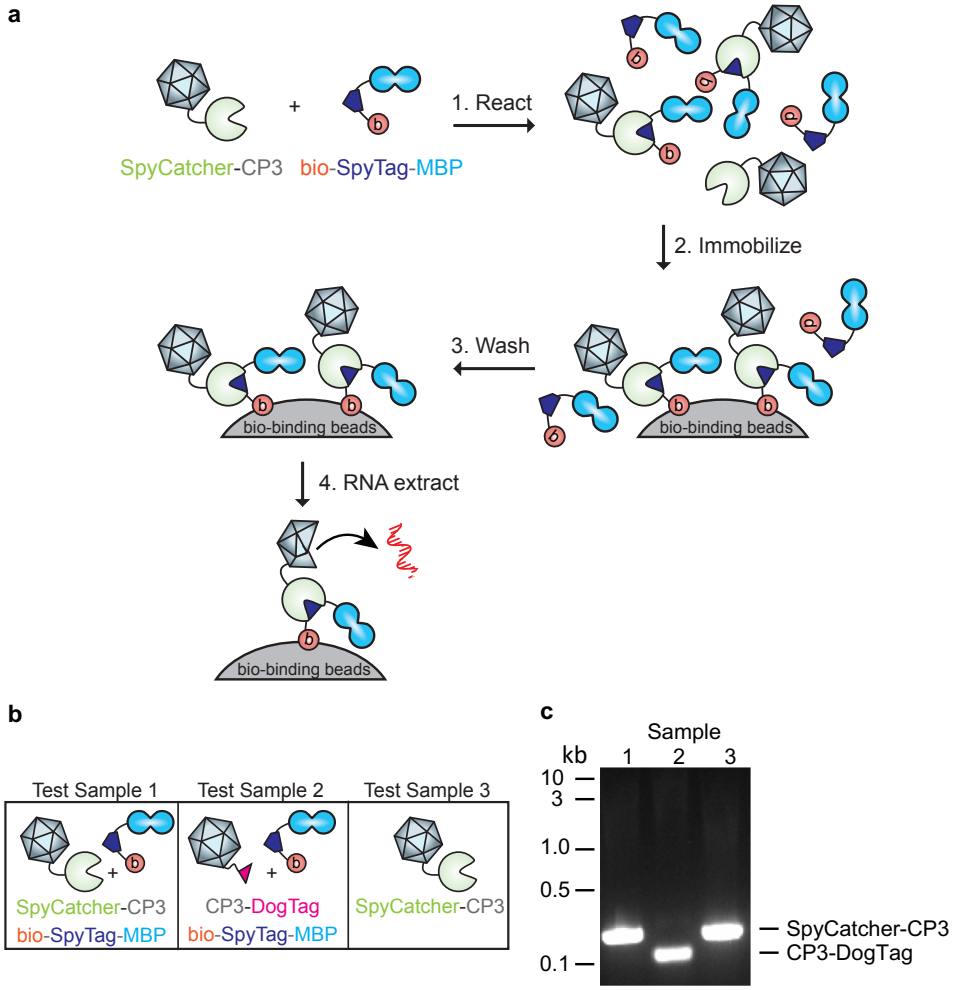


Figure 3.5. Optimizing the model selection for use in the directed evolution of SpyCatcher-CP3. (a) Cartoon of the model selection principle. Biotinylated-SpyTag002-MBP is incubated with SpyCatcher-CP3 VLPs to form a covalently bonded species. This species is then immobilized on magnetic biotin-binding beads and unconjugated VLPs are washed away. The bound VLPs are then lyzed directly while still bound to the beads and the RNA is purified and amplified via RT-PCR. **(b)** Cartoon of the three different test conditions used during optimization trials to stimulate the desired selection (1), a negative control for SpyCatcher-SpyTag binding specificity (2), and a negative control for non-specific binding on beads (3). **(c)** A sample agarose gel showing the DNA product band after bead incubation with protein sample, bead washing, RNA purification and RT-PCR for each of the three test conditions. Non-specific binding to the beads is observed in sample 2 and sample 3.

Table 3.1. Optimization of the model selection conditions.

	Conditions				Sample		
ID	Blocking	SpyTag	Other changes	Washing	1[a]	2[b]	3[a]
1	3 % BSA	bio-SpyTag-MBP	NA	3× A, 1× B	+	+	+
2	3 % BSA	bio-SpyTag-MBP	NA	3× B, 1× C	+	+	+
3	3 % BSA	bio-SpyTag-MBP	NA	3× C, 1× B	+	+	+
4	3 % casein	bio-SpyTag-MBP	NA	3× B, 1× C	+	+	+
5	3 % BSA	bio-SpyTag-MBP	Streptavidin resin	3× B, 1× C	+	+	+
6	10 % BSA	bio-SpyTag-TEV-MBP	Pre-clearing	3× C, 1× B	+	-	+
7	10 % BSA	bio-SpyTag-TEV-MBP	Pre-clearing, TEV cleavage	3× C, 1× B	+	+	+
8	10 % BSA	SpyTag-HaloTag	HaloLink beads	3× C, 1× B	+	+	-
9	10 % BSA	SpyTag-HaloTag	HaloLink beads, pre-clearing	3× C, 1× B	++	+	-
10	10 % BSA	SpyTag-HaloTag	HaloLink beads, pre-clearing, TEV cleavage	3× C, 1× B	+++	-	-
11	10 % BSA	bio-SpyTag-TEV-MBP	Streptavidin resin, pre-clearing, TEV cleavage	3× C, 1× B	+	++	-

A: 50 mM glycine, 25 mM sodium citrate, pH 8, 0.1 % Tween-20
B: 50 mM glycine, 25 mM sodium citrate, pH 8, 0.5 % Tween-20
C: 25 mM citrate-phosphate buffer, pH 4
[a] SpyCatcher-CP3 DNA band quantified
[b] CP3-DogTag DNA band quantified
+++ strong DNA band, ++ medium intensity DNA band
+ visible DNA band, - faint/no DNA visible

modifications ultimately did not have the desired effect (Table 3.1 line 6 and 7).

To improve the selectivity of the VLP capture I turned my attention to another selection system: reaction with SpyTag-TEV-HaloTag7 and capture with HaloLink magnetic beads. HaloTag is a modified bacterial haloalkane dehalogenase that forms a covalent bond with synthetic HaloTag ligands (Los et al., 2008). HaloLink beads capture HaloTag proteins rapidly, with high binding capacity, and with low non-specific binding. Although the HaloTag system did not initially seem to be better than the biotin-streptavidin capture (Table 3.1 line 8), once the procedure was tested with all the previous modifications (10 % BSA blocking, pre-clearing, and TEV cleavage) the desired selectivity was finally seen (Table 3.1 line 10, Figure 3.6c).

Since I had seen qualitatively that the model selection conditions were working, I decided to do quantitative-PCR (qPCR) to more accurately determine how much better the selection of SpyCatcher-VLPs was compared to my negative controls. I first created a standard curve with known amounts of plasmid DNA from SpyCatcher-CP3 and CP3-DogTag. The qPCR data from the standard curve is shown in Figure 3.7a,b. I then took the RNA that I extracted from each sample following the newly optimized model selection procdure (Figure 3.6b), performed reverse-transcription PCR, and quantified the DNA amount by qPCR. The results from qPCR indicated that SpyCatcher-CP3 VLPs from sample 1 were enriched between $\sim 10^4$ to 10^5 compared to negative control CP3-DogT VLPs (sample 2) and negative control SpyCatcher-CP3 VLPs with no bait (Sample 3).

3.3.4 Library construction

Since I had performed a number of the necessary initial validations, I turned my attention to creating the library of variants that I would be screening during the directed evolution. The gene I targeted for mutagenesis was CP3 of AP205 which forms the basis of the SpyCatcher-VLP vaccine platform. There are many different techniques for gene diversification, each with different advantages and disadvantages (Packer and Liu, 2015; Jäckel et al., 2008).

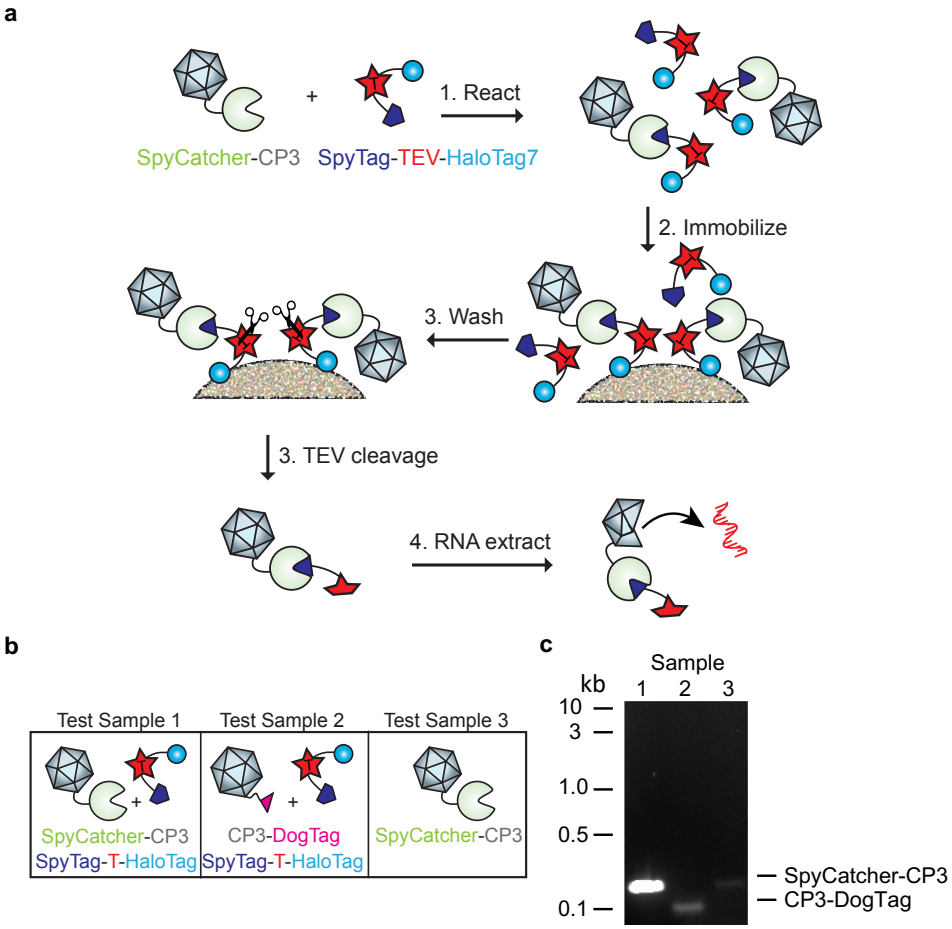


Figure 3.6. Optimized VLP capture conditions for the directed evolution of SpyCatcher-CP3. **(a)** Cartoon of the altered and optimized model selection principle. SpyTag002-HaloTag7 containing a TEV cleavage site is incubated with SpyCatcher-CP3 VLPs to form a covalently bonded species. This species is then immobilized on HaloLink magnetic beads and unconjugated VLPs are washed away. The bound VLPs are then incubated with TEV protease. Cleaved VLPs in the supernatant are lysed and RNA is extracted and amplified via RT-PCR. **(b)** Cartoon of the three different test conditions used during optimization trials to stimulate the desired selection (1), a negative control for SpyCatcher-SpyTag binding specificity (2), and a negative control for non-specific binding on beads (3). **(c)** A sample agarose gel of the DNA band from the three test conditions shows desired selectivity. Bands of high saturation are highlighted in red.

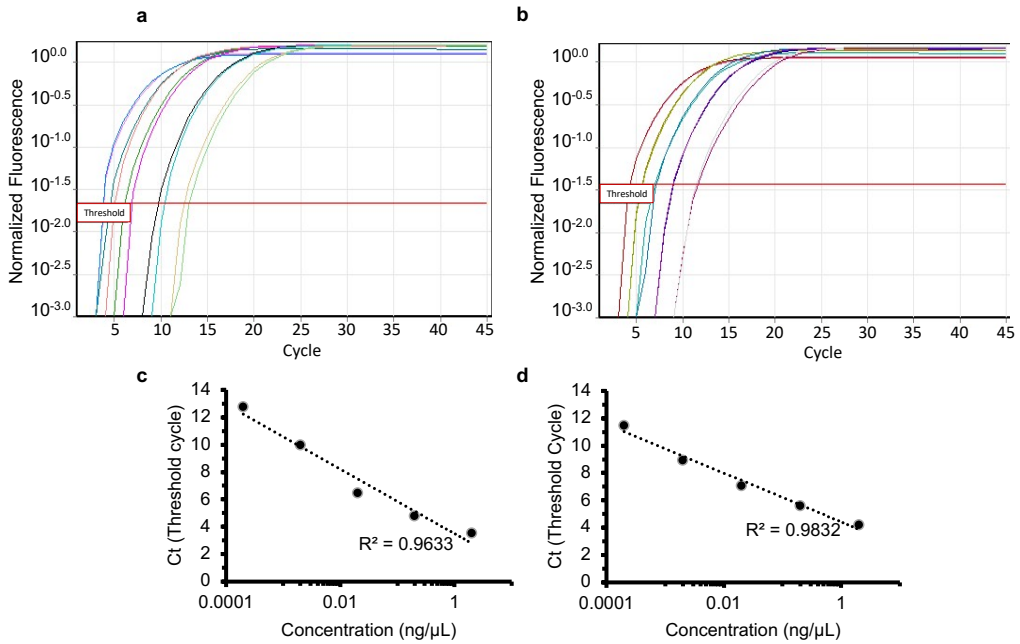


Figure 3.7. Quantitiative-PCR (qPCR) to assess RNA amounts in model selection experiments. (a,b) Examples of the quantitation data of a series of dilutions with known DNA amounts of SpyCatcher-CP3 and CP3-DogTag. A standard curve generated using a dilution series with a known amount of SpyCatcher-CP3 DNA **(c)** and SpyCatcher-CP3 DNA **(d)** in duplicate.

When amino acid positions that likely impact on a desired function are known, or when there is a region (such as an enzyme active site) that should be avoided, focused mutagenesis strategies are often employed. Focused mutagenesis has the advantage of theoretically sampling an entire chosen mutational space. The largest library size that can be achieved with current protocols is $\sim 10^{15}$ which is far lower than would be needed to sample all the unique combinations of any completely randomized protein (Packer and Liu, 2015). However, if protein structure or function is not well understood random mutagenesis gives a better chance of finding mutations in advantageous areas.

The most common strategies for random mutagenesis include error-prone PCR (epPCR), chemical mutagenesis, and mutator strains (Packer and Liu, 2015; Tee and Wong, 2013). I chose epPCR since it is quick and easy to control the mutagenesis rate. To mutagenize CP3, I used the GeneMorph II Kit (Agilent) which uses a blend of two error prone DNA polymerases to minimize mutational bias compared to wild-type *Taq* polymerase (Table 3.2).

Using the kit, mutation rates of 1-16 mutations/kb can be achieved by varying the initial amount of target DNA or cycle number. I initially tested four different DNA amounts (50 ng, 5 ng, 0.5 ng, 0.05 ng). After cloning the mutated sequence into my expression vector and transforming competent cells with the DNA, I was able to sequence colonies from each library. Screening libraries is crucial before beginning an evolution to make sure that the mutation rate is not too high or too low, i.e. that the library is of good quality. Using the online tool MUTANALYST (Ferla, 2016) (http://www.mutanalyst.com/), I was able to estimate the mutational rate and mutational spectrum of my libraries. I decided to combine the libraries from my two intermediate conditions since they both had a medium mutational rate of ~ 6 mutations/kb (0.1 mutations/doubling/kb), with a good distribution of mutations across the genetic sequence. Libraries with high mutational rates are more likely to encode a higher proportion of non-functional misfolded proteins, or proteins containing premature stop codons and frameshift mutations (Tee and Wong, 2013). Likewise, for the success of any directed evolution having an even mutational spectrum is crucial for more thorough sampling of a given gene's sequence space. In Table 3.2 I list the analysis of the mutation spectrum from my library compared with the reference values for GeneMorph II and *Taq*. My library correlated well with expected values for the Mutazyme II DNA polymerase compared to *Taq* DNA polymerase and overall did not have a bias for transitions over transversions (T_s/T_v ratio of 0.5), although adenine $\leftrightarrow$ thymine was by far the most common transversion.

3.4 Directed evolution 1

The target of the directed evolution was to create a SpyCatcher-CP3 VLP that would be higher-yielding and more soluble. Due to the fact that expression of SpyCatcher-CP3 was so poor, Dr.Karl Brune devoted a very significant portion of his thesis developing a VLP specific protocol. The protocol compared to a standard expression protocol is summarized in Table 3.3. However, even with this non-standard method, the yields I achieved were never

Table 3.2. Mutational spectrum of the CP3 library compared to reported results.

	Taq polymerase*	MutazymeII polymerase*	CP3 library
Bias Indicator			
Ts/Tv	0.8	0.9	0.5
AT→GC/GC→AT	1.9	0.6	0.8
A→N, T→N (%)	75.9	50.7	69.4
G→N, C→N (%)	19.6	43.8	30.6
Transitions			
A→G, T→C (%)	27.6	17.5	16.5
G→A, C→T (%)	13.6	25.5	16.7
Transversions			
A→T, T→A (%)	40.9	28.5	47.7
A→C, T→G (%)	7.3	4.7	5.2
G→C, C→G (%)	1.4	4.1	3.2
G→T, C→A (%)	4.5	14.1	10.6

*Values from GeneMorph II Random Mutagenesis Kit (Agilent) Catalog #200550

more than 1 mg/L culture. Thus, I decided to screen my library by subjecting the protein variants to expression under standard conditions to find a variant that could express highly under a cheap, easy, and scalable production method. I knew the selection pressure would not be that high, since some wild-type SpyCatcher-CP3 could be expressed during standard conditions. However, a variant with 2-fold, 5-fold, or 10-fold better expression should, over a couple of rounds, dominate the culture.

An illustration of the directed evolution methodology is shown in Figure 3.8a. The library I created, described in 3.3.4, was approximately 10^6 cfu (colony forming units) and was transformed into home-made electro-competent BL21(DE3) cells of competency 10^8 cfu/µg. After expression under standard conditions the VLPs were purified by IMAC, spun for 30 min to remove aggregates and protein yield was determined by BCA assay. In each round VLPs were treated with benzonase before model capture using the optimized conditions described in 3.3.3. The results from four rounds of evolution are summarized in Figure 3.8b.

Unfortunately, the results from the first four rounds of evolution were not encouraging. Had the evolution been working I would expect to see an enrichment of improved variants and

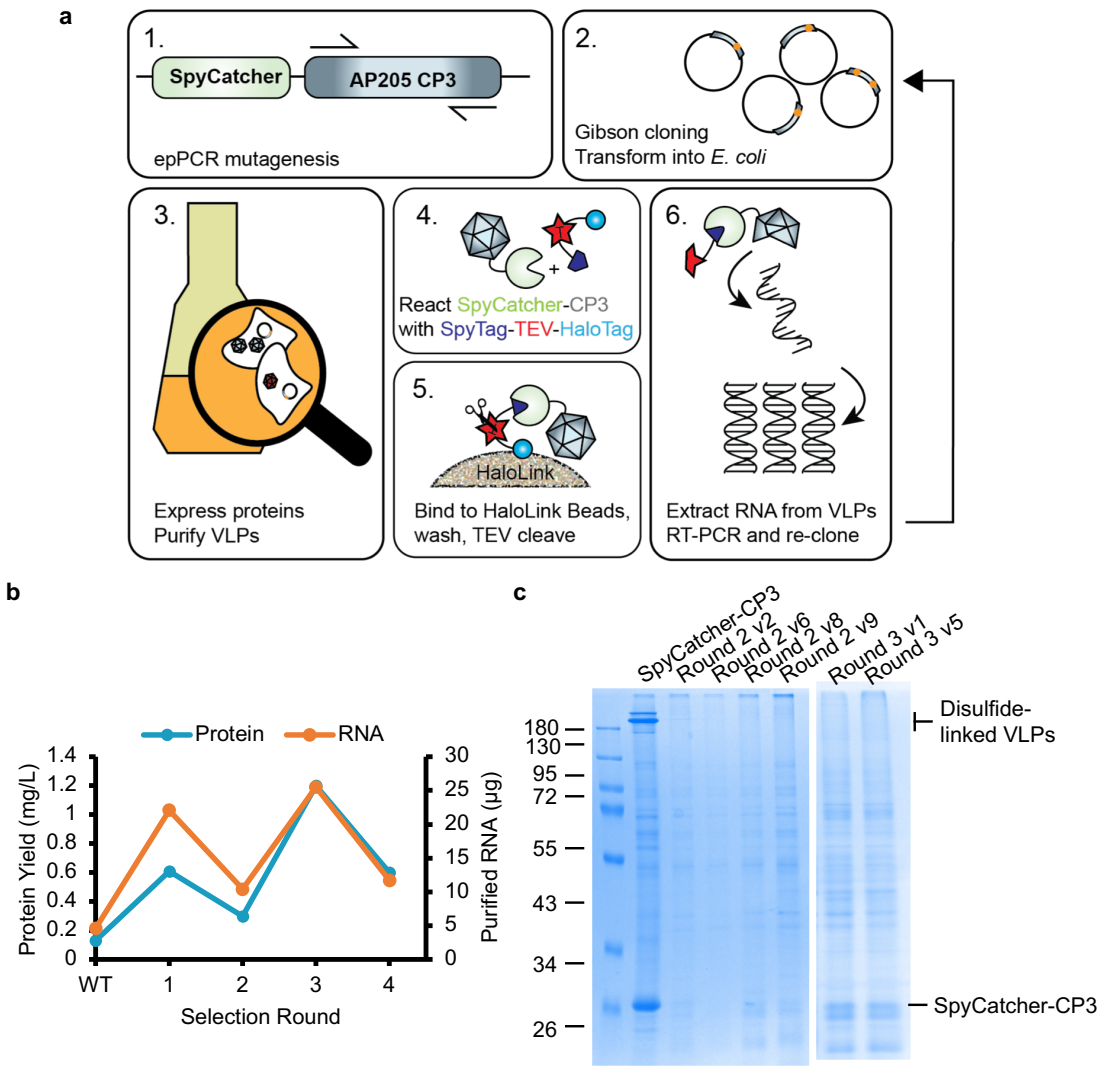


Figure 3.8. Results from directed evolution 1 indicated a problem in the methodology. **(a)** Schematic of the methodology for the directed evolution of SpyCatcher-AP205. Mutagenesis of the coat protein followed by expression of the library, model capture, RNA extraction, and cloning. **(b)** Graph showing the purified protein and RNA yield of SpyCatcher-VLPs as a function of each consecutive round of evolution. **(c)** SDS-PAGE of IMAC-purified variants from round 2 and round 3 of the evolution compared to wild-type SpyCatcher-CP3.

Table 3.3. VLP expression protocol versus standard expression for soluble protein.

SpyCatcher-CP3 VLP Protocol	Standard Expression Protocol
Day 1	
Transform into C41(DE3) cells, plate for single colonies overnight	Transform into expression strain, plate for single colonies overnight
Day 2	
Pick 8 colonies into 1 L 2× TY media and incubate overnight at 37 °C with shaking 30 RPM	Pick a single colony into 10 mL media and incubate overnight at 37 °C with shaking 200 RPM
Day 3	
Dilute 1 L starter culture into another 1 L of fresh media, shake at 100 RPM at 37 °C until A_{280} 0.5, cool to 22 °C for 30 min, induce with IPTG, grow overnight at 200 RPM	Dilute overnight culture 1/1000 in fresh media, incubate at 200 RPM at 37 °C until A_{280} 0.5, induce with IPTG, grow at 30 °C for 4-5 h. Harvest.
Day 4	
Harvest	

thus an increase in purified protein from round to round. Instead, the total protein amount fluctuated and decreased from round 1 to round 2 and from round 3 to 4. These results indicated that either the selection pressure was not strong enough or the model selection not stringent enough. This hypothesis was strengthened when I individually expressed some variants following round 2 and round 3 of the evolution and saw no VLPs following IMAC purification (Figure 3.8c). Thus, proteins that were worse than the wild-type were evading the measures set in place to ensure selection and propagation of RNA encapsulating VLPs, essentially "cheating" the evolution.

3.5 Optimization of methodology

Since the evolution methodology had proven to be flawed I turned my attention to investigating potential problem spots - areas in the protocol where there may be bias toward a non-VLP forming variant of SpyCatcher-CP3. I identified four areas that could potentially be problematic and thus four questions that I wanted to address. These were: 1. transforma-

tion bias (do non-VLP-forming sequences cause less toxicity and thus make more bacterial colonies?), 2. grow-up bias (do VLP-forming colonies grow up less reliably/more slowly so that in mixtures they become over-run?), 3. insufficient bias from RNA protection (do non-VLP-forming CP3 variants aggregate and thus protect RNA from benzonase degradation?), 4. TEV-protease elution bias (could the need for more anchor points linking well-formed VLPs to HaloTag resin favour the elution of bad assemblies?). To test transformation and grow-up bias, I expressed a cheater from the evolution (variant 3.1: A29V,K55R,N73Y) side-by-side with SpyCatcher-CP3. There was no bias towards the variant in either BL21(DE3) cells or C41 cells (Figure 3.9a,b). I then investigated RNA protection. I ran equal amounts of SpyCatcher-CP3 and a non-VLP forming variant 2.9 (N2Y,A41T,A58V) on an agarose gel, which I stained with SybrSafe and then Coomassie dye to visualize protein and RNA co-localization. The agarose gel showed a compact protein and RNA band in the same location for SpyCatcher-CP3 VLPs (Figure 3.9c). In contrast, the agarose gel showed a smear of protein for non-VLP forming variant 2.9, likely corresponding to aggregates (Figure 3.9c). Additionally, no RNA band was visible. However, it was concerning that, when the same proteins were subjected to RNA extraction and RT-PCR, a strong nucleic acid band was amplified from both samples, even after benzonase treatment (Figure 3.9d). This indicated that the aggregated variant was able to protect RNA from benzonase degradation. Additionally, it indicated that even when the RNA amount was negligible and not visible by SybrSafe staining, the sensitivity of RT-PCR meant that the RNA would still get amplified.

To address this issue, I decided to try an enhanced digestion protocol. Whereas initially I was incubating VLPs with 1 µL benzonase (>250 U/µL) for 1 h at 25 °C, I decided to double the amount of benzonase and incubate for 3 h at 37 °C, with shaking at 600 RPM. After enhanced digestion, model selection, RNA lysis and RT-PCR, agarose gel analysis showed that SpyCatcher-CP3 DNA was preserved and isolated in greater amounts than the aggregated protein (Figure 3.9e). However, I was concerned about the faint band on the agarose gel from the variant, indicating that even the enhanced digestion was not 100 %

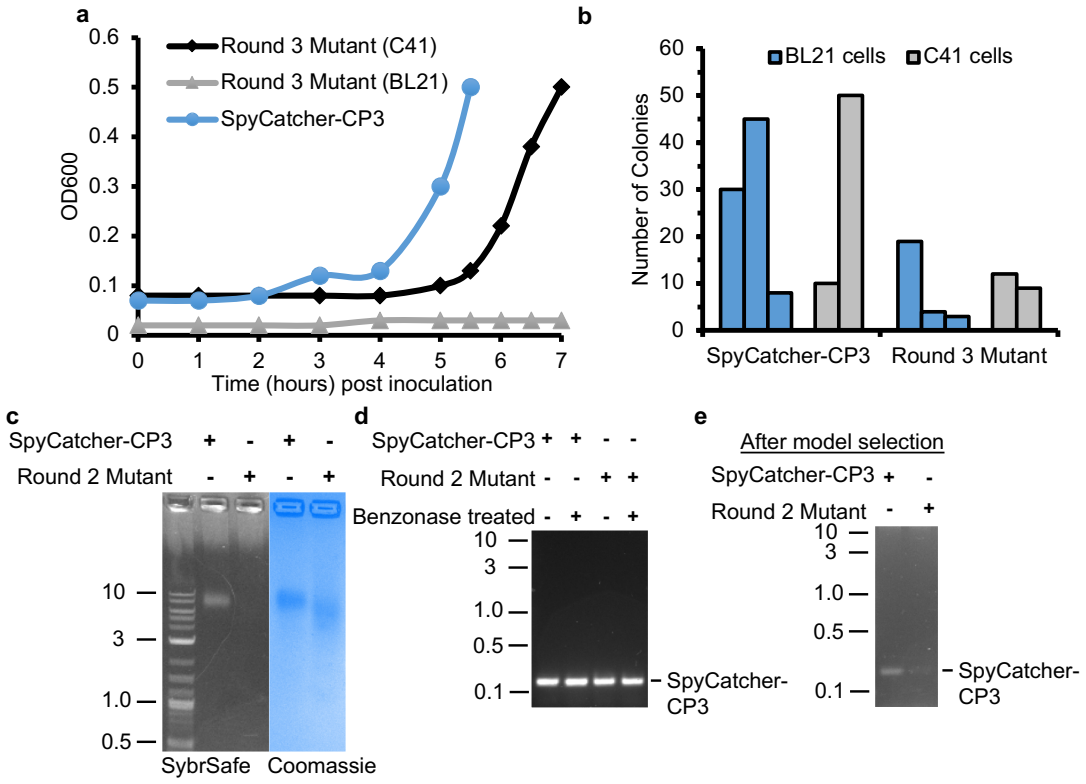


Figure 3.9. Investigating bias for non-VLP forming mutants in the evolution methodology. **(a)** SpyCatcher-CP3 WT was grown at the same time under the same conditions as two mutants from DE1 to observe if non-VLP forming mutants grow more quickly. **(b)** The same amount of DNA was transformed into two different cell strains to see if non-VLP forming mutants cause less toxicity and thus form more bacterial colonies. Each bar represents the colonies found on one plate following growth overnight. **(c)** Agarose gel comparing the protein and RNA co-localization of WT VLPs compared to a mutant. **(d)** DNA product after RNA extraction and RT-PCR of WT VLPs and a mutant before and after benzonase treatment. Benzonase does not degrade mutant RNA. **(e)** DNA from RT-PCR following increased enhanced benzonase degradation and model selection. VLP DNA is enriched compared to variant DNA.

effective at removing RNA from aggregates. Since even enhanced digestion could not remove all the RNA from the aggregates I reasoned that it would be more efficient to try and remove all aggregates from solution in the first place.

IMAC purification of VLPs was not sensitive enough to resolve aggregates from VLPs, despite washing Ni-NTA bound protein multiple times with 200 mM imidazole before elution at 2 M imidazole. As a second purification step I decided to try density gradient ultra-centrifugation, a commonly used technique for purifying viruses to homogeneity (Effio and Hubbuch, 2015). Density gradient centrifugation relies on layering solutions of dense media in a tube (from increasing to decreasing density). The solution to be purified is placed on top of the layers and after centrifuging at high speed, particles become distributed in solution in different layers depending on their size, shape, and density (Brakke, 1961). Puncture of the tube and subsequent fractionation allows for the collection of layers containing the protein of interest.

Before using ultra-centrifugation in the evolution, I tested and optimized different protocols from the literature (Buck et al., 2004; Buck and Thompson, 2007; Thrane et al., 2016). The optimized conditions involved layering IMAC-purified VLPs on top of a gradient made from three layers (23, 29, 35 %) of Optiprep (a sterile solution of iodixanol) (Sigma). Following centrifugation for 16 h at 4 °C at 140,000 $\times g$, layers were fractionated, analyzed by SDS-PAGE, and fractions containing VLPs pooled. Ultra-centrifugation was able to improve the purity of VLPs as analyzed by SDS-PAGE (Figure 3.10a). The method was even sensitive enough to separate between two distinct populations of VLPs, one of which appeared as a double band and one as a single band (Figure 3.10a). These VLPs samples were analyzed by TEM to confirm proper assembly (Figure 3.10b). Manual measurement of the particles from TEM confirmed that the two populations were of different average size, explaining their differing migration speed during centrifugation (Figure 3.10c). The average diameter of the double band particles was 23.5 ± 5.5 nm and the single band particles had an average diameter of 16.5 ± 5 nm (n = 100).

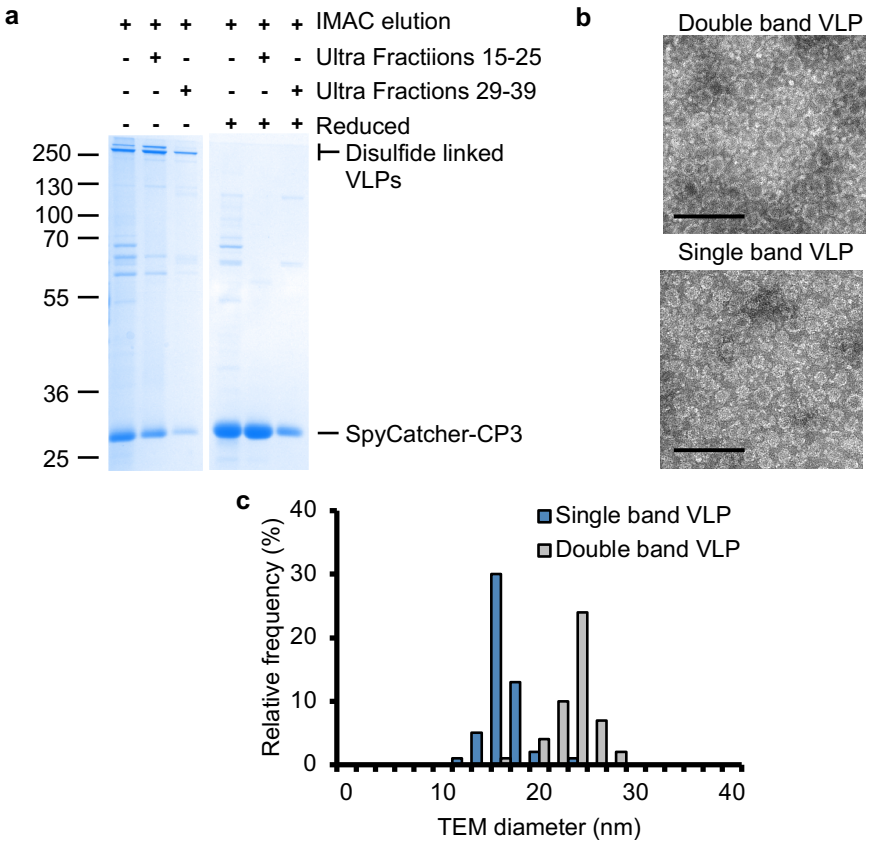


Figure 3.10. Ultra-centrifugation as an improved purification method for SpyCatcher-CP3 VLPs. **(a)** Gel filtration using an OptiPrep media gradient shows improved purity and separation of VLPs compared to IMAC purification. **(b)** Negatively-stained TEM image of double-band and single-band SpyCatcher-CP3 VLPs following ultra-centrifugation and concentration. Scale bar 100 nm. **(c)** Size distribution of SpyCatcher-CP3 VLP samples from TEM as measured by using FIJI Image processor (n=100).

3.6 Directed evolution 2

I decided to retry the DE with the same general protocol as DE1 (Figure 3.8a), but with a number of modifications in place. First, I transformed my library into C41(DE3) cells rather than BL21(DE3). C41(DE3) cells have better plasmid retention and are better at expressing toxic proteins (Kwon et al., 2015). I also introduced ultra-centrifugation as a second purification step after IMAC and used the harsher RNA degradation conditions. Whereas before I was adding SpyTag-HaloTag in a 1:1 molar ratio to SpyCatcher-CP3 monomers, I now used a 0.5:1 ratio to ensure more efficient TEV cleavage of well-formed VLPs with multiple anchor points to the HaloLink beads.

The library I created for the DE2 was approximately 10^7 cfu and was transformed into commercial electro-competent BL21(DE3) cells of competency 10^9 cfu/µg. The results from the first three rounds of the evolution seemed promising: the total purified protein increased from round to round in a trend that would be expected if improved variants in the library were becoming enriched (Figure 3.11a). To analyze what was happening on a genetic level, I sequenced $\sim$ 10 variants after round 2 and round 3 of the evolution. A number of the sequenced variants had silent mutations. A sequence alignment of the variants is shown in Figure 3.11c. The location of mutations that appeared in both round 2 and round 3 are highlighted in the PyMOL structure of one coat protein (Figure 3.11b). To check the assembly characteristics of the variants, I individually expressed some of the variants from round 2 and round 3. Disappointingly, none of the variants expressed better than the wild-type and the majority of the protein was seen by SDS-PAGE to be unassembled monomeric protein (Figure 3.11d). Even in cases where a faint HMW band was present (for example variant 2.2.8), analysis by DLS showed no peak of VLP size (Figure 3.11e). Out of all the variants I individually expressed and tested from both round 2 and round 3, only one variant seemed to form VLPs as seen by DLS (2.2.7) (Figure 3.11e). Thus, I concluded that even with the modifications and optimization of the methodology the directed evolution was still not selecting successfully for improved SpyCatcher-CP3 variants.

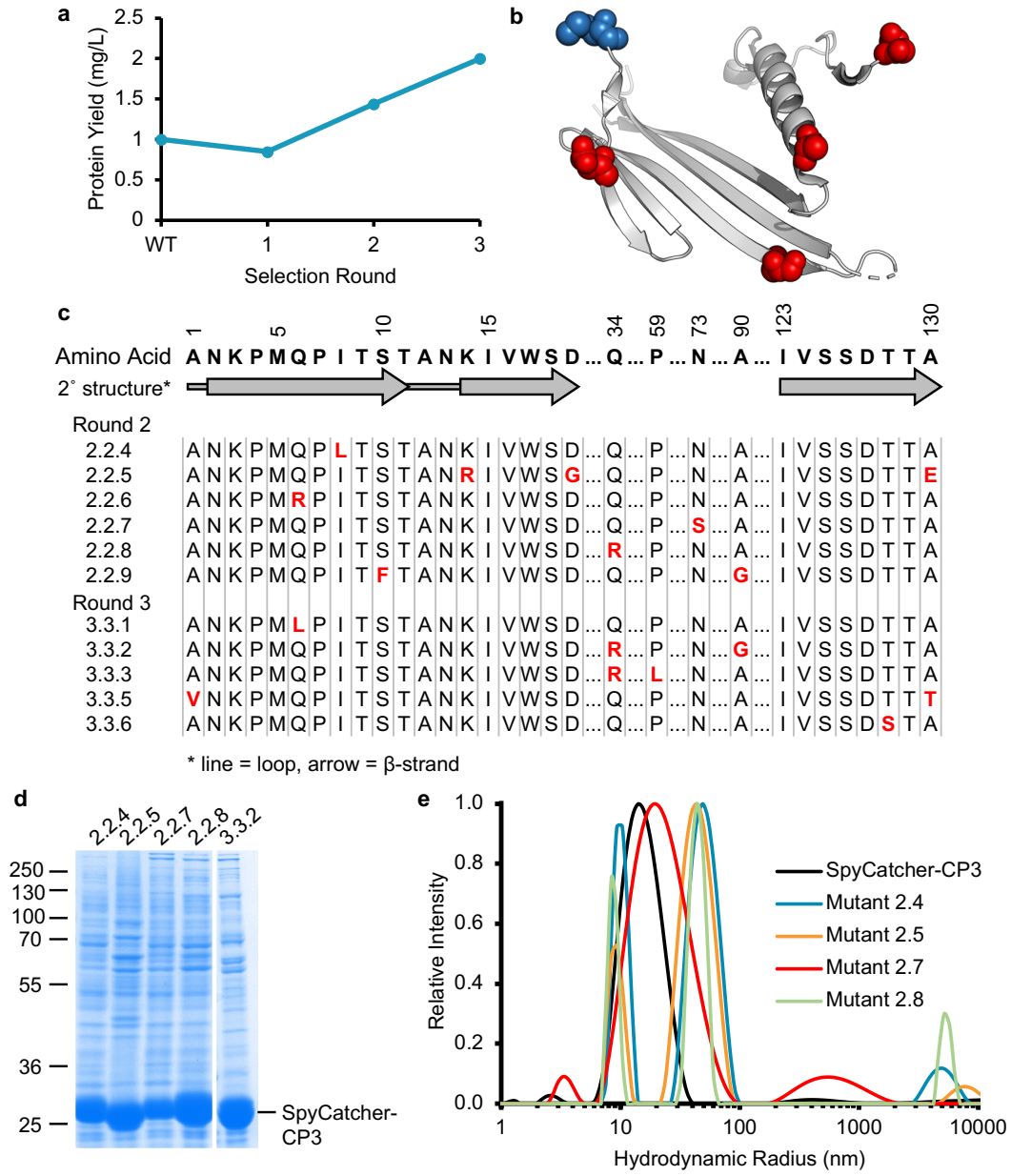


Figure 3.11. Results from directed evolution 2. **(a)** Purified protein yield (mg/L culture) as a function of selection round. Protein was quantified by BCA assay following IMAC elution and ultracentrifugation. **(b)** Monomer of AP205 cp3 (5JZR) with mutations appearing in both rounds shown in red. N-terminus in blue. **(c)** Alignment of SpyCatcher-CP3 to sequenced variants from round 2 and round 3. Mutations shown in red. No variant had more than three mutations and a number had silent mutations (not shown). **(d)** SDS-PAGE analysis of some IMAC purified mutants from round 2 and round 3 compared to WT SpyCatcher-CP3. Protein yield, purity, and ratio of assembled VLP to monomer is not improved in mutants compared to WT. **(e)** DLS analysis of WT SpyCatcher-CP3 compared to variants from round 2.

3.7 VLP assembly and disassembly

The optimized methodology for DE2 had failed to efficiently select for improved variants of SpyCatcher-CP3 as seen by SDS-PAGE and DLS analysis of individual variants. Although I initially began investigating further optimizations to the methodology (for example, heat-promoted aggregation, increasing selection pressure, changing the evolution aim), analysis by DLS revealed new information that indicated the SpyCatcher-CP3 VLP may be unsuitable for evolution. First, I discovered that VLPs could assemble from SpyCatcher-CP3 monomers slowly over time. For example, although the initial DLS trace of variant 2.2.4 showed scattered peaks, after 3 weeks incubation at 4 °C, the DLS trace changed drastically (Figure 3.12). The DLS trace after the prolonged incubation indicated the formation of new particles in the size range expected for SpyCatcher-CP3 VLPs.

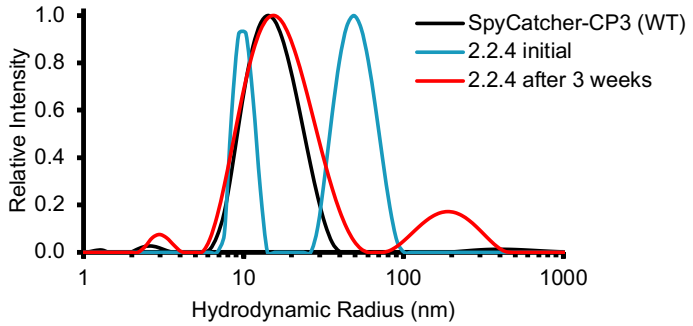


Figure 3.12. A variant from the evolution showed assembly over time. Variant 2.2.4 from the evolution showed assembly into VLP as analyzed by DLS after incubation at 4 °C for 3 weeks. A DLS trace of wild-type SpyCatcher-CP3 VLPs (black) shown for comparison.

If SpyCatcher-CP3 VLPs could assemble over time, I hypothesized that these VLPs could also disassemble once already assembled. From different expression and purifications I had seen a high degree of heterogeneity in the VLP batches by DLS (Figure 3.13). Although all these VLPs were purified in the same way and stored in the same buffer (50 mM glycine, 25 mM sodium citrate, pH 8.5), the average hydrodynamic radius varied between 15.9 ± 6.05 nm to 20 ± 9.9 nm. However, while I knew that the SpyCatcher-CP3 VLPs were often heterogeneous, I was not sure if the particles could change once formed.

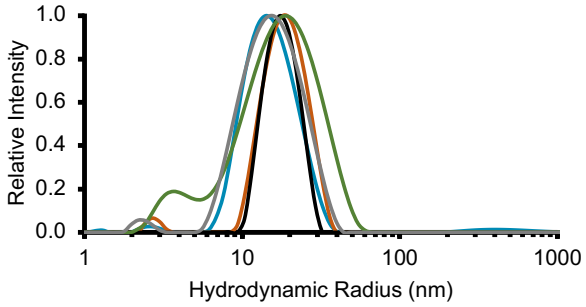


Figure 3.13. SpyCatcher-CP3 VLP sizes varied widely under the same purification and storage conditions. Different DLS traces are shown from unique SpyCatcher-CP3 VLP preparations, all purified in the same way and stored in the same buffer (50 mM glycine, 25 mM sodium citrate, pH 8.5). Average size and DLS trace varied widely depending on the VLP batch.

There are many examples in the literature of salt conditions being crucial to viral nanoparticle stability (Khudyakov and Pumpens, 2015). However, depending on the VLP, salt can have either a stabilizing (McCarthy et al., 1998), or a destabilizing effect (Chen et al., 2015).

As an initial crude experiment, I decided to try and trigger assembly/disassembly by changing the salt concentration of the VLP buffer. An IMAC-purified batch of SpyCatcher-CP3 was buffer exchanged into the standard buffer (50 mM glycine, 25 mM sodium citrate, pH 8.5) with the addition of 1 M NaCl buffer. The particles were assayed by DLS and found to be 27.8 $\pm$ 4.9 nm, much larger in standard buffer preparations (Figure 3.14). When I restored the VLPs to the normal buffer through another round of dialysis, the size of the particles changed to 20 $\pm$ 8 nm (Figure 3.14).

This experiment alone cannot prove that SpyCatcher-CP3 VLPs are subject to reversible disassembly/assembly. However, considering the negative results from the two DEs, and the general heterogeneity and instability of SpyCatcher-CP3 VLPs, I questioned whether the genotype-phenotype relationship of the VLPs was consistent. The evidence suggested that rather than evolving CP3, using a more robust particle for plug-and-display immunization could be a more successful route to creating a modular vaccine platform.

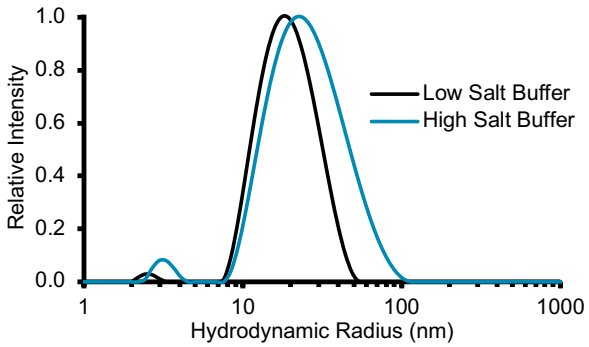


Figure 3.14. SpyCatcher-CP3 VLP size changed after dialysis into a high-salt buffer. SpyCatcher-CP3 VLPs in 1 M NaCl, 50 mM glycine, 25 mM sodium citrate at pH 8.5 were dialyzed to remove the salt. Hydrodynamic radius was measured by DLS before and after buffer exchange.

3.8 Discussion

Directed evolution is a valuable and widespread technique in the biological sciences. However, although the principles of a successful evolution are well understood, designing an evolution is complicated. In this chapter, I describe two attempted evolutions of SpyCatcher-CP3 VLPs. In both cases, I was trying to evolve the VLP to find a more soluble and high yielding protein. In both cases, I failed to successfully select for a better version of the original protein. There are a number of aspects of the evolution procedure which may account for this result.

Although the genetic diversity and library size could have been fine-tuned, another problem in the evolution was the model capture and enrichment strategy. From the beginning, the use of magnetic beads to capture biotinylated-SpyTag:SpyCatcher-VLPs was problematic. Non-specific interactions between the streptavidin coated beads seemed to entrap CP3 VLPs strongly (i.e. washing, shaking, and blocking did not have a significant effect). Although I initially hypothesized that it might be the surface of the beads themselves, when I tried streptavidin resin the same problem was seen. The interaction between streptavidin and biotin is a non-covalent interaction with high specificity (Chivers et al., 2011). However, perhaps the highly repetitive clusters of SpyCatcher on the surface of the VLPs non-specifically interacted with streptavidin. Previous use of the streptavidin coated beads

to capture SpyCatcher-phage variants had found the use of a glycine pH 2 wash crucial for getting rid of non-specifically bound species (Keeble et al., 2017). However, SpyCatcher-CP3 VLPs dissociate at low pH. Thus, the washes I was able to use were limited. When I switched to using the HaloTag-HaloLink bead capture system, the selectivity improved but I still had non-specific binding. Had the selection pressure been very strong, this might not have been a problem, as a stronger selection eliminates poorer variants. However, under the expression and purification conditions I was using, both wild-type and non-VLP forming recombinant protein were co-purified. Thus, the combination of mild selection pressure and a leaky model enrichment/capture step may have overwhelmed the evolution. It is possible that attempting an evolution of AP205 VLPs under conditions that avoid the use of magnetic bead capture or that have a harsher selection pressure (for example evolving for stability at low pH) would yield more successful variants.

However, even if all these elements of the evolution had been optimized further, it is impossible to run an evolution without a genotype-phenotype correlation. This was one of the very first things I attempted to address with the experiment involving co-purifying VLPs in the presence of sfGFP (3.3.2). Although this initial experiment indicated that foreign RNA was excluded from the interior of the VLPs, there are a number of factors I did not consider at the time. First of all, SpyCatcher-CP3 VLPs may disassemble/re-assemble during other points in the evolution. The experiment with SpyCatcher-sfGFP RNA only tested VLP encapsulation during purification. Furthermore, even if the VLPs had been in dynamic equilibrium in the presence of the sfGFP RNA it is possible that they would exhibit stronger preference for their cognate RNA, thus excluding the sfGFP RNA.

The pathway and interactions that govern coat protein (CP) assembly in VLPs is complex and varies from VLP to VLP. Both CP-CP and CP-cargo (most often negatively charged RNA) interactions are important (Maassen et al., 2018). Interestingly, depending on the solution conditions (i.e. pH) the importance of one type of interaction may predominate over the other (Maassen et al., 2018). Concentration and stoichiometry are also impor-

tant components that impact assembly and the interaction between coat proteins and RNA (Faivre-Moskalenko et al., 2014; Zandi and van der Schoot, 2009). For ssRNA phage, electrostatic interactions between the positive charges of the CP and negative charges on ssRNA drive spontaneous self-assembly (Pumpens et al., 2016; van der Holst et al., 2018). There are many examples of VLPs packaging heterologous nucleic acids and even packaging heterologous RNA more efficiently than the cognate viral RNA (Pascual et al., 2017; Cadena-Nava et al., 2012; Comas-Garcia et al., 2012; Patel et al., 2017). For many ssRNA phage, distinct packaging signals (PS) in the RNA have been found that interact with coat proteins and help explain the specificity of RNA packaging despite the abundance of mRNA in the cytosol (Rolfsson et al., 2016; Patel et al., 2017). However, no specific RNA-protein interactions have been discovered for AP205 (Klovins et al., 2002; Shishovs et al., 2016). Additionally, based on cryo-EM reconstructions, it appears that the RNA inside AP205 may interact less tightly than other known ssRNA phages (Shishovs et al., 2016). This may be at the root of some of the difficulties seen during the evolution. One can imagine that even if the coat proteins of SpyCatcher-CP3 have a weak preference for their own RNA, in the context of the evolution many mutated RNA sequences could have similar binding affinities and could mix with other coat proteins during disassembly and reassembly. Additionally, the CP3 coat protein sequence I was working with had been codon-optimized by Karl Brune. Although RNA was still being packaged, if the affinity of this packaging was weakened, the genotype-phenotype relationship may have become further exacerbated during the evolution. That being said, it is interesting that essentially no mutations were observed in the β-sheets which line the inside of the VLP and are points of contact with the RNA. This brings up a general limitation of the evolution: if better VLPs formed but had mutations that hindered RNA from binding, they would never get detected. In general, it would have been advantageous to deep-sequence the libraries at different rounds of the evolution to get a better sense of what was happening on a global genetic level.

SpyCatcher-CP3 VLP disassembly could have been studied in greater detail. In the buffer

exchange experiment on SpyCatcher-CP3 VLPs, I used only DLS to measure VLPs before and after changing the ionic strength of the solution (Figure 3.14). DLS is a quick method of assessing nanoparticles but is known to have limitations (Hinterwirth et al., 2013). DLS can be misleading when measuring non-monodisperse solutions, since large particles scatter light more and will thus hide the presence of smaller particles. As well, the presentation of DLS data (either by size, number, or intensity), can skew the distribution curve. Thus, when it comes to characterizing nanoparticles, the consensus is that a combination of methods will always give a more reliable measurement than DLS alone (Hinterwirth et al., 2013; Fissan et al., 2014; Mahl et al., 2011). Throughout my work with SpyCatcher-CP3 I could have employed TEM in greater frequency to characterize the VLP assembly state after various manipulations. In the case of the buffer exchange, it would have been interesting to perform the same experiment in the presence of benzonase and then visualize RNA packaging in VLPs by agarose gel. If the VLPs really were disassembling, the RNA should be unprotected at times and thus degrade. This experiment could provide more evidence that SpyCatcher-CP3 VLPs disassemble and assemble. More sophisticated characterization of SpyCatcher-CP3 VLP assembly and stability would also have been possible. For example, a recent paper was able to study the disassembly and assembly of the parvovirus minute virus of mice (MVM) VLP *in vitro* by using a combination of TEM and high-resolution atomic force microscopy (AFM) (Medrano et al., 2016). Characterizing the profile of recombinant AP205 VLP formation more completely will help guide future optimization experiments. A combination of computational techniques and rational engineering may also provide an alternate route for improving SpyCatcher-CP3 VLPs.

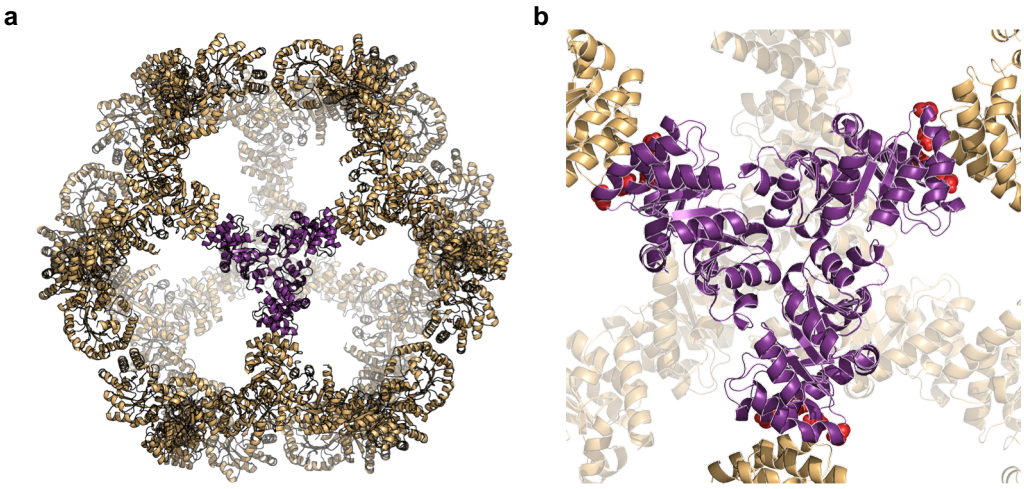
Chapter 4

Characterization of SpyCatcher-MI3 as a vaccine scaffold

4.1 Chapter Introduction

Virus-like particles (VLPs) are the basis of many current licensed vaccines (López-Sagaseta et al., 2016). However, there is also great interest in the field of bionanotechnology to develop alternative multimerization platforms that may have the advantage of stability, ease of scale up, and fine-tunable properties like antigen orientation and valency. Examples of non-protein platforms include gold nanoparticles and liposomes (Irvine et al., 2015; Smith et al., 2015). Other interesting research has focused on using coiled-coils (Brune et al., 2017; Li et al., 2016), or exploiting non-viral protein cages like vault particles and ferritin (Rother et al., 2016; Karch and Burkhard, 2016).

In the previous chapter I described an attempt to improve the solubility/yield of SpyCatcher-AP205. SpyCatcher-AP205 proved the feasibility of creating plug-and-display modular vaccine platforms but the VLP had limited potential for industrial or clinical application. In this chapter, I describe the development of a new vaccine scaffold based on a computationally designed nanoparticle that overcomes many of the limits seen in AP205.



c

KDPG Aldolase	1	MKMEELFKKHKIVAVLRANSVEEAKEKALAVFEGGVHLIEITFTVPDADTV	51
I301	1	MKMEELFKKHKIVAVLRANSVEEAKKALAVFLGGVHLIEITFTVPDADTV	51
KDPG Aldolase	52	IKELSFLKEKGAIIGAGTVTSVEQCRKAVESGAEFIVSPHLDEEISQFCKE	102
I301	52	IKELSFLKEMGAIIGAGTVTSVEQCRKAVESGAEFIVSPHLDEEISQFCKE	102
KDPG Aldolase	103	KGVFYMPGVMTPTELVKAMKLGHTILKLFPGEVVGPQFVKAMKGPFPNVKF	153
I301	103	KGVFYMPGVMTPTELVKAMKLGHTILKLFPGEVVGPQFVKAMKGPFPNVKF	153
KDPG Aldolase	154	VPTGGVNLDNVCEWFKAGVLAVGVGSALVKGTPDEVREKAKAFVEKIRGCTE	205
I301	154	VPTGGVNLDNVCEWFKAGVLAVGVGSALVKGTPVEVAEKAKAFVEKIRGCTE	205

Figure 4.1. I3-01 forms a hollow dodecahedral protein nanocage after mutations at key interface residues. (a) The 60-meric I3-01 protein scaffold is shown with a trimer coloured in purple (based on the designed structure PyMOL file). **(b)** A close-up of one I3-01 trimer with the mutations at each interface shown in red. **(c)** Alignment of amino acid sequences for *Thermotoga maritima* KDPG aldolase and I3-01. Mutations shown in red.

The particle we chose to work with is one of a number of synthetic protein cages computationally designed by David Baker and his team of scientists at the University of Washington (Bale et al., 2016; Hsia et al., 2016; King et al., 2012, 2014). Their method builds on the observation that multi-protein assemblies in nature form symmetrical structures that involve key interactions between repeated subunit building blocks. In one example, Hsia et al. took trimeric protein building blocks, arranged them into the desired higher order symmetric architecture, and used computational analysis to design low energy protein-protein interfaces to promote close packing and assembly (Hsia et al., 2016). The modified genes were then

expressed in *E. coli* and experimentally validated for assembly.

One such designed protein, I3-01, was found to form a dodecahedral 60-subunit assembly (Figure 4.1a). I3-01 is based on a KDPG (2-dehydro-3-deoxy-phosphogluconate) aldolase from the hyperthermophilic bacterium *Thermotoga maritima* (Griffiths et al., 2002). There are five mutations in I3-01 at the interface between trimers including four non-polar mutations (E33L, L61M, N187V, R190A) and E26K (Figure 4.1b,c).

I3-01 is an attractive nanoparticle for vaccine scaffold technology. The N-terminus is surface exposed and thus provides a point for SpyCatcher fusion and further particle functionalization (Figure 4.2a). The particle also has a diameter of 25 nm which is similar to many VLPs and is optimal for direct draining to lymph nodes, a crucial aspect of stimulating a good immune response (Bachmann and Jennings, 2010).

In this chapter, I will describe the development of SpyCatcher-MI3, a vaccine scaffold based on the rational engineering of I3-01 to minimize its propensity to aggregate. I show that SpyCatcher-MI3 is stable to high temperature, freezing, and lyophilization, is highly soluble, and can be produced simply and in high-yield from *E. coli*. I also validate its reactivity and conjugation efficiency and its ability to raise antibody titers with high avidity against a blood-stage malarial antigen.

4.2 Production of SpyCatcher-MI3

To begin the investigation of the suitability of I3-01 for vaccine technologies, the I3-01 gene was synthesized by Genscript and then cloned into a pET28 expression plasmid. All cloning was performed by Dr. Anne-Marie Andersson. The initial construct had the organization N-terminal His_6, GSG spacer, ΔN1-SpyCatcher, (GGS)4 spacer, I3-01. Initial expression in *E. coli* and subsequent purification using Ni-NTA ran into difficulties arising from protein aggregation in cell lysate. A double band in the purified SpyCatcher-I301 protein by SDS-PAGE that was reduced to a single band upon addition of reductant led to the hypothesis

that the aggregation was caused by inter-molecular disulfide bonds. To mediate this problem two mutations were introduced in surface-exposed cysteines C76A and C100A, creating a mutated-I3-01 that is hitherto referred to as MI3 (Figure 4.2a). The constructs were further altered by the replacement of the N-terminal His-Tag with a C-terminal C-tag (EPEA). A His_6 tag was initially used since the PyMOL structure indicated that the C-terminus is internally oriented and thus it was not clear if protein capture by C-tag resin would be feasible. However, C-tag allows for more efficient downstream processing for vaccine applications and was therefore installed for testing (Jin et al., 2017). In total, four different constructs were cloned as potential vaccine scaffolds and a schematic of their sequence organization as well as their name identifiers are shown in Figure 4.2b. Since a monomer of SpyCatcher-MI3 is ~34 kDa the 60-mer is expected to have a molecular weight (Mw) of 2.0 MDa (60×34 kDa = 2.0 MDa). Not only were C-tagged proteins captured by Capture Select C-Tag Affinity Matrix but further purification by size-exclusion chromatography showed a major peak eluting in the expected megadalton range for all four proteins, indicating nanoparticle assembly (Figure 4.2c).

Following the initial cloning the first thing I did was set up two crude assays to assess stability of protein in solution when kept at 25 °C (room temperature) for 8 days or at 4 °C over the course of 4 weeks. At each time point the proteins were centrifuged for 30 min at high speed and the amount of protein in the soluble fraction measured by BCA assay. The amount of protein in the soluble fraction at day 0 was defined as 100 % and subsequent values plotted as a percentage (Figure 4.3). After 8 days at 25 °C, SpyCatcher-MI3 C-tag remained 100 % soluble while the remaining three proteins had experienced a reduction in soluble protein between 27-40 %. Similarly, after 4 weeks at 4 °C, 87 % of SpyCatcher-MI3 C-tag was left in the soluble fraction while the other three proteins experienced a reduction ranging from 22-70 % of the starting total. Thus, in both assays, the best performing construct (the construct that was least likely to aggregate) was SpyCatcher-MI3.

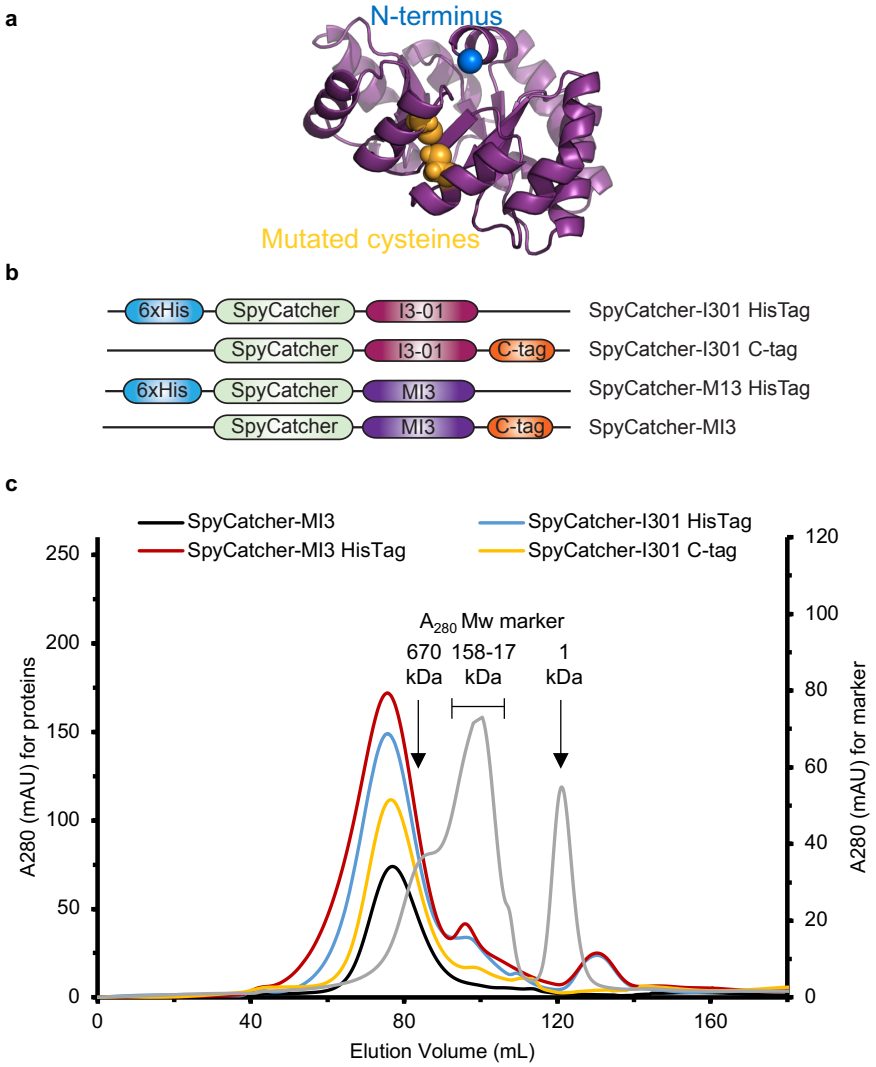


Figure 4.2. Modification of the I3-01 scaffold. **(a)** A single monomer of the I3-01 designed structure PyMOL file is shown. Two surface exposed cysteines, C76 and C100, were mutated to alanine to produce MI3. Mutations are shown in yellow and the N-terminus is highlighted in blue. **(b)** Schematic of the organization and names of the four initial nanoscaffold platform constructs. **(c)** Size-exclusion chromatography (Sephacryl S500) for determination of nanoparticle assembly by absorbance at A280 in comparison to molecular weight markers (gray line).

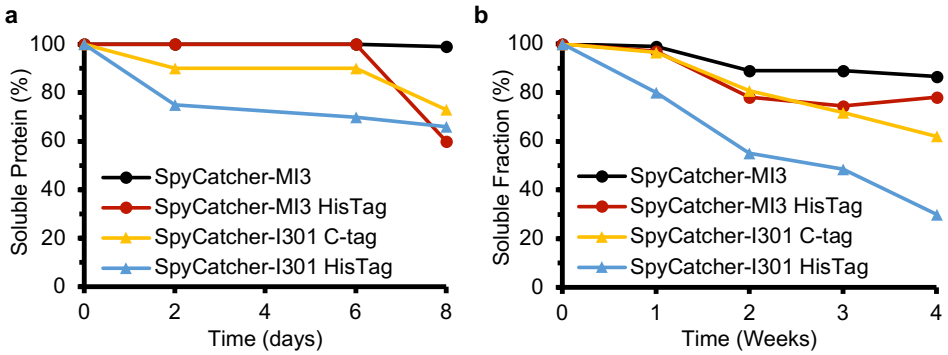


Figure 4.3. Mutations in I3-01 and the addition of C-tag improved the solubility of nanoparticles. A time course at 25 °C over eight days **(a)** and at 4 °C for 4 weeks **(b)**. At each time point soluble protein was quantified by BCA assay after centrifugation for 30 min at 16.9 $\times g$ to remove aggregates. Protein in soluble fraction at day 0 was defined as 100 %.

The assays also demonstrated a destabilizing effect caused by the N-terminal HisTag. At both temperatures SpyCatcher-I301 C-tag performed better than SpyCatcher-I301 HisTag and SpyCatcher-MI3 C-tag performed better than SpyCatcher-MI3 HisTag. Since installing the C-tag was beneficial for the particles, as well as being preferred for vaccine purposes, I continued my characterization of the effects of the cysteine mutations by comparing SpyCatcher-I301 C-tag with SpyCatcher-MI3 C-tag. By SDS-PAGE the double band that was seen in the I301 version of the purified protein was not present in MI3 (Figure 4.4a). I also expressed and purified SpyCatcher-MI3 under the same conditions as SpyCatcher-I301 and the yield of SpyCatcher-MI3 was 2-fold higher (n=3) (Figure 4.4b). The mutations also helped eliminate the aggregation that I saw in SpyCatcher-I301 by DLS after 5 weeks of storage (Figure 4.4c).

The studies showed that SpyCatcher-MI3 C-tag was the most desirable construct in terms of stability, yield, and solubility. In particular, the yield for SpyCatcher-MI3 (23 mg/L) was 10-fold higher than for SpyCatcher-AP205 and around the maximum our lab achieves for soluble protein in shake-flask *E. coli* culture. Thus, all further experiments employed SpyCatcher-MI3 C-tag which will hitherto be referred to just as SpyCatcher-MI3.

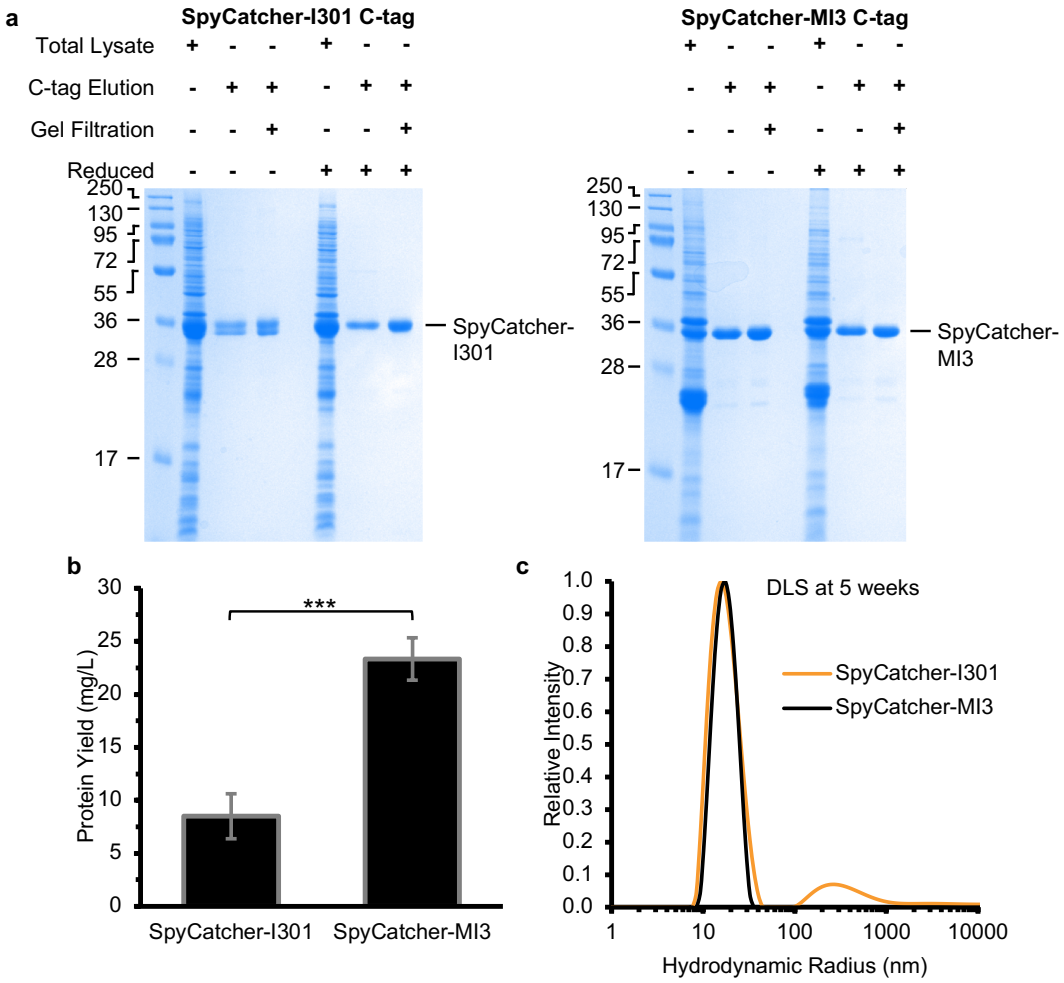


Figure 4.4. SpyCatcher-MI3 was high yielding and less prone to aggregation than SpyCatcher-I301. **(a)** MI3 increased the uniformity of the purified protein. Induction and purification gel, showing the elimination of the unwanted dimer in SpyCatcher-MI3, by SDS-PAGE with Coommassie staining. **(b)** MI3 enhanced nanoscaffold yield. Purified protein yield (mean ± 1 s.d., n=3) was compared for SpyCatcher-MI3 and SpyCatcher-I301. A Student's unpaired t-test was used to compare yields ($p = 0.0006$). *** $p < 0.001$. **(c)** SpyCatcher-MI3 showed greater stability to aggregation. SpyCatcher-I301 or SpyCatcher-MI3 were stored for 5 weeks at 4 °C and analyzed by DLS.

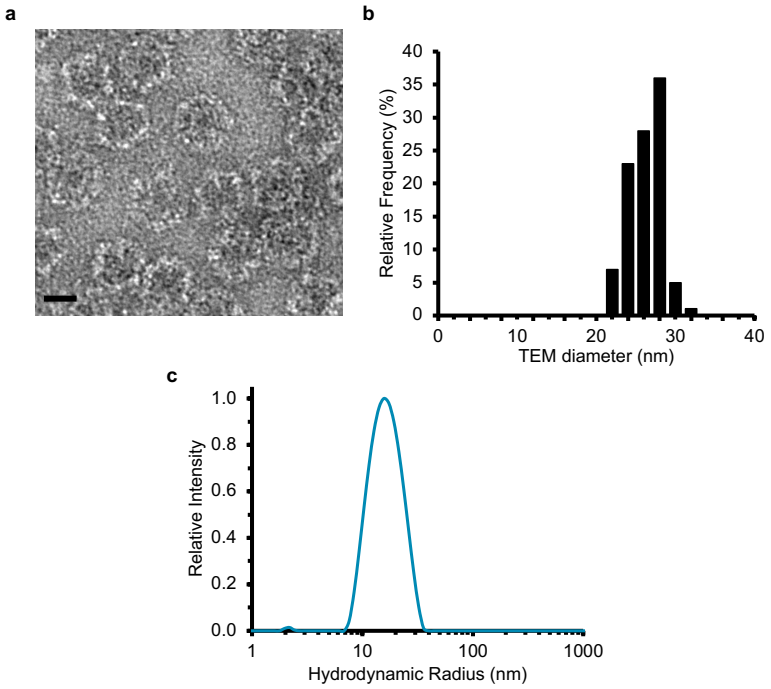


Figure 4.5. SpyCatcher-MI3 assembles into well-formed particles. (a) Negatively-stained TEM image of SpyCatcher-MI3 nanoparticles. Scale bar 25 nm. **(b)** Size distribution of SpyCatcher-MI3 nanoparticles from TEM (n = 100). **(c)** Dynamic light scattering (DLS) determination of hydrodynamic radius (R_h) of SpyCatcher-MI3.

4.3 Pushing the limits of SpyCatcher-MI3

4.3.1 Biophysical characterization

A particularly important criterion that determines a vaccine's ability to transition into the clinical setting is being able to ensure purity, composition, and uniformity of the vaccine formulation from batch to batch (Effio and Hubbuch, 2015). Thus, I looked to characterize SpyCatcher-MI3 in depth.

By negative-stained transmission electron microscopy (TEM) the presence of well-formed symmetrical dodecahedral particles was observed (Figure 4.5a). Size determination from TEM by manual measurement using ImageJ gave a particle diameter of 26 ± 2.0 nm (Figure 4.5b). Analysis by DLS also showed a uniform peak indicating an average hydrodynamic radius of 16.8 ± 5.7 nm (Figure 4.5c).

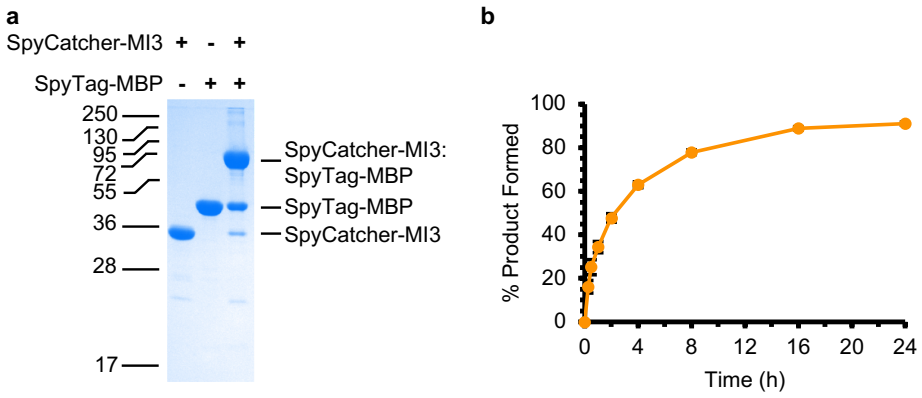


Figure 4.6. SpyCatcher-MI3 reaction with model protein partner SpyTag-MBP. **(a)** Conjugation was performed with SpyCatcher-MI3 in a 1:3 ratio with SpyTag-MBP at 25 °C for 16 h, followed by analysis on SDS-PAGE with Coomassie staining. **(b)** Conjugation was performed with SpyCatcher-MI3 in a 1:3 ratio with SpyTag-MBP at 25 °C for the indicated time, followed by analysis on SDS-PAGE with Coomassie staining. Values are the mean of triplicate ± 1 s.d. The reaction half-time is just under 2 h.

4.3.2 Reactivity and conjugation of particle

To initially validate SpyCatcher-MI3 reactivity, I used the model protein SpyTag-MBP. Upon mixing with SpyTag-MBP in 3× molar excess for 16 h, a clear band shift was observed by SDS-PAGE, indicating covalent bond formation (Figure 4.6a). A reaction time-course indicated that the reaction proceeded to 91 % completion after 16 h and further incubation (up to 24 h) did not increase conjugation (Figure 4.6b). The reaction half-time was just under 2 h. SpyTag-MBP is ∼ 45 kDa and complete conjugation is likely hindered by steric constraints on the surface of the nanoparticle.

After observing that SpyCatcher was functional and reactive on the surface of MI3, I decided to try conjugation with more challenging proteins of immunological relevance. Three SpyTagged antigens against malaria were tested: SpyTag-CIDR (cysteine-rich interdomain region), Pfs25-SpyTag, and CyRPA-SpyTag (cysteine-rich protective antigen) (Figure 4.7a-c). The CIDR protein domain is one of two domain types found on the extracellular portion of the variable *Plasmodium falciparum* erythrocyte membrane protein-1 family (PfEMP1) (Lau et al., 2015). PfEMP1 proteins are expressed on the surface of infected erythrocytes

and bind different human endothelial receptors to avoid spleen-mediated clearance and to further propagate the infection (Lennartz et al., 2017). The CIDR domain specifically binds to the endothelial protein C receptor (EPCR) and this interaction correlates with severe childhood malaria (Bernabeu and Smith, 2017; Jespersen et al., 2016). Pfs25 is a small protein that localizes to the surface of zygotes and ookinetes in the mosquito midgut during sexual-stages of the malaria parasite lifecycle (Kaslow et al., 1988). Pfs25 is a leading malaria transmission-blocking antigen that has shown promise in previous vaccine trials (Nikolaeva et al., 2015; Li et al., 2016; Talaat et al., 2016). CyRPA is a malaria blood-stage antigen that has a role during merozoite invasion of erythrocytes. A previous study showed that Abs raised against CyRPA were able to prevent merozoite invasion both *in vitro* and *in vivo* (Dreyer et al., 2012).

These three antigens all contained disulfide bonds (4 in CIDR, 5 in CyRPA, and 11 in Pfs25). The antigens were expressed in either *E. coli* (SpyTag-CIDR) or mammalian cells (CyRPA-SpyTag and Pfs25-SpyTag), and had SpyTag conjugated to either the N-terminus (CIDR) or the C-terminus (CyRPA and Pfs25). After reaction for 16 h at 25 °C, conjugation efficiency was determined by quantification via SDS-PAGE. The conjugation efficiency was $\sim$ 95 % for all the malaria antigens (Figure 4.7e).

Since SpyCatcher-MI3 had shown itself to be very reactive, I was interested to see if it could be functionalized while still in cleared lysate. Being able to conjugate nanoparticles while avoiding purification of one or both partners would greatly streamline assembly and reduce time and cost of vaccine production. To this end, I added purified SpyCatcher-mClover3 to cleared lysate expressing SpyCatcher-MI3. After reaction for 16 h I was able to see depletion of the SpyCatcher-MI3 band and formation of the conjugate SpyCatcher-MI3:SpyTag-mClover3 by SDS-PAGE both by fluorescent imaging and Coomassie staining (Figure 4.8). This result, as well as my previous trials with malaria antigens showed that SpyCatcher-MI3 reacted efficiently with antigens of varying size, from different expression hosts, and with varying SpyTag placement, and was even able to react with antigens while

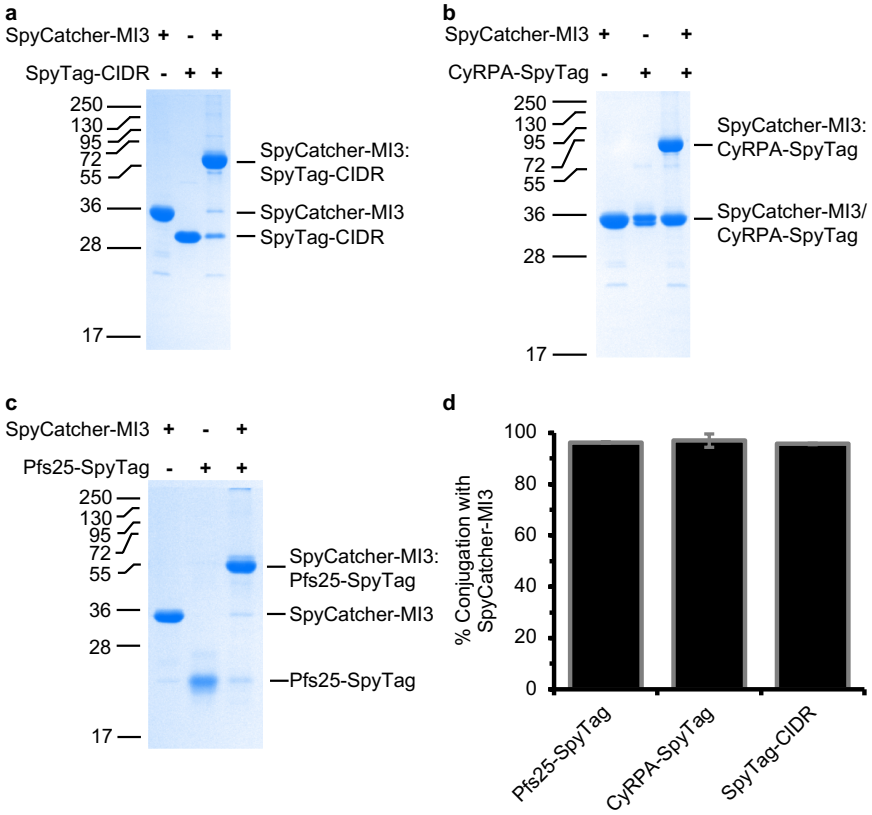


Figure 4.7. SpyCatcher-MI3 nanoparticles efficiently reacted with a variety of antigens. Conjugation was performed with SpyCatcher-MI3 in a 1:3 ratio with antigen at 25 °C for 16 h, followed by analysis on SDS-PAGE with Coomassie staining. **(a)** SpyTag-CIDR. **(b)** CyRPA-SpyTag **(c)** Pfs25-SpyTag. **(d)** Coupling efficiency of SpyCatcher-MI3 with antigens, quantified by SDS-PAGE with Coomassie staining. Values are the mean of triplicate ± 1 s.d. Some error bars too small to see.

in cleared lysate.

4.3.3 Robustness

After confirming the reactivity of the SpyCatcher-MI3 nanoparticles, I turned my attention to investigating their stability. Since vaccines often travel long distances to reach their destination their tolerance to a variety of conditions is necessary to ensure a viable end product (Preiss et al., 2016). Efforts in the vaccine field have focused on establishing a cold chain to preserve vaccines from manufacture to injection. However, the cold chain is difficult to maintain (this includes temperatures dropping too low as well as too high), particularly

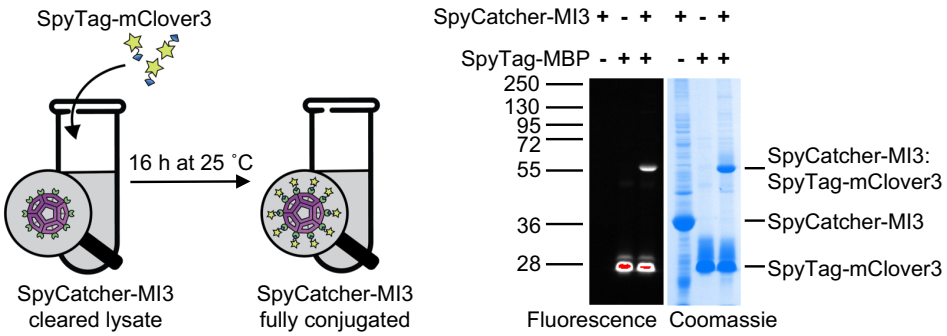


Figure 4.8. SpyCatcher-MI3 can be functionalized directly in lysate. Purified antigen (SpyTag-mClover3) was added directly to cleared lysate from *E. coli* expressing SpyCatcher-MI3 and incubated for 16 h at 25 °C. The cleared lysate was then analyzed via SDS-PAGE (samples were not boiled) by fluorescence (left) followed by Coomassie staining (right).

when vaccines must be delivered to remote, rural locations (Kumru et al., 2014; Hanson et al., 2017). Thus, in the clinical setting, there is an important need for robust vaccines that maintain their integrity despite heating, freezing, or long-term storage (Chen et al., 2009).

To test the effect of freezing on the nanoparticle scaffold, I subjected SpyCatcher-MI3 to multiple rounds of freeze-thawing. After four rounds of freeze-thaw at -80 °C approximately 85 % of protein was left in the soluble fraction. However, adding trehalose, a commonly used sugar stabilizer (Jain and Roy, 2010), minimized the aggregation and resulted in only a 3 % loss of protein after an equivalent four rounds of freeze-thaw (Figure 4.9a). Multiple rounds of freeze-thaw also did not impair the reactivity and conjugation efficiency of SpyCatcher-MI3 (Figure 4.9b) and the particles retained their shape as confirmed by DLS (Table 4.1).

I then tested whether or not SpyCatcher-MI3 could withstand lyophilization. Lyophilization of proteins is advantageous for a number of reasons, including minimizing storage space and energy costs during transportation (Matejtschuk, 2007). A sample of SpyCatcher-MI3 was lyophilized and then reconstituted in the same volume of buffer after 24 h. No protein in the soluble fraction was lost to lyophilization (Figure 4.9c) nor was the reactivity affected as analyzed by SDS-PAGE (Figure 4.9d). The particles also maintained their shape as seen

by DLS (Table 4.1).

I also wanted to investigate the thermoresilience of SpyCatcher-MI3, especially considering the hyperthermophilic origin of the aldolase that serves as the basis for MI3. I took purified SpyCatcher-MI3 and incubated the sample for 1 h in temperatures ranging from 25 to 95 °C. Samples were then spun at 16.9 $\times g$ for 30 min before determining protein % remaining in soluble fraction. Up to 75 °C, at least 80 % of protein remained in the soluble fraction, although interestingly the protein seemed to be more aggregation prone at 55 °C than at 75 °C (Figure 4.9e). To make sure that protein left in the soluble fraction was still assembled, I checked the particles by DLS. Even though at 95 °C only 33 % of protein remained soluble, DLS confirmed a narrow peak for the protein, indicating that whatever fraction was left was still able to assemble into nanoparticles (Table 4.1).

Table 4.1. Dynamic light scattering of SpyCatcher-MI3 nanoparticles after heating, freezing, and lyophilization.

Sample	Hydrodynamic radius (nm)	Peak area (%)
Initial	17.6 ± 4.4	100
Post 4× freeze-thaw	18.1 ± 5.8	99.8
Initial	17.6 ± 4.4	100
Reconstituted post lyophilization	18.2 ± 4.8	100
Initial	16.8 ± 5.7	99.7
1 h at 95 °C	16.8 ± 4.5	99

Solubility of a protein is also a very important quality and something that was particularly lacking in the AP205 VLP platform. I found that with SpyCatcher-MI3 I was able to obtain concentrations >1 mM (36 mg/mL) and this concentration was sustained even after freezing or storage at 4 °C for 1 week (Figure 4.10).

4.4 Immunization trial

After establishing that SpyCatcher-MI3 was a robust and reactive nanoparticle, it was time to address whether or not SpyCatcher-MI3 would be a successful immunogenic platform. For the immunization trial we had two aims. First, to see whether antigen displayed on the

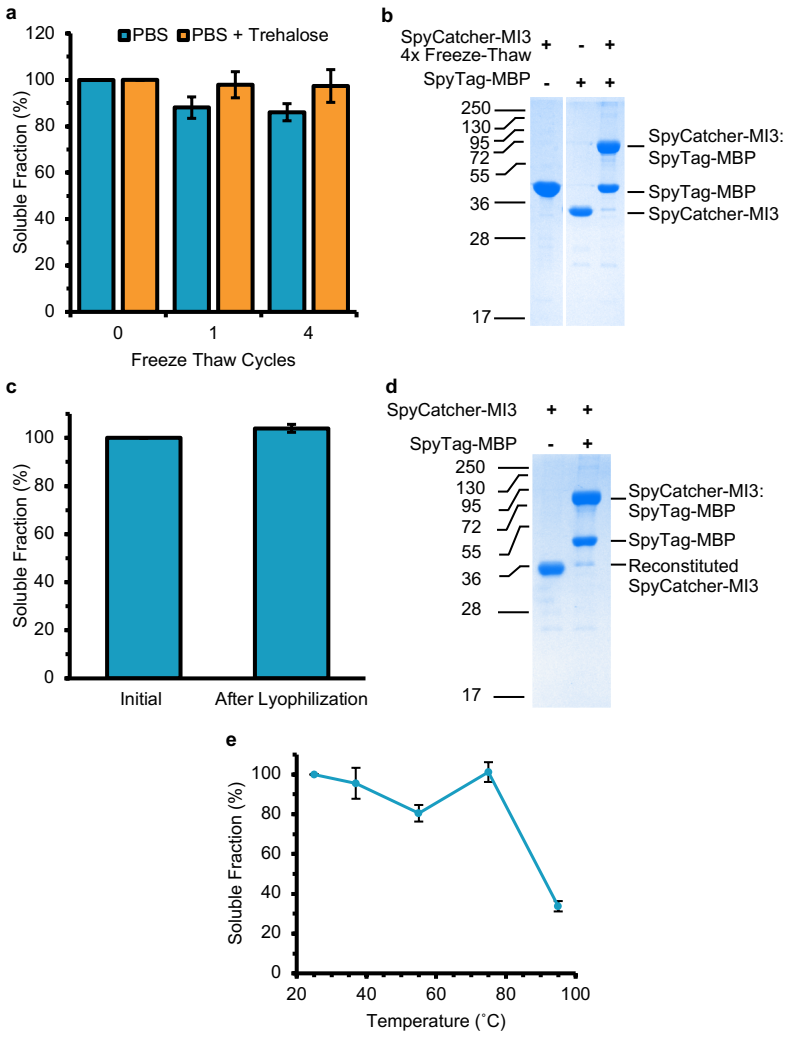


Figure 4.9. SpyCatcher-MI3 nanoparticles were robust to freezing, lyophilization, and heating. **(a)** SpyCatcher-MI3 remained soluble after freeze-thaw. Samples were centrifuged to remove aggregates and soluble protein was quantified by densitometry (mean ± 1 s.d., n = 3) after 1 or 4 cycles of freeze-thawing ± 1 M trehalose (mean ± 1 s.d., n = 3). **(b)** SpyCatcher-MI3 retained reactivity after freezing. Reaction of SpyCatcher-MI3 with SpyTag-MBP at 25 °C for 16 h was analyzed by SDS-PAGE with Coomassie staining. **(c)** SpyCatcher-MI3 soluble fraction, before and after lyophilization with reconstitution in the same buffer volume (mean ± 1 s.d., n = 3). **(d)** SpyCatcher-MI3 retained reactivity after lyophilization. Reaction of SpyCatcher-MI3 with SpyTag-MBP at 25 °C for 16 h was analyzed by SDS-PAGE with Coomassie staining. **(e)** SpyCatcher-MI3 remained soluble after high temperatures. SpyCatcher-MI3 was incubated for 1 h at the indicated temperatures and soluble protein quantified as in **(a)**. The sample held at 25 °C was defined as 100 % soluble.

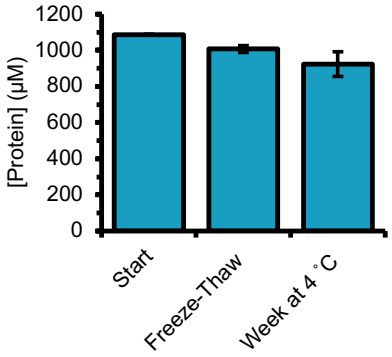


Figure 4.10. SpyCatcher-MI3 is highly soluble and stable to storage. SpyCatcher-MI3 was concentrated and stored for 1 week at 4 °C or subjected to one round of freeze-thaw. Protein concentration was assayed by BCA after spinning down sample to remove aggregates. All values are the mean of triplicate ± 1 s.d.

particle would induce more antibodies compared to free antigen. Improved immunogenicity as a result of multimerization has been seen many times in the literature (Leneghan et al., 2017; Brune et al., 2016; Jennings and Bachmann, 2008). The second aim was to see whether SpyCatcher-MI3 would be as good at stimulating an immune response as SpyCatcher-AP205, a phage-derived virus-like particle.

However, before beginning the immunization trial we were also interested in checking the MI3 sequence for similarity to human sequences since stimulating an autoimmune response would be dangerous. No ortholog of the KDPG aldolase exists in humans. Sequence alignment of MI3 against the human protein database using BLAST also did not reveal any substantial similarity, by coincidence, to a human protein (Figure 4.11). The top hit was a fragment of Interleukin-1 receptor-associated kinase 3 (IRAK3) (score 64, sequence identity 40.6 %, E-value: 9.4). For comparison the same assessment was done for ΔN1-SpyCatcher for which the top hit was a fragment of Hemicentin-2 (score: 62, sequence identity 29.7 %, E-value: 2.8). E-values of 0.1 or greater are not considered to be significant (Pearson, 2013).

For the immunization trial we decided to focus on immunizing against CyRPA, since an efficient malaria vaccine continues to be an urgent unmet global need (Healer et al., 2017; Rabinovich et al., 2017). Conjugation of CyRPA-SpyTag to SpyCatcher-MI3 and SpyCatcher-AP205 was done at 25 °C for 16 h. Free antigen was removed by vigorous dialysis

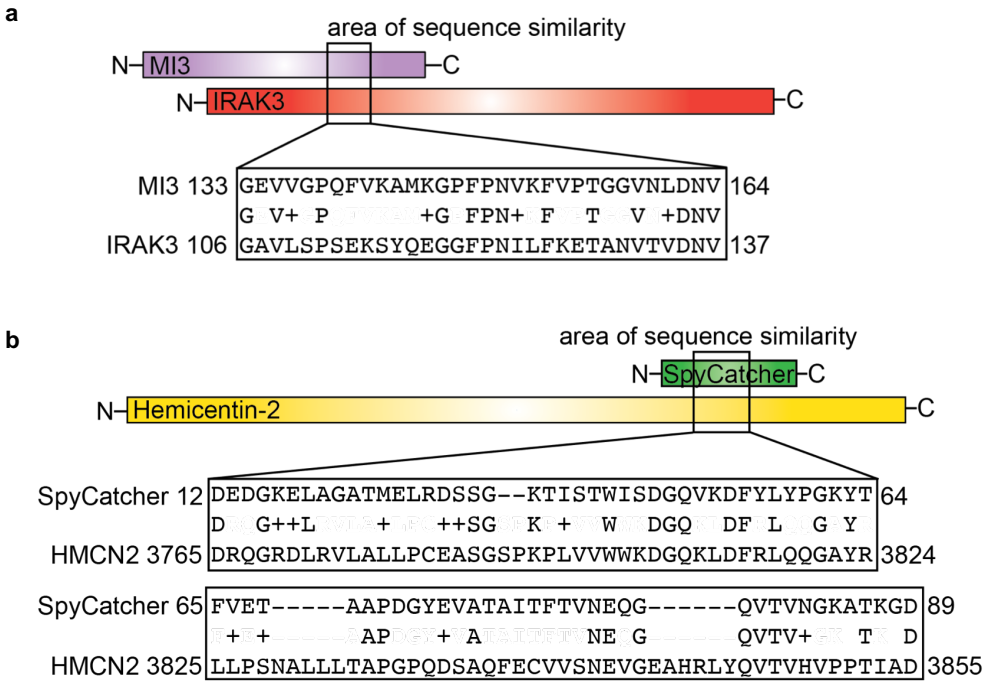


Figure 4.11. Minimal sequence similarity to MI3 or SpyCatcher in the human genome. Sequence alignment of the top hit after BLAST against the UniProtKB human database for **(a)** MI3 and **(b)** SpyCatcher.

using a high molecular weight cut-off (MWCO) membrane and conjugation was validated by SDS-PAGE (Figure 4.12a). Proper assembly of particles following conjugation to antigen was also assessed by DLS. For SpyCatcher-MI3 a small, but distinct, shift in the peak was observed between unconjugated particle (17.6 ± 4.4 nm) and conjugated particle (20.9 ± 5.8 nm) (Figure 4.12b). For SpyCatcher-AP205 a similar shift was observed following reaction with antigen from 16.2 ± 6.9 nm to 20.3 ± 6.2 nm (Figure 4.12c).

Particularly important for the vaccines was the removal of lipopolysaccharides (LPS) before injection. The presence of endotoxins in vaccines has not only been shown to be able to modulate immune responses by activating Toll-like receptor 4 (TLR4) (Wakelin et al., 2006; Tumban et al., 2013), but it can also have side-effects like endotoxin shock or death in humans, and can cause pain in animals after injection (Tateda et al., 1996; Magalhães et al., 2007). To remove endotoxin from the nanoparticle vaccines, I used a protocol based on Triton X-114 phase-separation and verified endotoxin depletion by the

LAL assay (ThermoScientific) (Aida and Pabst, 1990). All immunogens for injection had an endotoxin level of <1 EU/mL.

Injections in mice were performed by Dr.Anne-Marie Andersson. For each group (CyRPA-SpyTag alone, SpyCatcher-MI3:CyRPA-SpyTag, and SpyCatcher-AP205:CyRPA-SpyTag), 6 mice were immunized intramuscularly with 1 µg of CyRPA. The immunization schedule, involving a prime followed by a boost of the same dosage 14 days later, is shown (Figure 4.13a). All immunizations were also performed with the addition of AddaVax, which is a squalene-oil-in-water adjuvant that is based on the MF59 adjuvant currently licensed for use in influenza vaccines (Alving et al., 2012; Mbow et al., 2010; Mantile et al., 2014). Antibody titer against CyRPA was measured post-prime (day 13) and post-boost (day 27) by enzyme-linked immunosorbent assay (ELISA) (Figure 4.13b,c).

After the prime 6/6 mice in each of the nanoparticle groups had responded to the vaccine while, in comparison, only 4/6 of the mice injected with monomeric antigen showed a response (Figure 4.13b). Although the difference in titer was not significant between groups, the lack of response in 2/6 mice injected with free antigen shows that antigen alone can produce variable results. Following the boost the endpoint titer in each group was compared again. At this time point 6/6 mice in each group had a measurable antibody response. The titer in the mice immunized with the SpyCatcher-MI3 platform was significantly higher than free antigen ($p = 0.011$, $n = 6$, Kruskal-Wallis test followed by Dunn's multiple comparison post-test) (Figure 4.13c). There was no significant difference between SpyCatcher-AP205 and monomeric antigen or between AP205 and MI3 groups.

Besides quantitatively measuring antibody responses we also wanted to assay the quality of the antibodies. Thus, we looked at the avidity of the antibodies produced by each group. Antibody avidity ELISA was performed by Dr.Anne-Marie Andersson. The experiment involves displacing bound antibodies with sodium thiocyanate in increasing concentrations to determine the half-maximal inhibitory concentration (IC_{50}) of each group compared to an untreated control (Luxton and Thompson, 1990).

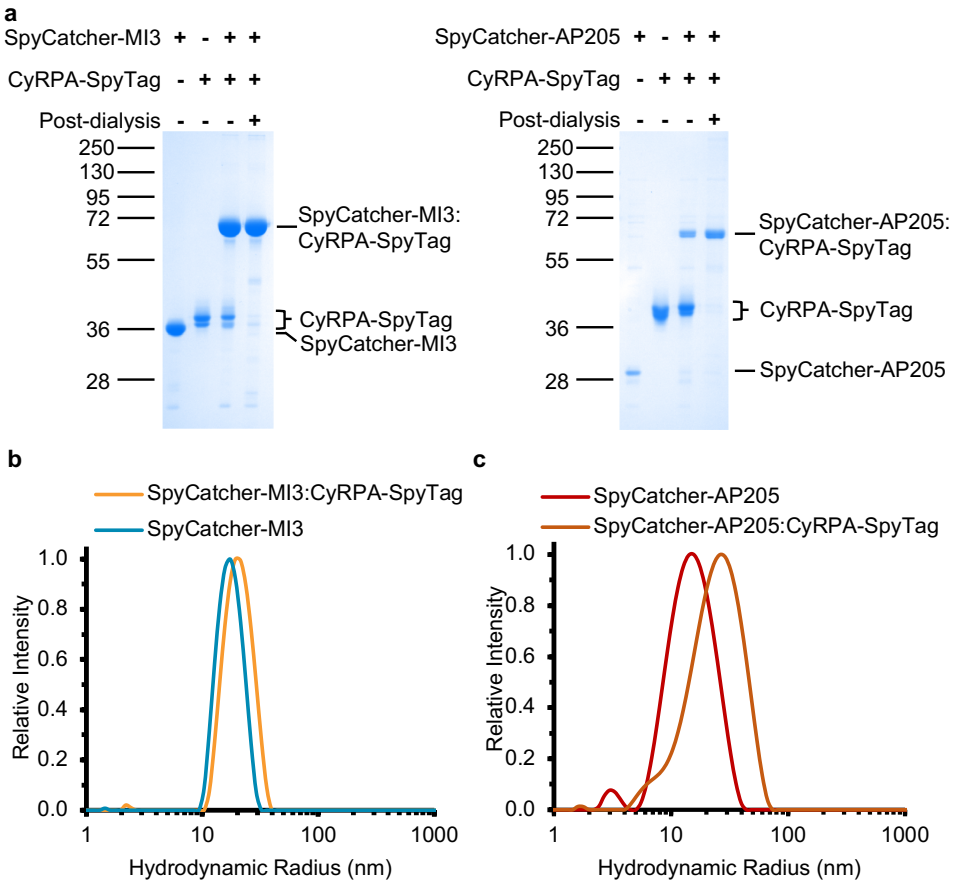


Figure 4.12. Preparation of SpyCatcher-nanoparticle immunogens. **(a)** SpyCatcher-MI3 and SpyCatcher-AP205 were conjugated with CyRPA-SpyTag and unreacted antigen was removed by dialysis, as analyzed by SDS-PAGE with Coomassie staining. **(b)** DLS characterization of SpyCatcher-MI3 with or without CyRPA-SpyTag conjugation. **(c)** DLS characterization of SpyCatcher-AP205 with or without CyRPA-SpyTag conjugation.

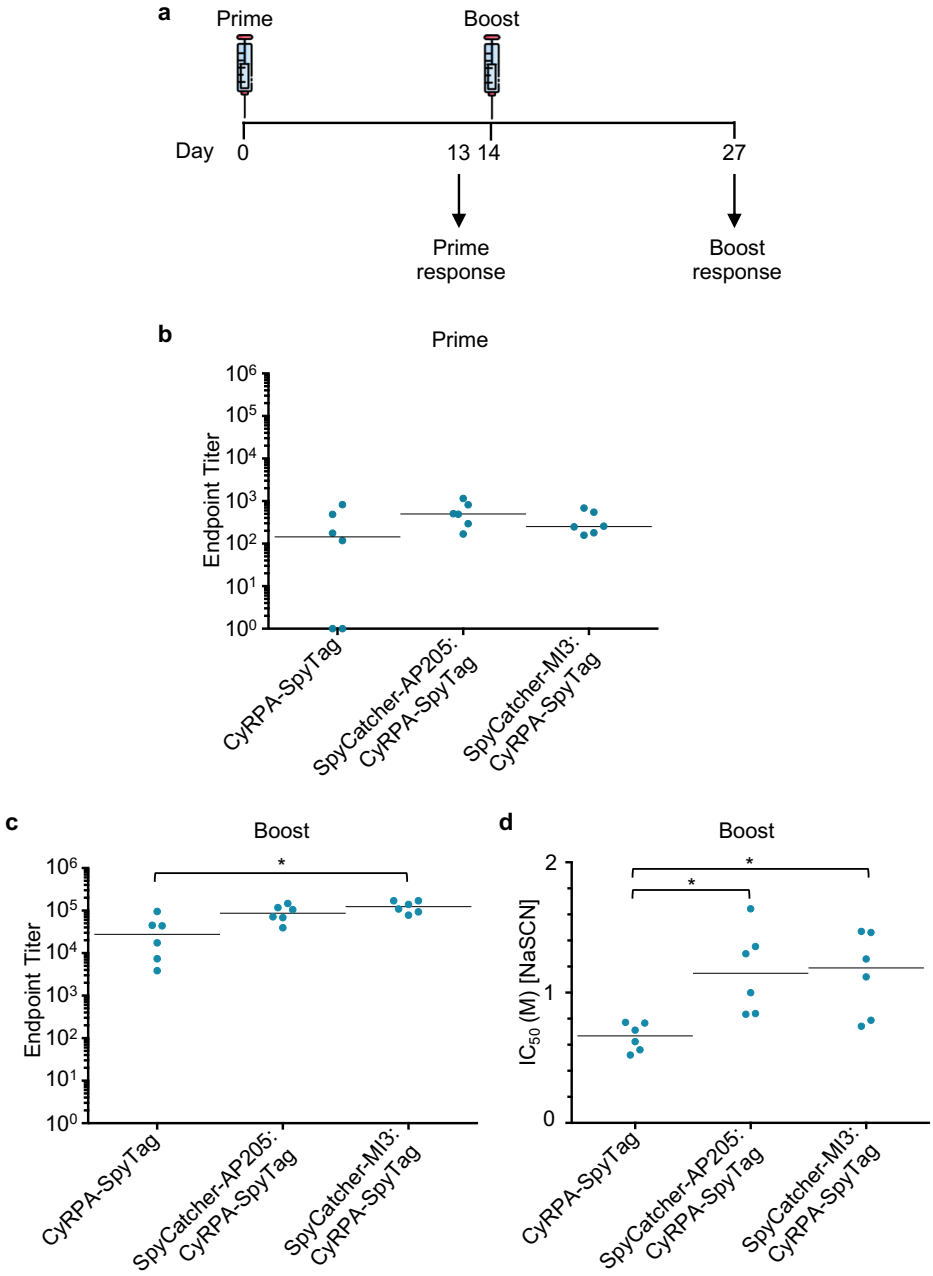


Figure 4.13. Plug-and-Display immunization with CyRPA immunogens. **(a)** Time course of immunization regimen. **(b)** Antibody titer to CyRPA after the prime. **(c)** Antibody titer to CyRPA after the boost. **(d)** Nanoassembly enhanced antibody avidity. The avidity of anti-CyRPA antibodies from each group was assayed after boosting, based on resistance to NaSCN-induced dissociation. In each case, the value is plotted for each mouse. The horizontal bar represents the median and a Kruskal-Wallis test followed by Dunn's multiple comparison post-test was performed. *p <0.05, n.s. p >0.05, n = 6.

For both SpyCatcher-MI3 and SpyCatcher-AP205, the induced antibodies had a significantly higher avidity than CyRPA-SpyTag alone ($p = 0.028$ for SpyCatcher-MI3, $p = 0.011$ for SpyCatcher-AP205, $n = 6$, Kruskal-Wallis test followed by Dunn's multiple comparison post-test) (Figure 4.13d). There was no significant difference in avidity between SpyCatcher-MI3 and SpyCatcher-AP205.

4.5 Discussion

In the previous chapter I described my attempt to evolve SpyCatcher-AP205 to produce a soluble and high-yield modular vaccine scaffold. Although SpyCatcher-AP205 successfully induces high antibody titers when conjugated to diverse antigens (Palladini et al., 2017; Thrane et al., 2016; Brune et al., 2016), a number of characteristics hamper its use, not just on a lab-scale but also on a clinical and industrial level.

In this chapter, I describe the establishment of a simple and robust platform for modular multimerization of proteins. I show that the designed protein nanocage I301 tolerated fusion of SpyCatcher to its N-terminus and was improved by rational engineering of two surface-exposed cysteines. The modified platform could be expressed and purified in high-yield from *E. coli* and was robust to freezing, heating, and lyophilization. An important thing to explore in the future is whether the stability of the platform is the same once decorated with antigen. However, properly characterizing a conjugated vaccine necessitates immunization in mice to see how any given treatment (i.e. freezing) affects the induction of antibodies.

During the initial testing of the four constructs (4.2, Figure 4.3) I observed a destabilizing effect caused by the N-terminal HisTag compared to the C-terminal C-tag. On the one hand, there are reported cases in the literature of His_6-Tags causing destabilization of proteins, changing the structure, and also influencing protein structure depending on placement at the N- or C- terminus (Zhao and Huang, 2016; Majorek et al., 2014; Klose et al., 2004; McDonald et al., 2007). The elution trace from size-exclusion chromatography of the four

constructs also supported the observations from the storage stability assays. It is only in the two HisTagged constructs that we see two major secondary peaks eluting in the <158 kDa region (according to a Mw marker), indicating likely unassembled trimeric and monomeric intermediates (Figure 4.2c). On the other hand, analysis of the I301 protein in PyMOL revealed that two amino acids away from the C-terminus lies C203, which is in close contact with C165. The distance between C203 and C165 is $\sim$ 2.1 Å (as measured in PyMOL), which is within the expected range of $\sim$ 2 Å for a disulfide bond (Rubinstein and Fiser, 2008). Therefore, it may be possible that installing a C-tag near these atoms somehow affects the disulfide bond and thus the structure of the protein nanocage during assembly and subsequent storage.

While testing the robustness of the platform I also showed that SpyCatcher-MI3 could efficiently conjugate to purified SpyTag-protein partner while still in cleared lysate. This could have important consequences for streamlining vaccine production and reducing cost. It would be interesting in the future to try mixing both unpurified antigen and unpurified nanoparticle to see if the process could be streamlined even further. Another potential experiment would be the use of pETDuet-1 plasmids which can co-express two target genes. It would be useful to see if co-expression of SpyCatcher-MI3 and a SpyTag-antigen that is amenable to expression in bacterial hosts (for example SpyTag-CIDR), would result in a conjugated particle in high yield. If optimized, such a procedure would increase the efficacy and ease of vaccine production.

The purification method of SpyCatcher-MI3 could also be optimized. Currently, a two-step method is employed using affinity resin capture followed by size-exclusion chromatography. While this results in a pure product, using affinity resin is not typically done in industry as it is very expensive and not easily scalable (Effio and Hubbuch, 2015). The most common method for virus purification in industry is still ultra-centrifugation, something which has not been tried for SpyCatcher-MI3 (Effio and Hubbuch, 2015). There are also a number of new chromatography matrices and techniques being developed for the specific purpose of pu-

rifying large biomolecules in adherence with good manufacturing practices. Some examples include monoliths, gigapore resins, and steric-exclusion chromatography using PEG (Effio and Hubbuch, 2015; Effio et al., 2016; Gagnon et al., 2014).

Our immunization trial in mice showed that CyRPA was quite efficient at stimulating antibodies on its own. Future immune studies with antigens that are quite poorly immunogenic on their own may show a greater benefit to multimerization on the SpyCatcher-MI3 platform. However, assessing the avidity of the antibodies showed that the quality of the antigens produced by MI3 was significantly better. Thus, even in the case of an antigen that can stimulate high endpoint titers on its own there may still be important qualitative benefits to immunizing with a vaccine platform.

There are also additional tests that can be performed to further assess the relevance of raised antibodies in the context of disease. For example, for blood-stage malarial antigens there are a variety of in vitro growth-inhibition assays (GIAs) that assess the raised antibodies' ability to stop the invasive capacity of merozoites in red-blood cells (Duncan et al., 2012; Boyle et al., 2010). However, the link between in vitro GIA results and efficacy of blood-stage malarial vaccines in real-world application is still being validated (Duncan et al., 2012). In general, finding accurate ways of predicting which promising antigens from the lab will translate into a clinical setting is of major importance for malarial vaccine development (Miura, 2016).

Crucially, in this chapter, we showed that the engineered MI3 protein nanoparticles are as immunogenic as phage-derived virus-like particles. There are many relevant differences between MI3 and AP205 which could affect their immuno-stimulatory properties. AP205 has a larger number of antigens displayed on its surface (180) versus MI3 (maximum 60). The antigen spacing and clustering on the surface of both platforms is also different which could potentially impact B-cell receptor cross-linking efficiency. Furthermore, AP205 packages RNA which can act act as a natural adjuvant simulating immune responses through Toll-like receptor (TLR) 7 and 8 signalling (Schmitz et al., 2012). Further studies comparing

MI3 to other leading VLP-based platforms and comparison using different antigens would be relevant to confirm that the results seen in this preliminary trial are generalizable. Thanks to the ease with which large amounts of MI3 can be produced and also its general robustness it is possible that the particle will be of use to other areas of bionanotechnology including imaging, catalysis, and therapeutics (Uchida et al., 2018; Wilhelm et al., 2016; Shi et al., 2017).

Chapter 5

Summary and General Discussion

Nanoparticle platforms for antigen multimerization are powerful tools for stimulating the immune system (Bachmann and Jennings, 2010). VLP-based vaccines avoid the safety issues of live/attenuated vaccines and can improve the poor immunogenicity of protein subunit vaccines (Wu et al., 2015). However, installing antigens onto nanoparticles to create robust vaccines is still a process that can require tedious optimization and engineering (Janssens et al., 2010; Caldeira and Peabody, 2011; Frietze et al., 2016). In this thesis, I have sought to address this challenge by focusing on the evolution and creation of modular vaccine scaffolds.

In Chapter 3, I describe the development of a methodology for the directed evolution of SpyCatcher-VLPs and the subsequent attempts to evolve the AP205 coat protein for solubility and yield. The strategy for the evolution exploited the fact that AP205 VLPs package their own RNA. After using error-prone PCR to mutagenize the VLP coat protein, I expressed the library using a standard *E. coli* protocol that was challenging for the wild-type SpyCatcher-VLP construct. After purifying the SpyCatcher-VLP library, I incubated the VLPs with SpyTag-HaloTag bait and captured the conjugated species with HaloLink magnetic beads. VLP cleavage off the beads using MBP-TEV protease helped improve the selectivity of the model enrichment phase, as did the use of extensive blocking and wash steps. Lysis of the cleaved VLP species, RNA purification, and RT-PCR afforded the genetic

sequences of enriched species for re-cloning and continued rounds of selection.

After sequencing and expressing selected variants from directed evolution 1, it was evident that the evolution strategy needed improvement. Investigation into potential weak points of the methodology revealed a few areas that were amenable to optimization. Particularly problematic was the realization that RNA-containing aggregates of misfolded protein were not easily distinguishable from properly folded VLPs. To try to remove aggregates, an ultracentrifugation purification step, after IMAC-purification of the VLPs, was introduced in directed evolution 2. Other modifications included switching the *E. coli* expression strain to C41(DE3) cells, using harsher RNA degradation conditions, and using a decreased amount of SpyTag-HaloTag bait.

Although the purified protein yield of SpyCatcher-VLPs increased in the first three rounds of DE 2, expression of individual variants indicated that, once again, the evolution did not select for improved variants of SpyCatcher-CP3 VLPs. All of the individually expressed variants following round 2 and round 3 of selection either expressed in very low yield, and/or failed to assemble into VLPs following IMAC-purification. Interestingly, some of the SpyCatcher-CP3 variants assembled into VLPs after incubation at 4 °C for two weeks. Some preliminary experiments then indicated that SpyCatcher-AP205 VLPs may be prone to disassembly and assembly depending on the buffer conditions. The ability to disassemble and re-assemble, potentially packing other VLP RNA in the process, would account for the inability to selectively differentiate between variants in the directed evolution.

As a result of my attempt to evolve SpyCatcher-CP3, I learned that the AP205 VLPs were more unstable than expected. It is possible that fusion of SpyCatcher to the coat protein affects assembly of AP205. However, many VLPs, both chimeric and wild-type recombinant constructs, are influenced by purification and storage conditions like pH, temperature, and buffer ionic-strength (Kim et al., 2018; Effio and Hubbuch, 2015; Lan et al., 2018; Zahid et al., 2015). For any VLP or nanoparticle-based platform it will be crucial to carefully study the factors which can affect its formulation. For example, production of HPV VLPs

in insect cells compared to yeast cells not only produced differently sized particles but also resulted in a >2-fold increase in the antibody titer during immunization trials (Kim et al., 2018).

During my Masters, I have shipped SpyCatcher-AP205 to multiple laboratories who have wanted to make use of the platform for diverse vaccine applications. Similar to my own personal experience, the vast majority of laboratories reported difficulty in expressing, purifying, and handling the VLP. However, the demand for the particle indicates the broad applicability and scientific interest in using a modular VLP platform. Thus, I turned my attention in Chapter 4 of this thesis to the characterization of a new modular scaffold: SpyCatcher-MI3.

The computationally-derived synthetic nanocage I3-01 (Hsia et al., 2016) resembles a VLP in size and geometry. By fusing SpyCatcher to the N-terminus of I3-01 and using rational engineering to remove two surface-exposed cysteines, the SpyCatcher-MI3 protein scaffold was created. SpyCatcher-MI3 had a reduced tendency to aggregate compared to SpyCatcher-I301. SpyCatcher-MI3 could be purified in high yield using a simple and cheap *E. coli* expression protocol. Through a number of different experiments I demonstrated the stability of SpyCatcher-MI3. SpyCatcher-MI3 nanoparticles were stable to heating for prolonged periods at high temperature and remained soluble after repeated rounds of freeze-thawing. The nanoparticles could also be lyophilized, which is an advantage for storage and transportation (Matejtschuk, 2007). Significant research is devoted to exploring vaccine formulations that can help reduce production costs, eliminate the cold chain, and improve vaccine stability (Lua et al., 2014). SpyCatcher-MI3 is able to satisfy many of these requirements.

In immunization trials, SpyCatcher-MI3 conjugated to CyRPA-SpyTag was able to induce high-avidity antibodies against CyRPA. Crucially, comparison indicated no significant difference in titer or avidity of CyRPA antibodies raised by either conjugated SpyCatcher-MI3 or conjugated SpyCatcher-AP205. Thus, multimerization of an antigen to MI3 affords the

same immunological benefits as multimerization to AP205. MI3 also adopted a much more stable and uniform conformation compared to AP205 based on DLS and TEM. Thus, the work in this thesis has demonstrated there can be advantages to using a synthetic nanoparticle. However, the stability and fusion tolerance of any other new nanoparticle would need to be empirically determined.

The existence of a number of other synthetic protein cages also opens up the ability to systematically investigate factors that can affect and improve immunogenicity. The same laboratory that designed I3-01 has also created nanoparticles of different geometries (e.g. tetrahedral and icosahedral), different sizes (15-40 nm), and different assembly states (e.g. assembly from one or two unique components) (Bale et al., 2016; King et al., 2014, 2012; Bale et al., 2015). Hitherto, the approach to creating modular vaccine platforms in the Howarth lab has focused on fusing SpyCatcher to an exposed N- or C- terminus of a VLP coat protein. Due to the size of SpyCatcher ($\sim$ 15 kDa), insertion in the middle of a protein sequence can be challenging and inhibit proper protein folding. However, not every protein nanocage will have easily functionalizable, externally presented termini. The recent creation of the SnoopLigase system can help address this challenge (Buldun et al., 2018). SnoopLigase is able to catalyze an isopeptide bond between two small peptide tags of 12 and 23 amino acid length. The small size of the two tags means the geometry of antigen display on the surface of a given nanoparticle can be changed depending on the fusion site. A smaller tag could also potentially be inserted into various parts of an antigen which, when functionalized to a nanoparticle, may expose different important immunogenic binding sites of the epitope (Scally et al., 2017). The development of SnoopLigase-functionalized vaccine platforms may also be advantageous for minimizing antibodies generated against the platform itself. Currently, an investigation into the effect of pre-existing antibodies against SpyCatcher on future immunizations has not been performed. However, it is known that off-target antigenicity can reduce the immune response to the antigen of choice (Ringe et al., 2017). Hence, the use of a system with minimal protein scars may be desirable.

The immunization trial presented here used a prime-boost scheme. However, for both antigen-sparing, time, and cost-efficiency, a single immunization is preferable (Quan et al., 2009). It would be interesting to see if SpyCatcher-MI3 nanoparticles could induce protective immunity after one dose. Another facet of SpyCatcher-MI3 that has not been investigated is the platform's ability to stimulate T-cells. T-cells in addition to B-cells are thought to be important in attacking pathogens that establish chronic infections in individuals (Irvine et al., 2015). SpyCatcher-MI3's ability to efficiently stimulate T-cells would increase its potential as a vaccine platform for diseases that have evaded current vaccine efforts (Delany et al., 2014). It is also possible to engineer and enhance the immunogenicity of a vaccine platform (Irvine et al., 2015; Frietze et al., 2016). For example, by using the orthogonal pairs SpyCatcher/SpyTag and SnoopCatcher/SnoopTag, nanoparticles can be designed that carry two antigens (Brune et al., 2017). Since SpyCatcher-MI3 has an external N- terminus and an internal C- terminus, one could create particles with an N-terminally fused antigen and an encapsulated C-terminally fused helper T-cell antigen. Such a delivery has been shown to promote efficient T-cell and B-cell responses, with minimal antibodies raised against the T-cell peptides (Hanson et al., 2015).

Even though directed evolution for SpyCatcher-AP205 VLPs did not achieve the objective, directed evolution as a protein engineering strategy could be applied to future modular platforms. A synthetic icosahedral nanocage, 153-50, was recently engineered to encapsulate RNA through electrostatic interactions and then evolved to improve RNA loading (Butterfield et al., 2017). Such a particle could serve as the base of a modular vaccine platform that could be evolved for other desirable properties. Characteristics that could be important for vaccine applications include pH-tolerance (oral delivery), fusion-tolerance, and long-term stability. Additionally, *in vivo* selections in mice could be performed to find particles that have enhanced T-cell stimulation, specific organ-targeting, or enhanced APC uptake. For SpyCatcher-MI3 specifically, further rational engineering strategies could be employed to improve the platform. For example, linker type and linker length between MI3 and Spy-

Catcher are important structural features that have not been optimized (Chen et al., 2013; Klein et al., 2014). The effect of conjugation to the C-terminus of SpyCatcher-MI3 should also be investigated further. During my characterization of the platform I found that a C-terminal C-tag improved the stability of the particle compared to a C-terminal His_6-Tag. However, in the case of HBcAg-VLPs, the placement of a C-terminal polyhistidine-peptide was found to improve the stability of the chimeric VLP (Schumacher et al., 2018). It would be interesting to investigate if other internally conjugated peptides could further improve the stability of SpyCatcher-MI3. Additionally, it could be advantageous to install disulfide bonds at key residues between the trimeric subunits of MI3. Disulfide bonds have been engineered into VLPs to improve thermostability and assembly (Schumacher et al., 2018; Lu et al., 2015; Fiedler et al., 2012a; Ashcroft et al., 2005). Covalent linkages between subunits of SpyCatcher-MI3 could help further improve the robustness of the platform. Having a series of modular vaccine platforms with fine-tuned properties will help speed up lab-bench to bed-side production of new vaccines for some of the most urgent, unmet medical needs.

Bibliography

Adams, W. R. and A. M. Prince (1957). An electron microscope study of the morphology and distribution of the intracytoplasmic virus-like particles of Ehrlich ascites tumor cells. *The Journal of biophysical and biochemical cytology*, 3(2):161–70.

Aida, Y. and M. J. Pabst (1990). Removal of endotoxin from protein solutions by phase separation using Triton X-114. *Journal of immunological methods*, 132:191–5.

Alegre-Cebollada, J., C. L. Badilla, and J. M. Fernández (2010). Isopeptide bonds block the mechanical extension of pili in pathogenic Streptococcus pyogenes. *The Journal of biological chemistry*, 285(15):11235–42.

Alving, C. R., K. K. Peachman, M. Rao, and S. G. Reed (2012). Adjuvants for human vaccines. *Current opinion in immunology*, 24:310–5.

Arnold, F. H., P. L. Wintrode, K. Miyazaki, and A. Gershenson (2001). How enzymes adapt: lessons from directed evolution. *Trends in Biochemical Sciences*, 26(2):100–106.

Asensio, M. A., N. M. Morella, C. M. Jakobson, E. C. Hartman, J. E. Glasgow, B. Sankaran, P. H. Zwart, and D. Tullman-Ercek (2016). A Selection for Assembly Reveals That a Single Amino Acid Mutant of the Bacteriophage MS2 Coat Protein Forms a Smaller Virus-like Particle. *Nano Letters*, 16(9):5944–5950.

Ashcroft, A., H. Lago, J. B. Macedo, W. Horn, N. Stonehouse, and P. Stockley (2005).

Engineering Thermal Stability in RNA Phage Capsids via Disulphide Bonds. *Journal of Nanoscience and Nanotechnology*, 5(12):2034–2041.

Azuma, Y., M. Herger, and D. Hilvert (2018). Diversification of Protein Cage Structure Using Circularly Permuted Subunits. *Journal of the American Chemical Society*, 140(2):558–561.

Bachmann, M. F. and G. T. Jennings (2010). Vaccine delivery: a matter of size, geometry, kinetics and molecular patterns. *Nature reviews. Immunology*, 10:787–96.

Bale, J. B., S. Gonen, Y. Liu, W. Sheffler, D. Ellis, C. Thomas, D. Cascio, T. O. Yeates, T. Gonen, N. P. King, and D. Baker (2016). Accurate design of megadalton-scale two-component icosahedral protein complexes. *Science.*, 353:389–394.

Bale, J. B., R. U. Park, Y. Liu, S. Gonen, T. Gonen, D. Cascio, N. P. King, T. O. Yeates, and D. Baker (2015). Structure of a designed tetrahedral protein assembly variant engineered to have improved soluble expression. *Protein science: a publication of the Protein Society*, 24(10):1695–701.

Bernabeu, M. and J. D. Smith (2017). EPCR and Malaria Severity: The Center of a Perfect Storm. *Trends in Parasitology*, 33(4):295–308.

Boyle, M. J., D. W. Wilson, J. S. Richards, D. T. Riglar, K. K. A. Tetteh, D. J. Conway, S. A. Ralph, J. Baum, and J. G. Beeson (2010). Isolation of viable Plasmodium falciparum merozoites to define erythrocyte invasion events and advance vaccine and drug development. *Proceedings of the National Academy of Sciences of the United States of America*, 107(32):14378–83.

Brakke, M. K. (1961). Density Gradient Centrifugation And its Application to Plant Viruses. *Advances in Virus Research*, 7:193–224.

Brito, L. A. and M. Singh (2011). Acceptable levels of endotoxin in vaccine formulations during preclinical research. *Journal of pharmaceutical sciences*, 100(1):34–7.

Brune, K. D., C. M. Buldun, Y. Li, I. J. Taylor, F. Brod, S. Biswas, and M. Howarth (2017). Dual Plug-and-Display Synthetic Assembly Using Orthogonal Reactive Proteins for Twin Antigen Immunization. *Bioconjugate Chemistry*, 28:1544–1551.

Brune, K. D., D. B. Leneghan, I. J. Brian, A. S. Ishizuka, M. F. Bachmann, S. J. Draper, S. Biswas, and M. Howarth (2016). Plug-and-Display: decoration of Virus-Like Particles via isopeptide bonds for modular immunization. *Scientific reports*, 6:19234.

Buck, C. B., D. V. Pastrana, D. R. Lowy, and J. T. Schiller (2004). Efficient intracellular assembly of papillomaviral vectors. *Journal of virology*, 78(2):751–7.

Buck, C. B. and C. D. Thompson (2007). Production of Papillomavirus-Based Gene Transfer Vectors. In *Current Protocols in Cell Biology*, chapter 26. Hoboken, NJ, USA: John Wiley & Sons, Inc.

Buldun, C. M., J. Jean, M. R. Bedford, and M. Howarth (2018). SnoopLigase catalyzes peptide-peptide locking and enables solid-phase conjugate isolation. *Journal of the American Chemical Society*, 140:3008–3018.

Bundy, B. C., M. J. Franciszkowicz, and J. R. Swartz (2008). Escherichia coli-based cell-free synthesis of virus-like particles. *Biotechnology and Bioengineering*, 100(1):28–37.

Bundy, B. C. and J. R. Swartz (2011). Efficient disulfide bond formation in virus-like particles. *Journal of Biotechnology*, 154(4):230–239.

Butterfield, G. L., M. J. Lajoie, H. H. Gustafson, D. L. Sellers, U. Nattermann, D. Ellis, J. B. Bale, S. Ke, G. H. Lenz, A. Yehdego, R. Ravichandran, S. H. Pun, N. P. King, and D. Baker (2017). Evolution of a designed protein assembly encapsulating its own RNA genome. *Nature*, 552:415–420.

Cabral, G. A., F. Marciano-Cabral, G. A. Funk, Y. Sanchez, F. B. Hollinger, J. L. Melnick, and G. R. Dreesman (1978). Cellular and Humoral Immunity in Guinea Pigs to Two Major

Polypeptides Derived from Hepatitis B Surface Antigen. *Journal of General Virology*, 38(2):339–350.

Cadena-Nava, R. D., M. Comas-Garcia, R. F. Garmann, A. L. N. Rao, C. M. Knobler, and W. M. Gelbart (2012). Self-assembly of viral capsid protein and RNA molecules of different sizes: requirement for a specific high protein/RNA mass ratio. *Journal of virology*, 86(6):3318–26.

Caldeira, J. C. and D. S. Peabody (2011). Thermal stability of RNA phage virus-like particles displaying foreign peptides. *Journal of nanobiotechnology*, 9:22.

Chackerian, B. (2007). Virus-like particles: flexible platforms for vaccine development. *Expert review of vaccines*, 6(381):390.

Chackerian, B., J. d. C. Caldeira, J. Peabody, and D. S. Peabody (2011). Peptide epitope identification by affinity selection on bacteriophage MS2 virus-like particles. *Journal of molecular biology*, 409(2):225–37.

Chackerian, B., D. R. Lowy, and J. T. Schiller (2001). Conjugation of a self-antigen to papillomavirus-like particles allows for efficient induction of protective autoantibodies. *The Journal of clinical investigation*, 108(3):415–23.

Champion, C. I., V. A. Kickhoefer, G. Liu, R. J. Moniz, A. S. Freed, L. L. Bergmann, D. Vaccari, S. Raval-Fernandes, A. M. Chan, L. H. Rome, and K. A. Kelly (2009). A vault nanoparticle vaccine induces protective mucosal immunity. *PloS one*, 4(4):e5409.

Chen, D., A. Tyagi, J. Carpenter, S. Perkins, D. Sylvester, M. Guy, D. D. Kristensen, and L. T. J. Braun (2009). Characterization of the freeze sensitivity of a hepatitis B vaccine. *Human Vaccines*, 5:26–32.

Chen, X., J. L. Zaro, and W.-C. Shen (2013). Fusion protein linkers: property, design and functionality. *Advanced drug delivery reviews*, 65(10):1357–69.

Chen, Y., Y. Zhang, C. Quan, J. Luo, Y. Yang, M. Yu, Y. Kong, G. Ma, and Z. Su (2015). Aggregation and antigenicity of virus like particle in salt solutionA case study with hepatitis B surface antigen. *Vaccine*, 33(35):4300–4306.

Cheng, L.-F., F. Wang, L. Zhang, L. Yu, W. Ye, Z.-Y. Liu, Q.-K. Ying, X.-A. Wu, Z.-K. Xu, and F.-L. Zhang (2016). Incorporation of GM-CSF or CD40L Enhances the Immunogenicity of Hantaan Virus-Like Particles. *Frontiers in cellular and infection microbiology*, 6:185.

Chivers, C. E., A. L. Koner, E. D. Lowe, and M. Howarth (2011). How the biotin-streptavidin interaction was made even stronger: investigation via crystallography and a chimaeric tetramer. *The Biochemical journal*, 435(1):55–63.

Comas-Garcia, M., R. D. Cadena-Nava, A. L. N. Rao, C. M. Knobler, and W. M. Gelbart (2012). In vitro quantification of the relative packaging efficiencies of single-stranded RNA molecules by viral capsid protein. *Journal of virology*, 86(22):12271–82.

Crossey, E., K. Frietze, D. L. Narum, D. S. Peabody, and B. Chackerian (2015). Identification of an Immunogenic Mimic of a Conserved Epitope on the Plasmodium falciparum Blood Stage Antigen AMA1 Using Virus-Like Particle (VLP) Peptide Display. *PLOS ONE*, 10(7):e0132560.

Dalod, M., R. Chelbi, B. Malissen, and T. Lawrence (2014). Dendritic cell maturation: functional specialization through signaling specificity and transcriptional programming. *The EMBO journal*, 33(10):1104–16.

Delany, I., R. Rappuoli, and E. De Gregorio (2014). Vaccines for the 21st century. *EMBO molecular medicine*, 6(6):708–20.

Dreyer, A. M., H. Matile, P. Papastogiannidis, J. Kamber, P. Favuzza, T. S. Voss, S. Wittlin, and G. Pluschke (2012). Passive immunoprotection of Plasmodium falciparum-infected

mice designates the CyRPA as candidate malaria vaccine antigen. *Journal of immunology (Baltimore, Md. : 1950)*, 188:6225–37.

Duncan, C. J. A., A. V. S. Hill, and R. D. Ellis (2012). Can growth inhibition assays (GIA) predict blood-stage malaria vaccine efficacy? *Human vaccines & immunotherapeutics*, 8(6):706–14.

Effio, C. L. and J. Hubbuch (2015). Next generation vaccines and vectors: Designing downstream processes for recombinant protein-based virus-like particles. *Biotechnology Journal*, 10:715–727.

Effio, C. L., S. A. Oelmeier, and J. Hubbuch (2016). High-throughput characterization of virus-like particles by interlaced size-exclusion chromatography. *Vaccine*, 34(10):1259–1267.

Fairhead, M. and M. Howarth (2015). Site-Specific biotinylation of purified proteins using BirA. *Site-Specific Protein Labeling: Methods and Protocols*, 1266:171–184.

Faivre-Moskalenko, C., J. Bernaud, A. Thomas, K. Tartour, Y. Beck, M. Iazykov, J. Danial, M. Lourdin, D. Muriaux, and M. Castelnovo (2014). RNA control of HIV-1 particle size polydispersity. *PloS one*, 9(1):e83874.

Ferla, M. P. (2016). Mutanalyst, an online tool for assessing the mutational spectrum of epPCR libraries with poor sampling. *BMC Bioinformatics*, 17(1):152.

Fiedler, J. D., C. Higginson, M. L. Hovlid, A. A. Kislukhin, A. Castillejos, F. Manzenrieder, M. G. Campbell, N. R. Voss, C. S. Potter, B. Carragher, and M. Finn (2012a). Engineered Mutations Change the Structure and Stability of a Virus-Like Particle. *Biomacromolecules*, 13(8):2339–2348.

Fiedler, J. D., C. Higginson, M. L. Hovlid, A. A. Kislukhin, A. Castillejos, F. Manzenrieder, M. G. Campbell, N. R. Voss, C. S. Potter, B. Carragher, and M. G. Finn (2012b).

Engineered mutations change the structure and stability of a virus-like particle. *Biomacromolecules*, 13(8):2339–48.

Fierer, J. O., G. Veggiani, and M. Howarth (2014). SpyLigase peptide-peptide ligation polymerizes affibodies to enhance magnetic cancer cell capture. *Proceedings of the National Academy of Sciences of the United States of America*, 111:E1176–E1181.

Fissan, H., S. Ristig, H. Kaminski, C. Asbach, and M. Epple (2014). Comparison of different characterization methods for nanoparticle dispersions before and after aerosolization. *Analytical Methods*, 6(18):7324.

Fletcher, J. M., A. L. Boyle, M. Bruning, S. J. Bartlett, T. L. Vincent, N. R. Zaccai, C. T. Armstrong, E. H. Bromley, P. J. Booth, R. L. Brady, A. R. Thomson, and D. N. Woolfson (2012). A basis set of de novo coiled-Coil peptide oligomers for rational protein design and synthetic biology. *ACS Synthetic Biology*, 1(6):240–250.

Frietze, K. M., D. S. Peabody, and B. Chackerian (2016). Engineering virus-like particles as vaccine platforms. *Current Opinion in Virology*, 18:44–49.

Gagnon, P., P. Toh, and J. Lee (2014). High productivity purification of immunoglobulin G monoclonal antibodies on starch-coated magnetic nanoparticles by steric exclusion of polyethylene glycol. *Journal of chromatography. A*, 1324:171–80.

Galen, J. E., R. Curtiss, and 3rd (2014). The delicate balance in genetically engineering live vaccines. *Vaccine*, 32(35):4376–85.

Gibson, D. G., L. Young, R.-Y. Chuang, J. C. Venter, C. A. Hutchison, and H. O. Smith (2009). Enzymatic assembly of DNA molecules up to several hundred kilobases. *Nature methods*, 6(5):343–5.

Gillam, E. M., J. N. Copp, and D. F. Ackerley (2014). *Directed evolution library creation : methods and protocols*, second edition. New York: Humana Press.

Griffiths, J. S., N. J. Wymer, E. Njolito, S. Niranjanakumari, C. A. Fierke, and E. J. Toone (2002). Cloning, isolation and characterization of the Thermotoga maritima KDPG aldolase. *Bioorganic & medicinal chemistry*, 10(3):545–50.

Hajj Hussein, I., N. Chams, S. Chams, S. El Sayegh, R. Badran, M. Raad, A. Gerges-Geagea, A. Leone, and A. Jurjus (2015). Vaccines Through Centuries: Major Cornerstones of Global Health. *Frontiers in public health*, 3:269.

Hanson, C. M., A. M. George, and A. Sawadogo (2017). Is freezing in the vaccine cold chain an ongoing issue? A literature review. *Vaccine*, 35:2127–2133.

Hanson, M. C., W. Abraham, M. P. Crespo, S. H. Chen, H. Liu, G. L. Szeto, M. Kim, E. L. Reinherz, and D. J. Irvine (2015). Liposomal vaccines incorporating molecular adjuvants and intrastructural T-cell help promote the immunogenicity of HIV membrane-proximal external region peptides. *Vaccine*, 33(7):861–8.

Harakuni, T., K. Andoh, R.-i. Sakamoto, Y. Tamaki, T. Miyata, H. Uefuji, K.-i. Yamazaki, and T. Arakawa (2016). Fiber knob domain lacking the shaft sequence but fused to a coiled coil is a candidate subunit vaccine against egg-drop syndrome. *Vaccine*, 34(27):3184–3190.

He, D. and J. Marles-Wright (2015). Ferritin family proteins and their use in bionanotechnology. *New biotechnology*, 32(6):651–7.

Healer, J., A. F. Cowman, D. C. Kaslow, and A. J. Birkett (2017). Vaccines to Accelerate Malaria Elimination and Eventual Eradication. *Cold Spring Harbor perspectives in medicine*, 7:a025627.

Hinterwirth, H., S. K. Wiedmer, M. Moilanen, A. Lehner, G. Allmaier, T. Waitz, W. Lindner, and M. Lämmerhofer (2013). Comparative method evaluation for size and size-distribution analysis of gold nanoparticles. *Journal of Separation Science*, 36(17):2952–2961.

Hsia, Y., J. B. Bale, S. Gonen, D. Shi, W. Sheffler, K. K. Fong, U. Nattermann, C. Xu, P.-S. Huang, R. Ravichandran, S. Yi, T. N. Davis, T. Gonen, N. P. King, and D. Baker (2016). Design of a hyperstable 60-subunit protein icosahedron. *Nature*, 535:136–139.

Huang, D. B., J. J. Wu, and S. K. Tyring (2004). A review of licensed viral vaccines, some of their safety concerns, and the advances in the development of investigational viral vaccines. *Journal of Infection*, 49:179–209.

Irvine, D. J., M. C. Hanson, K. Rakhra, and T. Tokatlian (2015). Synthetic Nanoparticles for Vaccines and Immunotherapy. *Chemical Reviews*, 115(19):11109–11146.

Jäckel, C., P. Kast, and D. Hilvert (2008). Protein Design by Directed Evolution. *Annual Review of Biophysics*, 37(1):153–173.

Jain, N. K. and I. Roy (2010). Trehalose and Protein Stability. In *Current Protocols in Protein Science*, volume Chapter 4, Pp. 4.9.1–4.9.12. Hoboken, NJ, USA: John Wiley & Sons, Inc.

Jain, N. K., N. Sahni, O. S. Kumru, S. B. Joshi, D. B. Volkin, and C. Russell Middaugh (2015). Formulation and stabilization of recombinant protein based virus-like particle vaccines. *Advanced Drug Delivery Reviews*, 93:42–55.

Janssens, M. E., D. Geysen, K. Broos, I. De Goeyse, J. Robbens, F. Van Petegem, J.-P. Timmermans, and Y. Guisez (2010). Folding properties of the hepatitis B core as a carrier protein for vaccination research. *Amino Acids*, 38:1617–1626.

Jennings, G. T. and M. F. Bachmann (2008). The coming of age of virus-like particle vaccines. *Biological chemistry*, 389:521–36.

Jespersen, J. S., C. W. Wang, S. I. Mkumbaye, D. T. Minja, B. Petersen, L. Turner, J. E. Petersen, J. P. Lusingu, T. G. Theander, and T. Lavstsen (2016). Plasmodium falciparum

var genes expressed in children with severe malaria encode CIDRα1 domains. *EMBO Molecular Medicine*, 8(8):839–850.

Jin, J., K. A. Hjerrild, S. E. Silk, R. E. Brown, G. M. Labbé, J. M. Marshall, K. E. Wright, S. Bezemer, S. B. Clemmensen, S. Biswas, Y. Li, A. El-Turabi, A. D. Douglas, P. Hermans, F. J. Detmers, W. A. de Jongh, M. K. Higgins, R. Ashfield, and S. J. Draper (2017). Accelerating the clinical development of protein-based vaccines for malaria by efficient purification using a four amino acid C-terminal 'C-tag'. *International journal for parasitology*, 47:435–446.

Kanekiyo, M., W. Bu, M. G. Joyce, G. Meng, J. R. R. Whittle, U. Baxa, T. Yamamoto, S. Narpala, J.-P. Todd, S. S. Rao, A. B. McDermott, R. A. Koup, M. G. Rossmann, J. R. Mascola, B. S. Graham, J. I. Cohen, and G. J. Nabel (2015). Rational Design of an Epstein-Barr Virus Vaccine Targeting the Receptor-Binding Site. *Cell*, 162(5):1090–100.

Kang, H. J. and E. N. Baker (2009). Intramolecular isopeptide bonds give thermodynamic and proteolytic stability to the major pilin protein of Streptococcus pyogenes. *The Journal of biological chemistry*, 284(31):20729–37.

Kang, H. J., F. Coulibaly, F. Clow, T. Proft, and E. N. Baker (2007). Stabilizing isopeptide bonds revealed in gram-positive bacterial pilus structure. *Science (New York, N.Y.)*, 318(5856):1625–8.

Karch, C. P. and P. Burkhard (2016). Vaccine technologies: From whole organisms to rationally designed protein assemblies. *Biochemical pharmacology*, 120:1–14.

Kaslow, D. C., I. A. Quakyi, C. Syin, M. G. Raum, D. B. Keister, J. E. Coligan, T. F. McCutchan, and L. H. Miller (1988). A vaccine candidate from the sexual stage of human malaria that contains EGF-like domains. *Nature*, 333(6168):74–6.

Keeble, A. H., A. Banerjee, M. P. Ferla, S. C. Reddington, I. N. Anuar, and M. Howarth

(2017). Evolving Accelerated Amidation by SpyTag/SpyCatcher to Analyze Membrane Dynamics. *Angewandte Chemie - International Edition*, 56:16521–16525.

Khudyakov, Y. E. and P. Pumpens, eds. (2015). *Viral nanotechnology*. Boca Raton: CRC Press.

Kim, H. and H.-J. Kim (2017). Yeast as an expression system for producing virus-like particles: what factors do we need to consider? *Letters in Applied Microbiology*, 64(2):111–123.

Kim, H. J., S. Y. Cho, M.-H. Park, and H.-J. Kim (2018). Comparison of the size distributions and immunogenicity of human papillomavirus type 16 L1 virus-like particles produced in insect and yeast cells. *Archives of Pharmacal Research*, Pp. 1–10.

King, N. P., J. B. Bale, W. Sheffler, D. E. McNamara, S. Gonen, T. Gonen, T. O. Yeates, and D. Baker (2014). Accurate design of co-assembling multi-component protein nanomaterials. *Nature*, 510(7503):103–8.

King, N. P., W. Sheffler, M. R. Sawaya, B. S. Vollmar, J. P. Sumida, I. Andre, T. Gonen, T. O. Yeates, and D. Baker (2012). Computational Design of Self-Assembling Protein Nanomaterials with Atomic Level Accuracy. *Science*, 336(6085):1171–1174.

Klein, J. S., S. Jiang, R. P. Galimidi, J. R. Keeffe, and P. J. Bjorkman (2014). Design and characterization of structured protein linkers with differing flexibilities. *Protein engineering, design & selection : PEDS*, 27(10):325–30.

Klose, J., N. Wendt, S. Kubald, E. Krause, K. Fechner, M. Beyermann, M. Bienert, R. Rudolph, and S. Rothemund (2004). Hexa-histidin tag position influences disulfide structure but not binding behavior of in vitro folded N-terminal domain of rat corticotropin-releasing factor receptor type 2a. *Protein science : a publication of the Protein Society*, 13(9):2470–5.

Klovins, J., G. P. Overbeek, S. H. E. van den Worm, H. W. Ackermann, and J. van Duin (2002). Nucleotide sequence of a ssRNA phage from Acinetobacter: Kinship to coliphages. *Journal of General Virology*, 83(6):1523–1533.

Koho, T., T. O. Ihalainen, M. Stark, H. Uusi-Kerttula, R. Wieneke, R. Rahikainen, V. Blazevic, V. Marjomäki, R. Tampé, M. S. Kulomaa, and V. P. Hytönen (2015). His-tagged norovirus-like particles: A versatile platform for cellular delivery and surface display. *European journal of pharmaceutics and biopharmaceutics*, 96:22–31.

Könning, D. and H. Kolmar (2018). Beyond antibody engineering: directed evolution of alternative binding scaffolds and enzymes using yeast surface display. *Microbial Cell Factories*, 17(1):32.

Kueh, C. L., C. Y. Yong, S. Masoomi Dezfooli, S. Bhassu, S. G. Tan, and W. S. Tan (2016). Virus-like particle of Macrobrachium rosenbergii nodavirus produced in Spodoptera frugiperda (Sf9) cells is distinctive from that produced in Escherichia coli. *Biotechnology Progress*, 00:1–9.

Kumru, O. S., S. B. Joshi, D. E. Smith, C. R. Middaugh, T. Prusik, and D. B. Volkin (2014). Vaccine instability in the cold chain: Mechanisms, analysis and formulation strategies. *Biologicals*, 42:237–259.

Kushnir, N., S. J. Streatfield, and V. Yusibov (2012). Virus-like particles as a highly efficient vaccine platform: diversity of targets and production systems and advances in clinical development. *Vaccine*, 31(1):58–83.

Kwon, S.-K., S. K. Kim, D.-H. Lee, and J. F. Kim (2015). Comparative genomics and experimental evolution of Escherichia coli BL21(DE3) strains reveal the landscape of toxicity escape from membrane protein overproduction. *Scientific reports*, 5:16076.

Lan, N. T., H. J. Kim, H.-J. Han, D.-C. Lee, B. K. Kang, S. Y. Han, H. Moon, and H.-J. Kim

(2018). Stability of virus-like particles of red-spotted grouper nervous necrosis virus in the aqueous state, and the vaccine potential of lyophilized particles. *Biologicals*, 51:25–31.

Lau, C. K., L. Turner, J. S. Jespersen, E. D. Lowe, B. Petersen, C. W. Wang, J. E. Petersen, J. Lusingu, T. G. Theander, T. Lavstsen, and M. K. Higgins (2015). Structural conservation despite huge sequence diversity allows EPCR binding by the pfemp1 family implicated in severe childhood malaria. *Cell Host and Microbe*, 17(1):118–129.

Lee, K. L., R. M. Twyman, S. Fiering, and N. F. Steinmetz (2016). Virus-based nanoparticles as platform technologies for modern vaccines. *Wiley interdisciplinary reviews. Nanomedicine and nanobiotechnology*, 8(4):554–78.

Leneghan, D. B., K. Miura, I. J. Taylor, Y. Li, J. Jin, K. D. Brune, M. F. Bachmann, M. Howarth, C. A. Long, and S. Biswas (2017). Nanoassembly routes stimulate conflicting antibody quantity and quality for transmission-blocking malaria vaccines. *Scientific Reports*, 7:3811.

Lennartz, F., Y. Adams, A. Bengtsson, R. W. Olsen, L. Turner, N. T. Ndam, G. Ecklu-Mensah, A. Moussiliou, M. F. Ofori, B. Gamain, J. P. Lusingu, J. E. Petersen, C. W. Wang, S. Nunes-Silva, J. S. Jespersen, C. K. Lau, T. G. Theander, T. Lavstsen, L. Hviid, M. K. Higgins, and A. T. Jensen (2017). Structure-Guided Identification of a Family of Dual Receptor-Binding PfEMP1 that Is Associated with Cerebral Malaria. *Cell Host & Microbe*, 21(3):403–414.

Lenz, P., P. M. Day, Y. Y. Pang, S. A. Frye, P. N. Jensen, D. R. Lowy, and J. T. Schiller (2001). Papillomavirus-like particles induce acute activation of dendritic cells. *Journal of immunology*, 166(9):5346–55.

Li, Y., D. B. Leneghan, K. Miura, D. Nikolaeva, I. J. Brian, M. D. J. Dicks, A. J. Fyfe, S. E. Zakutansky, S. D. Cassan, C. A. Long, S. J. Draper, A. V. S. Hill, F. Hill, and S. Biswas (2016). Enhancing immunogenicity and transmission-blocking activity of malaria vaccines

by fusing Pfs25 to IMX313 multimerization technology. *Scientific Reports*, 6(November 2015):18848.

Liu, Z., H. Zhou, W. Wang, W. Tan, Y.-X. Fu, and M. Zhu (2014). A novel method for synthetic vaccine construction based on protein assembly. *Scientific Reports*, 4:7266.

López-Sagaseta, J., E. Malito, R. Rappuoli, and M. J. Bottomley (2016). Self-assembling protein nanoparticles in the design of vaccines. *Computational and structural biotechnology journal*, 14:58–68.

Lorand, L. and R. M. Graham (2003). Transglutaminases: crosslinking enzymes with pleiotropic functions. *Nature Reviews Molecular Cell Biology*, 4(2):140–156.

Los, G. V., L. P. Encell, M. G. McDougall, D. D. Hartzell, N. Karassina, C. Zimprich, M. G. Wood, R. Learish, R. F. Ohana, M. Urh, D. Simpson, J. Mendez, K. Zimmerman, P. Otto, G. Vidugiris, J. Zhu, A. Darzins, D. H. Klaubert, R. F. Bulleit, and K. V. Wood (2008). HaloTag: A Novel Protein Labeling Technology for Cell Imaging and Protein Analysis. *ACS Chemical Biology*, 3(6):373–382.

Lu, Y., W. Chan, B. Y. Ko, C. C. Vanlang, and J. R. Swartz (2015). Assessing sequence plasticity of a virus-like nanoparticle by evolution toward a versatile scaffold for vaccines and drug delivery. *Proceedings of the National Academy of Sciences of the United States of America*, 112(40):12360–12365.

Lu, Y., J. P. Welsh, W. Chan, and J. R. Swartz (2013). Escherichia coli-based cell free production of flagellin and ordered flagellin display on virus-like particles. *Biotechnology and Bioengineering*, 110(8):2073–2085.

Lua, L. H., N. K. Connors, F. Sainsbury, Y. P. Chuan, N. Wibowo, and A. P. Middelberg (2014). Bioengineering virus-like particles as vaccines. *Biotechnology and Bioengineering*, 111(3):425–440.

Luxton, R. and E. Thompson (1990). Affinity distributions of antigen-specific IgG in patients with multiple sclerosis and in patients with viral encephalitis. *Journal of Immunological Methods*, 131:277–282.

Maassen, s. J., M. V. de Ruiter, S. Lindhoud, and J. J. Cornelissen (2018). Oligonucleotide length dependent formation of virus-like particles. *Chemistry - A European Journal*, (December).

Magalhães, P. O., A. M. Lopes, P. G. Mazzola, C. Rangel-Yagui, T. C. V. Penna, and A. Pessoa (2007). Methods of endotoxin removal from biological preparations: a review. *Journal of pharmacy & pharmaceutical sciences: a publication of the Canadian Society for Pharmaceutical Sciences, Societe canadienne des sciences pharmaceutiques*, 10(3):388–404.

Mahl, D., J. Diendorf, W. Meyer-Zaika, and M. Epple (2011). Possibilities and limitations of different analytical methods for the size determination of a bimodal dispersion of metallic nanoparticles. *Colloids and Surfaces A: Physicochemical and Engineering Aspects*, 377(1-3):386–392.

Majorek, K. A., M. L. Kuhn, M. Chruszcz, W. F. Anderson, and W. Minor (2014). Double trouble-Buffer selection and His-tag presence may be responsible for nonreproducibility of biomedical experiments. *Protein science: a publication of the Protein Society*, 23(10):1359–68.

Malyala, P. and D. O'Hagan (2017). Polymeric Particles as Vaccine DeliverySystems. In *Immunopotentiators in Modern Vaccines*, Pp. 231–248. Elsevier.

Mantile, F., M. Trovato, A. Santoni, P. Barba, S. Ottonello, P. De Berardinis, and A. Prisco (2014). Alum and squalene-oil-in-water emulsion enhance the titer and avidity of anti-Aβ antibodies induced by multimeric protein antigen (1-11)E2, preserving the Igg1-skewed isotype distribution. *PloS one*, 9:e101474.

Matejtschuk, P. (2007). Lyophilization of Proteins. In *Methods in molecular biology (Clifton, N.J.)*, volume 368, Pp. 59–72.

Mateu, M. G. (2011). Virus engineering: Functionalization and stabilization. *Protein Engineering, Design and Selection*, 24(1-2):53–63.

Mbow, M. L., E. De Gregorio, N. M. Valiante, and R. Rappuoli (2010). New adjuvants for human vaccines. *Current Opinion in Immunology*, 22:411–416.

McCarthy, M. P., W. I. White, F. Palmer-Hill, S. Koenig, and J. A. Suzich (1998). Quantitative disassembly and reassembly of human papillomavirus type 11 viruslike particles in vitro. *Journal of virology*, 72(1):32–41.

McDonald, H. M., P. S. Pruett, C. Deivanayagam, I. I. Protasevich, W. M. Carson, L. J. DeLucas, W. J. Brouillette, C. G. Brouillette, and IUCr (2007). Structural adaptation of an interacting non-native C-terminal helical extension revealed in the crystal structure of NAD+ synthetase from Bacillus anthracis. *Acta Crystallographica Section D Biological Crystallography*, 63(8):891–905.

Medrano, M., M. Á. Fuertes, A. Valbuena, P. J. P. Carrillo, A. Rodríguez-Huete, and M. G. Mateu (2016). Imaging and Quantitation of a Succession of Transient Intermediates Reveal the Reversible Self-Assembly Pathway of a Simple Icosahedral Virus Capsid. *Journal of the American Chemical Society*, 138(47):15385–15396.

Meireles, L. C., R. T. Marinho, and P. Van Damme (2015). Three decades of hepatitis B control with vaccination. *World journal of hepatology*, 7(18):2127–32.

Menon, V., M. C. Kapulu, I. Taylor, K. Jewell, Y. Li, F. Hill, C. A. Long, K. Miura, and S. Biswas (2018). Assessment of Antibodies Induced by Multivalent Transmission-Blocking Malaria Vaccines. *Frontiers in Immunology*, 8(January).

Miura, K. (2016). Progress and prospects for blood-stage malaria vaccines. *Expert review of vaccines*, 15(6):765–81.

Mohsen, M. O., L. Zha, G. Cabral-Miranda, and M. F. Bachmann (2017). Major findings and recent advances in virus-like particle (VLP)-based vaccines. *Seminars in Immunology*, 34:123–132.

Moyle, P. M. and I. Toth (2013). Modern Subunit Vaccines: Development, Components, and Research Opportunities. *ChemMedChem*, 8(3):360–376.

Nestola, P., C. Peixoto, R. R. J. S. Silva, P. M. Alves, J. P. B. Mota, and M. J. T. Carrondo (2015). Improved virus purification processes for vaccines and gene therapy. *Biotechnology and Bioengineering*, 112:843–857.

Ng, S., M. R. Jafari, and R. Derda (2012). Bacteriophages and Viruses as a Support for Organic Synthesis and Combinatorial Chemistry. *ACS Chemical Biology*, 7(1):123–138.

Nikolaeva, D., S. J. Draper, and S. Biswas (2015). Toward the development of effective transmission-blocking vaccines for malaria. *Expert Rev Vaccines*, 14:653–680.

Ogun, S. A., L. Dumon-Seignovert, J.-B. Marchand, A. A. Holder, and F. Hill (2008). The oligomerization domain of C4-binding protein (C4bp) acts as an adjuvant, and the fusion protein comprised of the 19-kilodalton merozoite surface protein 1 fused with the murine C4bp domain protects mice against malaria. *Infection and immunity*, 76(8):3817–23.

Packer, M. S. and D. R. Liu (2015). Methods for the directed evolution of proteins. *Nature reviews. Genetics*, 16(7):379–394.

Palladini, A., S. Thrane, C. M. Janitzek, J. Pihl, S. B. Clemmensen, W. A. de Jongh, T. M. Clausen, G. Nicoletti, L. Landuzzi, M. L. Penichet, T. Balboni, M. L. Ianzano, V. Giusti, T. G. Theander, M. A. Nielsen, A. Salanti, P.-L. Lollini, P. Nanni, and A. F.

Sander (2017). Virus-like particle display of HER2 induces potent anti-cancer responses. *OncoImmunology*, 7.

Parkin, J. and B. Cohen (2001). An overview of the immune system. *The Lancet*, 357(9270):1777–1789.

Pascual, E., C. P. Mata, J. L. Carrascosa, and J. R. Castón (2017). Assembly/disassembly of a complex icosahedral virus to incorporate heterologous nucleic acids. *Journal of Physics: Condensed Matter*, 29(49):494001.

Patel, K. G. and J. R. Swartz (2011). Surface Functionalization of Virus-Like Particles by Direct Conjugation Using AzideAlkyne Click Chemistry. *Bioconjugate Chemistry*, 22:376–387.

Patel, N., E. Wroblewski, G. Leonov, S. E. V. Phillips, R. Tuma, R. Twarock, and P. G. Stockley (2017). Rewriting nature's assembly manual for a ssRNA virus. *Proceedings of the National Academy of Sciences of the United States of America*, 114(46):12255–12260.

Peabody, D. S. (1993). The RNA binding site of bacteriophage MS2 coat protein. *The EMBO Journal*, 12(2):595–600.

Peabody, D. S. and L. Al-Bitar (2001). Isolation of viral coat protein mutants with altered assembly and aggregation properties. *Nucleic acids research*, 29(22):E113.

Peabody, D. S., B. Manifold-Wheeler, A. Medford, S. K. Jordan, J. do Carmo Caldeira, and B. Chackerian (2008). Immunogenic display of diverse peptides on virus-like particles of RNA phage MS2. *Journal of molecular biology*, 380(1):252–63.

Pearson, W. R. (2013). An introduction to sequence similarity ("homology") searching. *Current protocols in bioinformatics*, 42:3.1.1–3.1.8.

Perez, E. M., J. Foley, T. Tison, R. Silva, J. G. Ogembo, E. M. Perez, J. Foley, T. Tison, R. Silva, and J. G. Ogembo (2016). Novel Epstein-Barr virus-like particles incorporating

gH/gL-EBNA1 or gB-LMP2 induce high neutralizing antibody titers and EBV-specific T-cell responses in immunized mice. *Oncotarget*, 5(0).

Pickart, C. M. (2001). Mechanisms underlying ubiquitination. *Annual review of biochemistry*, 70(1):503–33.

Plotkin, S. A. and S. L. Plotkin (2011). The development of vaccines: how the past led to the future. *Nature Reviews Microbiology*, 9(12):889–893.

Porter, J. L., R. A. Rusli, and D. L. Ollis (2016). Directed Evolution of Enzymes for Industrial Biocatalysis. *ChemBioChem*, 17(3):197–203.

Preiss, S., N. Garçon, R. Strugnell, and L. R. Friedland (2016). Vaccine provision: Delivering sustained & widespread use. *Vaccine*, 34:6665–6671.

Pumpens, P., R. Renhofa, A. Dishlers, T. Kozlovska, V. Ose, P. Pushko, K. Tars, E. Grens, and M. F. Bachmann (2016). The True Story and Advantages of RNA Phage Capsids as Nanotools. *Intervirology*, 59(2):74–110.

Quan, F. S., D.-G. Yoo, J.-M. Song, J. D. Clements, R. W. Compans, and S.-M. Kang (2009). Kinetics of immune responses to influenza virus-like particles and dose-dependence of protection with a single vaccination. *Journal of virology*, 83(9):4489–97.

Ra, J.-S., H.-H. Shin, S. Kang, and Y. Do (2014). Lumazine synthase protein cage nanoparticles as antigen delivery nanoplatforms for dendritic cell-based vaccine development. *Clinical and Experimental Vaccine Research*, 3(2):227.

Rabinovich, R. N., C. Drakeley, A. A. Djimde, B. F. Hall, S. I. Hay, J. Hemingway, D. C. Kaslow, A. Noor, F. Okumu, R. Steketee, M. Tanner, T. N. C. Wells, M. A. Whittaker, E. A. Winzeler, D. F. Wirth, K. Whitfield, and P. L. Alonso (2017). malERA: An updated research agenda for malaria elimination and eradication. *PLoS medicine*, 14:e1002456.

Rappuoli, R. and A. Aderem (2011). A 2020 vision for vaccines against HIV, tuberculosis and malaria. *Nature*, 473(7348):463–469.

Rehm, B. H. (2017). Bioengineering towards self-assembly of particulate vaccines. *Current Opinion in Biotechnology*, 48:42–53.

Reimann, J. and R. Schirmbeck (1999). Alternative pathways for processing exogenous and endogenous antigens that can generate peptides for MHC class I-restricted presentation. *Immunological Reviews*, 172(1):131–152.

Ringe, R. P., G. Ozorowski, K. Rantalainen, W. B. Struwe, K. Matthews, J. L. Torres, A. Yasmeen, C. A. Cottrell, T. J. Ketas, C. C. LaBranche, D. C. Montefiori, A. Cupo, M. Crispin, I. A. Wilson, A. B. Ward, R. W. Sanders, P. J. Klasse, and J. P. Moore (2017). Reducing V3 Antigenicity and Immunogenicity on Soluble, Native-Like HIV-1 Env SOSIP Trimers. *Journal of Virology*, 91(15):e00677–17.

Rohovie, M. J., M. Nagasawa, and J. R. Swartz (2017). Virus-like particles: Next-generation nanoparticles for targeted therapeutic delivery. *Bioengineering & translational medicine*, 2(1):43–57.

Roingeard, P. (2008). Viral detection by electron microscopy: past, present and future. *Biology of the Cell*, 100(8):491–501.

Rolfsson, Ó., S. Middleton, I. W. Manfield, S. J. White, B. Fan, R. Vaughan, N. A. Ranson, E. Dykeman, R. Twarock, J. Ford, C. Cheng Kao, and P. G. Stockley (2016). Direct Evidence for Packaging Signal-Mediated Assembly of Bacteriophage MS2. *Journal of Molecular Biology*, 428(2):431–448.

Rome, L. H. and V. A. Kickhoefer (2013). Development of the vault particle as a platform technology. *ACS nano*, 7(2):889–902.

Rother, M., M. G. Nussbaumer, K. Renggli, and N. Bruns (2016). Protein cages and synthetic polymers: a fruitful symbiosis for drug delivery applications, bionanotechnology and materials science. *Chem. Soc. Rev.*, 105:1445–1489.

Rubinstein, R. and A. Fiser (2008). Predicting disulfide bond connectivity in proteins by correlated mutations analysis. *Bioinformatics*, 24(4):498–504.

Sachsenhauser, V. and J. C. Bardwell (2018). Directed evolution to improve protein folding in vivo. *Current Opinion in Structural Biology*, 48:117–123.

Salunke, D., D. Caspar, and R. Garcea (1989). Polymorphism in the assembly of polyomavirus capsid protein VP1. *Biophysical Journal*, 56(5):887–900.

Scally, S. W., B. McLeod, A. Bosch, K. Miura, Q. Liang, S. Carroll, S. Reponen, N. Nguyen, E. Giladi, S. Rämisch, V. Yusibov, A. Bradley, F. Lemiale, W. R. Schief, D. Emerling, P. Kellam, C. R. King, and J.-P. Julien (2017). Molecular definition of multiple sites of antibody inhibition of malaria transmission-blocking vaccine antigen Pfs25. *Nature Communications*, 8(1):1568.

Schmitz, N., R. R. Beerli, M. Bauer, A. Jegerlehner, K. Dietmeier, M. Maudrich, P. Pumpens, P. Saudan, and M. F. Bachmann (2012). Universal vaccine against influenza virus: Linking TLR signaling to anti-viral protection. *European Journal of Immunology*, 42:863–869.

Schoene, C., J. O. Fierer, S. P. Bennett, and M. Howarth (2014). SpyTag/Spycatcher cyclization confers resilience to boiling on a mesophilic enzyme. *Angewandte Chemie - International Edition*, 53(24):6101–6104.

Schrand, A. M., M. F. Rahman, S. M. Hussain, J. J. Schlager, D. A. Smith, and A. F. Syed (2010). Metal-based nanoparticles and their toxicity assessment. *Wiley Interdisciplinary Reviews: Nanomedicine and Nanobiotechnology*, 2(5):544–568.

Schumacher, J., T. Bacic, R. Staritzbichler, M. Daneschdar, T. Klamp, P. Arnold, S. Jägle, Ö. Türeci, J. Markl, and U. Sahin (2018). Enhanced stability of a chimeric hepatitis B core antigen virus-like-particle (HBcAg-VLP) by a C-terminal linker-hexahistidine-peptide. *Journal of Nanobiotechnology*, 16(1):39.

Shi, J., P. W. Kantoff, R. Wooster, and O. C. Farokhzad (2017). Cancer nanomedicine: progress, challenges and opportunities. *Nature Reviews Cancer*, 17:20–37.

Shishovs, M., J. Rumnieks, C. Diebolder, K. Jaudzems, L. B. Andreas, J. Stanek, A. Kazaks, S. Kotelovica, I. Akopjana, G. Pintacuda, R. I. Koning, and K. Tars (2016). Structure of AP205 Coat Protein Reveals Circular Permutation in ssRNA Bacteriophages. *Journal of Molecular Biology*, 428(21):4267–4279.

Smith, J. D., L. D. Morton, and B. D. Ulery (2015). Nanoparticles as synthetic vaccines. *Current Opinion in Biotechnology*, 34:217–224.

Smith, M. T., A. K. Hawes, and B. C. Bundy (2013). Reengineering viruses and virus-like particles through chemical functionalization strategies. *Current Opinion in Biotechnology*, 24(4):620–626.

Smith, M. T., C. T. Varner, D. B. Bush, and B. C. Bundy (2012). The incorporation of the A2 protein to produce novel Qβ virus-like particles using cell-free protein synthesis. *Biotechnology Progress*, 28(2):549–555.

Stanley, M. (2008). Immunobiology of HPV and HPV vaccines. *Gynecologic Oncology*, 109(2):S15–S21.

Stockley, P. G. and R. A. Mastico (2000). Use of fusions to viral coat proteins as antigenic carriers for vaccine development. *Methods in Enzymology*, 326:551–569.

Sun, Q., Q. Chen, D. Blackstock, and W. Chen (2015). Post-Translational Modification of Bionanoparticles as a Modular Platform for Biosensor Assembly. *ACS nano*, 9(8):8554–61.

Talaat, K. R., R. D. Ellis, J. Hurd, A. Hentrich, E. Gabriel, N. A. Hynes, K. M. Rausch, D. Zhu, O. Muratova, R. Herrera, C. Anderson, D. Jones, J. Aebig, S. Brockley, N. J. MacDonald, X. Wang, M. P. Fay, S. A. Healy, A. P. Durbin, D. L. Narum, Y. Wu, and P. E. Duffy (2016). Safety and Immunogenicity of Pfs25-EPA/Alhydrogel®, a Transmission Blocking Vaccine against Plasmodium falciparum: An Open Label Study in Malaria Naïve Adults. *PLOS ONE*, 11:e0163144.

Tang, S., B. Xuan, X. Ye, Z. Huang, and Z. Qian (2016). A Modular Vaccine Development Platform Based on Sortase-Mediated Site-Specific Tagging of Antigens onto Virus-Like Particles. *Scientific reports*, 6(1):25741.

Tateda, K., T. Matsumoto, S. Miyazaki, and K. Yamaguchi (1996). Lipopolysaccharide-induced lethality and cytokine production in aged mice. *Infection and immunity*, 64(3):769–74.

Tee, K. L. and T. S. Wong (2013). Polishing the craft of genetic diversity creation in directed evolution. *Biotechnology Advances*, 31(8):1707–1721.

Thomassen, Y. E., A. G. van 't Oever, M. Vinke, A. Spiekstra, R. H. Wijffels, L. A. van der Pol, and W. A. Bakker (2013). Scale-down of the inactivated polio vaccine production process. *Biotechnology and Bioengineering*, 110(5):1354–1365.

Thrane, S., C. M. Janitzek, S. Matondo, M. Resende, T. Gustavsson, W. A. de Jongh, S. Clemmensen, W. Roeffen, M. van de VegteBolmer, G. J. van Gemert, R. Sauerwein, J. T. Schiller, M. A. Nielsen, T. G. Theander, A. Salanti, and A. F. Sander (2016). Bacterial superglue enables easy development of efficient virus-like particle based vaccines. *Journal of Nanobiotechnology*, 14:30.

Tissot, A. C., R. Renhofa, N. Schmitz, I. Cielens, E. Meijerink, V. Ose, G. T. Jennings, P. Saudan, P. Pumpens, and M. F. Bachmann (2010). Versatile Virus-Like Particle Carrier for Epitope Based Vaccines. *PLoS ONE*, 5(3):e9809.

Tomori, O. (2011). From smallpox eradication to the future of global health: Innovations, application and lessons for future eradication and control initiatives. *Vaccine*, 29:D145–D148.

Tsunetsugu-Yokota, Y., Y. Morikawa, M. Isogai, A. Kawana-Tachikawa, T. Odawara, T. Nakamura, F. Grassi, B. Autran, and A. Iwamoto (2003). Yeast-derived human immunodeficiency virus type 1 p55(gag) virus-like particles activate dendritic cells (DCs) and induce perforin expression in Gag-specific CD8(+) T cells by cross-presentation of DCs. *Journal of virology*, 77(19):10250–9.

Tumban, E., J. Peabody, D. S. Peabody, and B. Chackerian (2013). A universal virus-like particle-based vaccine for human papillomavirus: Longevity of protection and role of endogenous and exogenous adjuvants. *Vaccine*, 31(41):4647–4654.

Uchida, M., K. McCoy, M. Fukuto, L. Yang, H. Yoshimura, H. M. Miettinen, B. LaFrance, D. P. Patterson, B. Schwarz, J. A. Karty, P. E. Prevelige, B. Lee, and T. Douglas (2018). Modular Self-Assembly of Protein Cage Lattices for Multistep Catalysis. *ACS Nano*, 12:942–953.

van der Holst, B., W. K. Kegel, R. Zandi, and P. van der Schoot (2018). The different faces of mass action in virus assembly. *Journal of Biological Physics*, Pp. 1–17.

Veggiani, G., T. Nakamura, M. D. Brenner, R. V. Gayet, J. Yan, C. V. Robinson, and M. Howarth (2016). Programmable polyproteams built using twin peptide superglues. *Proceedings of the National Academy of Sciences of the United States of America*, 113(5):1202–7.

Veggiani, G., B. Zakeri, and M. Howarth (2014). Superglue from bacteria: Unbreakable bridges for protein nanotechnology. *Trends in Biotechnology*, 32:506–512.

Vicente, T., A. Roldão, C. Peixoto, M. J. Carrondo, and P. M. Alves (2011). Large-scale

production and purification of VLP-based vaccines. *Journal of Invertebrate Pathology*, 107:S42–S48.

Wakelin, S. J., I. Sabroe, C. D. Gregory, I. R. Poxton, J. L. Forsythe, O. J. Garden, and S. E. Howie (2006). Dirty little secretsEndotoxin contamination of recombinant proteins. *Immunology Letters*, 106(1):1–7.

Wang, Q., E. Kaltgrad, T. Lin, J. E. Johnson, and M. G. Finn (2002a). Natural supramolecular building blocks. Wild-type cowpea mosaic virus. *Chemistry & biology*, 9(7):805–11.

Wang, Q., T. Lin, J. E. Johnson, and M. G. Finn (2002b). Natural supramolecular building blocks. Cysteine-added mutants of cowpea mosaic virus. *Chemistry & biology*, 9(7):813–9.

Wang, S., H. L. True, E. M. Seitz, K. A. Bennett, D. E. Fouts, J. F. Gardner, and D. W. Celander (1997). Direct genetic selection of two classes of R17/MS2 coat proteins with altered capsid assembly properties and expanded RNA-binding activities. *Nucleic Acids Research*, 25(8):1649–1657.

Wang, Y., P. Vander Horn, and L. Xi (2011). Methods of using improved polymerases. *United States of America*, BioRad Inc(US patent EP1456394B2).

Wikoff, W. R., L. Liljas, R. L. Duda, H. Tsuruta, R. W. Hendrix, and J. E. Johnson (2000). Topologically linked protein rings in the bacteriophage HK97 capsid. *Science (New York, N.Y.)*, 289(5487):2129–33.

Wilhelm, S., A. J. Tavares, Q. Dai, S. Ohta, J. Audet, H. F. Dvorak, and W. C. W. Chan (2016). Analysis of nanoparticle delivery to tumours. *Nature Reviews Materials*, 1:16014.

Worsdorfer, B., K. J. Woycechowsky, and D. Hilvert (2011). Directed Evolution of a Protein Container. *Science*, 331(6017):589–592.

Wu, Y., D. L. Narum, S. Fleury, G. Jennings, and A. Yadava (2015). Particle-based platforms for malaria vaccines. *Vaccine*, 33(52):7518–7524.

Zabel, F., T. M. Kündig, and M. F. Bachmann (2013). Virus-induced humoral immunity: on how B cell responses are initiated. *Current Opinion in Virology*, 3(3):357–362.

Zahid, M., H. Lünsdorf, and U. Rinas (2015). Assessing stability and assembly of the hepatitis B surface antigen into virus-like particles during down-stream processing. *Vaccine*, 33(31):3739–3745.

Zakeri, B., J. O. Fierer, E. Celik, E. C. Chittock, U. Schwarz-Linek, V. T. Moy, and M. Howarth (2012). Peptide tag forming a rapid covalent bond to a protein, through engineering a bacterial adhesin. *Proceedings of the National Academy of Sciences of the United States of America*, 109:E690–E697.

Zakeri, B. and M. Howarth (2010). Spontaneous intermolecular amide bond formation between side chains for irreversible peptide targeting. *Journal of the American Chemical Society*, 132(13):4526–4527.

Zandi, R. and P. van der Schoot (2009). Size Regulation of ss-RNA Viruses. *Biophysical Journal*, 96(1):9–20.

Zeltins, A. (2013). Construction and Characterization of Virus-Like Particles: A Review. *Molecular Biotechnology*, 53(1):92–107.

Zhao, D. and Z. Huang (2016). Effect of His-Tag on Expression, Purification, and Structure of Zinc Finger Protein, ZNF191(243-368). *Bioinorganic chemistry and applications*, 2016:8206854.

Zylberberg, C. and S. Matosevic (2016). Pharmaceutical liposomal drug delivery: a review of new delivery systems and a look at the regulatory landscape. *Drug Delivery*, 23(9):3319–3329.

Appendix

Amino acid sequences of proteins employed in this thesis:

SpyCatcher-AP205 (Brune et al., 2016)

MGSSHHHHHHGSGDSATHIKFSKRDEDGKELAGATMELRDSSGKTISTWISDGQVK
DFYLYPGKYTFVETAAPDGYEVATAITFTVNEQGQVTVNGKATKGDAHIGGSGSA
NKPMQPITSTANKIVWSDPTRLSTTFSASLLRQRVKVGIAELNNVSGQYVSVYKRPA
PKPEGCADACVIMPNENQSIRTVISGSAENLATLKAEWETHKRNVDTLFASGNAGL
GFLDPTAAIVSSDTTA*

SpyTag-MBP (Zakeri et al., 2012)

MGSSHHHHHHSSGLVPRGSHMGAHIVMVDAYKPTKGSGESGKIEEGKLVIWINGDK
GYNGLAEVGKKFEKDTGIKVTVEHPDKLEEKFPQVAATGDGPDIIFWAHDRFGGY
AQSGLLAEITPDKAFQDKLYPFTWDAVRYNGKLIAYPIAVEALSLIYNKDLLPNPPK
TWEEIPALDKELKAKGKSALMFNLQEPYFTWPLIAADGGYAFKYENGKYDIKDVG
VDNAGAKAGLTFLVDLIKNKHMNADTDYSIAEAAFNKGETAMTINGPWAWSNIDT
SKVNYGVTVLPTFKGQPSKPFVGVLSAGINAASPNKELAKEFLENYLLTDEGLEAV
NKDKPLGAVALKSYEEELAKDPRIAATMENAQKGEIMPNIPQMSAFWYAVRTAVIN
AASGRQTVDEALKDAQTNSSS*

SpyTag002-TEV-HaloTag7

MGVPTIVMVDAYKRYKGSSGSGENLYFQGGGSGEIGTGFPFDPHYVEVLGERMHY
VDVGPRDGTPVLFLHGNPTSSYVWRNIIPHVAPTHRCIAPDLIGMGKSDKPDLGYFF
DDHVRFMDAFIEALGLEEVVLVIHDWGSALGFHWAKRNPERVKGIAFMEFIRPIPT
WDEWPEFARETFQAFRTTDVGRKLIIDQNVFIEGTLPMGVVRPLTEVEMDHYREP
FLNPVDREPLWRFPNELPIAGEPANIVALVEEYMDWLHQSPVPKLLFWGTPGVLIP
PAEAARLAKSLPNCKAVDIGPGLNLLQEDNPDLIGSEIARWLSTLEISGGSGSGSHHH
HHH*

CyRPA-SpyTag

MEFQTQVLMSLLLCMSGAAADSRHVFIRTELSFIKNNVPCIRDMFFIYKRELYNICLD

DLKGEEDETHIYVQKKVKDSWITLNDLFKETDLTGRPHIFAYVDVEEIIILLCEDEEF
SNRKKDMTCHRFYSNDGKEYNNAEITISDYILKDKLLSSYVSLPLKIENREYFLICGV
SPYKFKDDNKKDDILCMASHDKGETWGTKIVIKYDNYKLGVQYFFLRPYISKNDLS
FHFYVGDNINNVKNVNFIECTHEKDLEFVCSNRDFLKDNKVLQDVSTLNDEYIVSYG
NDNNFAECYIFFNNENSILIKPEKYGNTAAGCYGGTFVKIDENRALFIYSSSQGIYNIH
TIYYANYEGSGGSGGSGAHIVMVDAYKPTKGSGEPEA*

SpyTag-CIDR(IT4var07) (Brune et al., 2016)

MGHHHHHHENLYFQGGSAHIVMVDAYKPTKGGSEPAPDVKTTEINVIVSGDEQGII
TKKLQDFCMNPNNENGTNNQIWKCYYKDEKENKCKVETKSGNSTYKEKITSFDEF
FDFWVRKLLIDTIKWETELTYCINNTTNADCNNECNKNCVCFDKWVKQKEKEWK
NIMDLFTNKHDIPKKYYLNINDLFNSFFFQVIYKFNEGEAKWNKLKENLKKKIESSK
KNKGTKDSEAAIKVLFDHLKETATICKDNNTNEAC*

Pfs25-SpyTag (Brune et al., 2016)

MSGHLECKCENDLVLVNEETCEEKVLKCDEKTVNKPCGDFSKCIKIDGNPVSYACK
CNLGYDMVNNVCIPNECKQVTCGNGKCILDTSNPVKTGVCSCNIGKVPNVQDQNK
CSKDGETKCSLKCLKEQETCKAVDGIYKCDCKDGFIIDQESSICTAHIVMVDAYKPT
KEPEA*

SpyCatcher-I301 HisTag

MGSSHHHHHHGSGDSATHIKFSKRDEDGKELAGATMELRDSSGKTISTWISDGQVK
DFYLYPGKYTFVETAAPDGYEVATAITFTVNEQGQVTVNGKATKGDAHIGGSGGS
GGSGGSMKMEELFKKHKIVAVLRANSVEEAKKKALAVFLGGVHLIEITFTVPDADT
VIKELSFLKEMGAIIGAGTVTSVEQCRKAVESGAEFIVSPHLDEEISQFCKEKGVFYM
PGVMTPTELVKAMKLGHTILKLFPGEVVGPQFVKAMKGPFPNVKFVPTGGVNLD
NVCEWFKAGVLAVGVGSALVKGTPVEVAEKAKAFVEKIRGCTE*

SpyCatcher-I301 C-tag

MGSSDSATHIKFSKRDEDGKELAGATMELRDSSGKTISTWISDGQVKDFYLYPGKY
TFVETAAPDGYEVATAITFTVNEQGQVTVNGKATKGDAHIGGSGGSGGSGGSMKM

EELFKKHKIVAVLRANSVEEAKKKALAVFLGGVHLIEITFTVPDADTVIKELSFLKE
MGAIIGAGTVTSVEQCRKAVESGAEFIVSPHLDEEISQFCKEKGVFYMPGVMTPTEL
VKAMKLGHTILKLFPGEVVGPQFVKAMKGPFPNVKFVPTGGVNLDNVCEWFKAG
VLAVGVGSALVKGTPVEVAEKAKAFVEKIRGCTEGSGEPEA*

SpyCatcher-MI3 HisTag

MGSSHHHHHHGSGDSATHIKFSKRDEDGKELAGATMELRDSSGKTISTWISDGQVK
DFYLYPGKYTFVETAAPDGYEVATAITFTVNEQGQVTVNGKATKGDAHIGGSGGS
GGSGGSMKMEELFKKHKIVAVLRANSVEEAKKKALAVFLGGVHLIEITFTVPDADT
VIKELSFLKEMGAIIGAGTVTSVEQARKAVESGAEFIVSPHLDEEISQFAKEKGVFYM
PGVMTPTELVKAMKLGHTILKLFPGEVVGPQFVKAMKGPFPNVKFVPTGGVNLD
NVCEWFKAGVLAVGVGSALVKGTPVEVAEKAKAFVEKIRGCTE*

SpyCatcher-MI3

MGSSDSATHIKFSKRDEDGKELAGATMELRDSSGKTISTWISDGQVKDFYLYPGKY
TFVETAAPDGYEVATAITFTVNEQGQVTVNGKATKGDAHIGGSGGSGGSGGSMKM
EELFKKHKIVAVLRANSVEEAKKKALAVFLGGVHLIEITFTVPDADTVIKELSFLKE
MGAIIGAGTVTSVEQARKAVESGAEFIVSPHLDEEISQFAKEKGVFYMPGVMTPTEL
VKAMKLGHTILKLFPGEVVGPQFVKAMKGPFPNVKFVPTGGVNLDNVCEWFKAG
VLAVGVGSALVKGTPVEVAEKAKAFVEKIRGCTEGSGEPEA*